

ADVANCED OXIDATIVE WATER TREATMENT PROCESS FOR WATER DISINFECTION USING AN ELECTROHYDRAULIC DISCHARGE REACTOR AND TiO_2 IMMOBILIZED ON NANO FIBRES

Report to the
Water Research Commission

by

LF Petrik, OO Fatoba, E Mouele and T Totito
University of Western Cape



WRC Report No. 2132/1/15
ISBN 978-1-4312-0692-6

August 2015



Obtainable from

Water Research Commission
Private Bag X03
GEZINA, 0031

orders@wrc.org.za or download from www.wrc.org.za

DISCLAIMER

This report has been reviewed by the Water Research Commission (WRC) and approved for publication. Approval does not signify that the contents necessarily reflect the views and policies of the WRC, nor does mention of trade names or commercial products constitute endorsement or recommendation for use.

EXECUTIVE SUMMARY

BACKGROUND

Water pollution has become a global problem as a consequence of growing accumulation of persistent organic pollutants caused by natural and anthropogenic activities. These activities have impacted negatively on the availability and access to clean, safe and uncontaminated water. Most of these contaminants are highly recalcitrant, toxic and non-biodegradable with grave environmental consequences. Various health challenges have been reported due to exposure of the population to contaminated water among which is the vast spread of waterborne diseases that claims millions of life annually, especially amongst under age children. Thus, with this growing demand for safe drinking water and perpetually increasing water pollution, urgent practical and strategic water treatment solutions are required. Currently available conventional water treatment approaches are less capable of producing the desired results and often generate toxic intermediate products. These disadvantages have driven research interest into the development of new water treatment technologies that will supplement the existing approaches. Thus, the use of advanced oxidation technologies such as the electrohydraulic discharge (EHD) system for decomposing organics and inactivating microorganisms was considered due to its greater efficiency, energy saving, high speed, use of few or no chemicals, and non-destructive impacts upon the ecosystem.

This project investigated the design and methods for applying electrical energy to single or multiple electrodes. An assembly having a single or more electrodes may be configured such that the high voltage electrodes are submerged in the inner tubes positioned at parallel relative to one another and the grounded electrode is directly submerged into the setup of the water to be treated for production of a cocktail of active chemical species, such as ozone, hydrogen peroxide, singlet oxygen, superoxide radicals, hydroxyl radicals and other active species, which the system is capable of generating. The combination of these reactive species has been reported to be capable of degrading biological and chemical pollutants rapidly and efficiently. This technology development of advanced oxidation was initiated under WRC project K5/1897, funded at bench scale by Water Research Commission of South Africa under Prof Leslie Petrik's leadership at the University of Western Cape. (See WRC Report 1987/1/12.) The present project also aims to investigate optimization of the whole electrohydraulic discharge reactor (EHD) system, as well as detection and quantification of the free reactive species, both which have been some of the most challenging tasks in previous projects.

AIMS

The following were the aims of the project:

- To generate plasma directly in water which will produce radicals from water ionisation
- To optimize the reactor configuration using copper wire electrodes and study synergetic effects of advanced oxidation processes (AOP) on water treatment
- To identify and quantify the cocktail of chemicals species production, such as OH radicals, ozone and hydrogen peroxide which can target and attack the pollutants in the water without adding chemicals

- To integrate innovations in nanophotocatalysts in the proposed electrohydraulic system to maximally utilize the UV radiation produced in the reactor
- To investigate the effect of the optimised conditions of the EHD system on the removal and degradation of model solutions of dye as well as the inactivation of target micro-organisms
- To replace the initial conventional electrodes with nanowires
- To design and construct a new reactor system based on corona discharge principals using multiple electrodes to avoid corrosion on electrohydraulic mode, which will promote chemical oxidation reactions in the liquid phase, and produce a cocktail of oxidants

METHODOLOGY

The EHD system was optimized by investigating the effects of physico-chemical, electrical parameters and reactor configurations on methylene blue (MB) degradation efficiency. The physico-chemical parameters included MB concentration (0.5-10 mg/L), solution pH (2.5-10.5) and conductivity (5-20 mS/cm), solution volume (500-2000 mL), NaCl electrolyte concentration (10-50 g/L) air gap (2-6 mm) and air flow rate (2-4 L/min). As for electrical parameters, the effects of applied voltage (20-25 V), current (2-4 A), electrode type (copper, silver and stainless steel) and electrode size (0.5-1.5 mm) on MB degradation efficiency were evaluated. The effects of these parameters on MB degradation efficiency was assessed by varying one parameter at a time at the following fixed/constant conditions: reactor air gap 2 mm, solution volume 1500 mL, NaCl electrolyte concentration 50 g/L in electrode compartment, voltage 25 V (7.8 kV), airflow rate 3 L/min, 0.5 mm silver electrode and a running time of 60 minutes. In comparison to the preliminary experimental conditions the following optimum results were obtained based on the investigated parameters: optimum MB concentration (5 mg/L), solution pH (2.5), solution volume (1500 mL), air flow rate (3 L/min), 1.5 mm silver electrode, applied voltage (25 V), current (4 A), NaCl electrolyte (50 g/L) a contact time of 60 minutes.

In order to utilize the UV radiation generated during the operation of the EHD, supported photocatalysts were developed. In the previous WRC funded studies, it has been shown that titanium dioxide loaded carbon nanotube (CNT) nano-composites modified with silver nanoparticles was an effective photo-catalyst for the degradation of contaminants, using methylene blue (MB) as a model pollutant. In that work 1 g/L of catalyst with loading of 20 wt. % TiO₂ on CNT was enough to achieve a degradation rate of 83% of 500 mL of 50 mg/L aqueous MB solution in 10 h using UV light and at pH 8. The deposition of 2 wt. % Ag on 20 wt. % TiO₂/CNT resulted in a greater and faster degradation of MB of 92% in 4 h under the same conditions (Hintso et al., 2014). Furthermore, the powder TiO₂ decoloured 68% of the solution after 8 hrs.

Due to the toxicity problem, separation and light penetration issues of free floating nanoparticles in water, much effort was directed to preparing high surface area supported TiO₂ anatase nanocrystals. By combining photocatalysis with advanced oxidation systems much more complete degradation is possible. Methods to prepare high surface area TiO₂ anatase nanocrystals supported on a stainless steel mesh were developed. These new composite materials were used to remove methylene blue (MB) from aqueous solutions. The supporting procedure involved the thermal decomposition of a sol gel solution coated upon stainless steel mesh. The nanocrystalline anatase phase was formed by thermal decomposition of stainless steel mesh

coated with 8% PAN/DMF/TiO₂ sol gel formation calcined at varying temperatures of 300°C, 400°C, 500°C and 600°C. The heating rate of 50°C/min and holding times of 1 h, 2 h, 3 h and 4 h were applied to find the optimum supporting conditions. The synthesised TiO₂ nanocomposites materials were characterised using the following analytical techniques: XRD, HRSEM, EDS, HRTEM, SAED, FTIR and UV-Vis absorption spectroscopy. The photocatalytic activity of the TiO₂ nanocrystals supported on a stainless steel mesh were tested using 50 mg/L methylene blue solution under UV irradiation for 30, 60 and 90 minutes.

The specific EHD system developed, namely a dielectric barrier discharge (DBD) system was also employed for the treatment of real textile effluent and to inactivate *E. coli* bacteria in water at room temperature.

RESULTS AND DISCUSSION

No corrosion was observed with silver electrodes, whereas previously used copper electrodes showed significant corrosion after a few electrohydraulic cycles. Further increase in MB concentration above 5 mg/L resulted in a decrease in the decolourization rate under the optimised conditions.

With regards to the reactive species responsible for the decomposition of the organics, two of the active species, hydrogen peroxide and ozone (H₂O₂ and O₃), in the effluent were detected and quantified. It was observed that within the first 20 minutes, no significant amount of ozone was produced in solution. However, the concentration of generated hydrogen peroxide reached 6.05×10⁻⁷ mol/L in solution after 10 minutes and decreased to 4.76×10⁻⁷ mol/L after 20 minutes. This demonstrates that hydrogen peroxide rather than ozone is the first species to be formed and is possibly responsible for the initial MB degradation. After 20 minutes, the concentration of generated ozone increased to 0.5×10⁻⁷ mol/L. The complete decolourization of MB was ascribed to the combined effect of hydrogen peroxide and ozone within 40 minutes. Beyond this time, the concentration of hydrogen peroxide decreased continuously whereas that of ozone continued to rise in a sinusoidal fashion.

Furthermore, with application of the optimised conditions on MB decolourization/degradation, 99.99% MB decolourizations rate was achieved within 20 minutes of contact time. Therefore, the optimized EHD system showed an improvement in reduction of the treatment time with a corresponding 53% total organic carbon (TOC) reduction. The free reactive species (H₂O₂ and O₃) were also detected and quantified. After 10 minutes of experiment, about 3.73×10⁻⁵ mol/L H₂O₂ was produced which decreased to 2.93×10⁻⁵ mol/L with a low concentration of O₃ concentration. However, 0.5 mol/L of O₃ was detected after 20 minutes of contact time, thereafter, H₂O₂ concentration decreased continuously with time while that of O₃ fluctuated as the treatment time increased. Thus MB degradation in the optimized EHD configuration was mostly initiated by generated H₂O₂ and O₃. The report also demonstrates the details of the degradation mechanism of methylene blue. The effects of the physicochemical parameters (pH, conductivity of the water, additives) and discharge conditions (applied voltage polarity and pulse repetition rate) on hydrogen peroxide production were investigated. It was found that MB dye decolorized but decomposed to various intermediate by-products and the resulting aliphatic compounds such as carboxylic acids, aldehydes, amines, amides, were not fully oxidised into CO₂ and H₂O but remained in the solution. Hence it is necessary for the further

identification of intermediate products using Liquid chromatography Mass Spectroscopy or Gas Chromatography Mass Spectroscopy.

Because the single reactor tube was applied in EHD optimization, gas bubbles containing reactive species escaped the system, and a strong odour of ozone arose around the working system which could not be quantified. It is likely that other reactor configurations that sparge the bubbles more finely into the fluid, and utilize the reactive species more effectively and can handle higher volumes will show an effective maximum removal depending upon the applied conditions. A redesigned multiple tube reactor is presented in this report. Future work will focus on developing a new continuous mode reactor system that will recirculate the fluid, thus allowing better contact between reactive species in the gaseous phase and the liquid effluent to be treated.

The results of the characterisation of the synthesized TiO₂ nanocrystals supported on a stainless steel mesh indicated that they were in the anatase form, polycrystalline in nature, and contained additional carbon-carbon bonds from the polymer used during preparation with TiO₂ particle sizes ranging from 13.60±0.0091 nm to 2285.43±0.0010 nm depending upon the thermal conditions applied. The percentage degradation of MB achieved was 96.02% after 30 min under UV radiation in the presence of 0.3 g stainless steel mesh supported TiO₂ nanocrystals prepared by decomposition at 400°C for 2 h. This study clearly demonstrated that TiO₂ anatase nanocrystals supported on a stainless steel mesh effectively removed methylene blue from aqueous solution, hence can effectively utilize the UV radiation generated from the EHD system. This study has successfully produced stably adhered, supported TiO₂ anatase nanocrystals with a high surface area that eliminated the post separation problem of powdered forms of TiO₂ and which photocatalysts were highly effective for the degradation of complex organics such as methylene blue.

In terms of real textile effluent containing a plethora of dyes, it was demonstrated that a combination of coagulation-flocculation and electrohydraulic discharge treatment was able to remove the colour and lower the COD value of a real textile effluent to well below the discharge limit, depending upon the treatment process combination. The preliminary investigation conducted on the textile effluent indicated that removal of COD below the detection limit remains unrealistic via a single treatment system such as EDH alone. Thus, process integration was considered to be more economically advantageous and beneficial for the maintenance of environmental sustainability and protection. However, the application of the single cell configuration of the electrical discharge system for industrial wastewater treatment is costly to scale up thus may limit its full scale application for effluent treatment.

The treatment of wastewater containing microorganisms originating from different point and non-point sources has remained one of the cardinal objectives of most researchers. Most of these microorganisms, particularly bacteria, are not readily biodegradable and pose a serious threat to human health. Thus, it becomes imperative to develop an appropriate and effective treatment technique that could be used to remove the enteric bacteria from water. The specific EHD system developed, namely a dielectric barrier discharge (DBD) system was employed to inactivate *E. coli* bacteria in water at room temperature. Air was used as a feeding gas to raise the concentration of ozone generated during the plasma process. The

obtained results indicate an increase in the optical density of the bacteria during the first 10 minutes which drastically decreased with an increase of treatment time. After the first 10 minutes of exposure of *E. coli* to plasma discharge, the bacterial inactivation percentage increased from 11.3 to 59.4%. The increase in inactivation percentage was due to the combination of physical and chemical properties of the plasma generated within the discharge zone of the DBD system.

In summary, the DBD system was shown to be a viable technique for decomposing non-biodegradable organic pollutants and microorganisms such as *E. coli* commonly detected in water. This study developed an optimized single cell EHD system that can incorporate a supported UV active TiO₂ photocatalyst and the system is capable of degrading organic pollutants in wastewater within 20 minutes without chemical additives therefore presenting an advantage over current technologies.

RECOMMENDATIONS

Part of the recommended future work includes the use of pure oxygen as source of air to avoid formation of intermediate products such as nitrates from N₂ in the air. Further development of the combined advanced oxidation systems are being considered for the future.

ACKNOWLEDGEMENTS

The project team wishes to thank the following people for their contributions to the project.

Reference Group	Affiliation
Dr N Kalebaila	Water Research Commission (Chairperson)
Dr J Burgess	Water Research Commission (former Chairperson)
Dr M Botes	Stellenbosch University
Dr J Mans	University of Pretoria
Dr T Barnard	University of Johannesburg
Prof R Krause	Rhodes University
Prof C Ngila	University of Johannesburg
Prof L Tichagwa	Fort Hare University
Prof L Pillay	Stellenbosch University
Others	
Dr Godfrey Madzivire	University of the Western Cape (UWC)
Dr O Fatoba	University of the Western Cape (UWC)
Dr OS Ayanda	University of the Western Cape (UWC)
Ms A Abbott	University of the Western Cape (Committee Secretary)

CONTENTS

EXECUTIVE SUMMARY	iii
ACKNOWLEDGEMENTS	viii
CONTENTS	ix
LIST OF FIGURES	xii
LIST OF TABLES	xvi
ACRONYMS & ABBREVIATIONS	xvii
CHAPTER 1: BACKGROUND	1
1.1 INTRODUCTION.....	1
1.2 PROJECT AIMS.....	2
1.3 SCOPE AND LIMITATIONS.....	3
CHAPTER 2: LITERATURE REVIEW	4
2.1 INTRODUCTION.....	4
2.2 PLASMA TECHNOLOGY.....	4
2.3 STRUCTURE AND CHARACTERISTICS OF THE DIELECTRIC BARRIER DISCHARGE.....	9
2.4 WASTEWATER TREATMENT BY DIELECTRIC BARRIER DISCHARGE SYSTEM.....	13
2.5 DEGRADATION OF ORGANIC POLLUTANTS USING DBD PLASMA-AN OVERVIEW.....	15
2.6 TiO ₂ PHOTOCATALYSIS.....	19
CHAPTER 3: EXPERIMENTAL DESIGN AND METHODOLOGY	23
3.1 INTRODUCTION.....	23
3.2 UV-VIS SPECTROSCOPY.....	23
3.2.1 Sample preparation.....	23
3.2.2 Experimental set up for UV Vis spectroscopy.....	23
3.2.2.1 Procedure.....	24
3.3 PREPARATION OF METHYLENE BLUE STANDARD SOLUTIONS.....	26
3.4 EHD EXPERIMENTAL PROCEDURE.....	26
3.4.1 Effect of air gap between the outer and inner tubes of the EHD reactor.....	28
3.4.1.1 Procedure.....	28
3.4.2 The effect of pH on decolourization efficiency of MB.....	31
3.4.3 The effect of solution conductivity on decolourization efficiency of MB.....	31

3.4.4	The effect of MB volume on the degradation efficiency.....	31
3.4.5	The effect of air flow rate on MB decolourization efficiency	32
3.4.6	The effect of NaCl electrolyte on MB decolourization efficiency.....	32
3.4.7	The effect of electrical parameters: Applied voltage on decolourization efficiency of MB.....	32
3.4.8	The effect of electrode type on MB percentage removal.....	32
3.4.9	Optimization of the diameter of the electrode	33
3.4.10	Procedure of the EHD performed at optimal conditions	33
3.5	QUANTIFICATION OF ACTIVE SPECIES AT OPTIMUM CONDITIONS IN THE BULK SOLUTION	33
3.5.1	Quantification of H ₂ O ₂	33
3.5.2	Detection of ozone in the liquid phase.....	34
3.6	PRELIMINARY EXPERIMENTS ON REAL TEXTILE WATER.....	34
3.6.1	Experimental set-up	35
3.6.2	Electrohydraulic discharge treatment	35
3.7	MATERIALS AND PREPARATION FOR SUPPORTED TiO ₂ PHOTOCATALYSTS	35
3.7.1	Coating the 250 mm ² stainless steel mesh support with the 8% PAN/DMF/TiO ₂ sol gel solution	36
3.7.2	Characterization of supported TiO ₂ materials	36
3.8	DISINFECTION OF BACTERIAL USING DIELECTRIC BARRIER DISCHARGE.....	37
3.8.1	Preparation of <i>E. coli</i>	37
3.8.2	Experiment performed with blank solution of <i>E. coli</i>	37
3.8.3	Disinfection of <i>E. coli</i> using Dielectric barrier discharge.....	38
	3.8.3.1 DBD experimental procedure	38
	3.8.3.2 Procedure for <i>E. coli</i> inactivation.....	38
CHAPTER 4: RESULTS AND DISCUSSION		39
4.1	INTRODUCTION	39
4.2	EFFECT OF AIR GAP BETWEEN THE OUTER AND INNER TUBES OF THE EHD.....	39
4.3	CALCULATION OF DECOLOURIZATION EFFICIENCY USING INITIAL AND FINAL METHYLENE BLUE CONCENTRATIONS	42
4.4	RATE OF DEGRADATION.....	44
4.4.1	The effect of pH on decolourization efficiency of Methylene	45
4.4.2	The effect of conductivity on percentage MB colour removal.....	46
4.4.3	Effect of initial concentration on MB decolourization BY EHD.....	49
4.4.4	Quantification and detection of free reactive species	55
4.4.5	Effect of time on MB decolourization efficiency	57
4.5	ULTRA VIOLET – VISIBLE SPECTROSCOPY (UV-VIS).....	60
4.6	FT-IR SPECTRUM OF DEIONISED WATER AND MB SAMPLES	62
4.6.1	Quantitative parameters of MB degradation.....	64
4.7	DECOLOURIZATION EFFICIENCY OF MB AT NORMAL AND OPTIMUM CONDITIONS.....	66
4.8	PRELIMINARY RESULTS FOR TREATMENT OF A REAL TEXTILE EFFLUENT WITH EHD.....	68

4.9	REDESIGN OF THE EHD REACTOR.....	70
4.9.1	Materials of reactor construction.....	71
4.9.2	Results for optimization of supported TiO ₂ photocatalysts.....	72
4.10	DISINFECTION OF <i>E. COLI</i> BY DIELECTRIC BARRIER DISCHARGE.....	81
4.10.1	Simulation of <i>E. coli</i> solution by stirring with a magnetic stirrer within 60 minutes at room temperature.....	81
4.10.2	Inactivation of <i>E. coli</i> by dielectric barrier discharge system	82
CHAPTER 5: CONCLUSIONS AND RECOMMENDATIONS		85
5.1	CONCLUSIONS.....	85
5.2	RECOMMENDATIONS.....	90
REFERENCES		91
APPENDIX A: Multiple unit EHD reactor		99

LIST OF FIGURES

Figure 2.1: Different configurations for the initiation of streamer discharges in water. [A] Point plane geometry for liquid phase corona discharges. [B] Point-plane geometry for glow discharge initiation in the gas plenum above the water. [C] Hybrid geometry (Gupta, 2007).....	8
Figure 2.2: Schematic of the modified corona reactor for microbiological studies (Gupta, 2007).....	9
Figure 2.3: Double planar dielectric electrode configuration, (Lopez, 2008):.....	10
Figure 2.4: Single planar dielectric electrode configuration, (Lopez,	10
Figure 2.5: Cylindrical single dielectric electrode arrangement (Source: Nehra et al., 2008).....	11
Figure 2.6: Cylindrical double dielectric electrode arrangement, (Source: Nehra et al., 2008).....	11
Figure 2.7: Common dielectric barrier discharge configurations with one or two dielectric barriers (Kogelschatz et al., 2003).....	12
Figure 2.8: Single dielectric barrier discharge experimental setup for the treatment of endosulfan in aqueous medium (Reddy et al., 2014)	16
Figure 2.9: Cylindrical double DBD experimental setup (Source: Rong et al., 2014).	18
Figure 2.10: Scheme showing some photochemical and photophysical events that might take place on an irradiated semiconductor particle (Source: Chong et al., 2010).	20
Figure 3.1: Cuvettes pieces used in UV-vis analysis of samples.....	23
Figure 3.2: UV/Vis spectroscopy set up	24
Figure 3.3: Calibration curve of absorbance vs. concentrations of methylene blue at t = 0 minute.....	25
Figure 3.4: Actual DBD electrode/reactor arrangement.	27
Figure 3.5: Electro hydraulic experimental set up	28
Figure 3.6: Schematic representation of the DBD reactor (tube)1 (air gap =2 mm)	29
Figure 3.7: Schematic representation of the DBD reactor (tube) 2(air gap =4 mm)	30
Figure 3.8: Schematic representation of the DBD reactor (tube) 3(air gap =6 mm)	30
Figure 4.1: Effect of reactor configurations on MB degradation percentage. Varied parameters applied: air gap, [from 2 mm (R1), 4 mm (R2) and 6 mm (R3)]. Fixed parameters: MB concentration 5 mg/L, solution pH (various), air flow rate of 3 L/min, dye volume 1500 mL.....	41
Figure 4.2: Decolourization efficiency (%) of MB of different starting concentrations vs. time	43
Figure 4.3: Decolourization efficiency vs. concentration of MB.....	43
Figure 4.4: The influence of time and concentration on the reaction rate of methylene blue.	44

Figure 4.5: Effect of pH on decolourization efficiency of MB (experimental conditions: Applied voltage 25 V, Peak voltage 7.8 kV, air flow rate 3 L/min, air gap 2 mm, 0.5 mm silver electrode, 50 g/L of NaCl and running time 60 minutes)	45
Figure 4.6: Effect of optimum pH on the decolourization efficiency of MB (experimental conditions: Applied voltage 25 V, Peak voltage 7.8 kV, air flow rate 3 L/min, 0.5 mm silver electrode, 50 g/L of NaCl and running time 20 minutes)	46
Figure 4.7: Electrical conductivity vs. time during degradation of methylene blue using electrohydraulic discharge (experimental conditions: applied voltage 25 V, peak voltage 7.8 kV, air flow rate 3 L/min, air gap 2 mm, MB concentration 5 mg/L, solution, pH 6, 50	47
Figure 4.8: Effect of optimum electrical conductivity on degradation of methylene blue using electrohydraulic discharge (experimental conditions: applied voltage 25 V, peak voltage 7.8 kV, air flow rate 3 L/min, air gap 2 mm, MB concentration 5 mg/L, solution, pH 6	47
Figure 4.9: Effect of methylene blue volume on the degradation efficiency (experimental conditions: Voltage 25 V, peak voltage 8 kV, air flow rate of 3 L/min, air gap 2 mm, pH 6, MB concentration of 5 mg/L, 50 g/L NaCl electrolyte, silver electrode and running time 60 minutes)	49
Figure 4.10: MB solutions obtained within 60 minutes at concentrations from: 0.5 to 5 mg/L (a) and above 5 mg/L (b, c, d, e and f) at the following experimental conditions: solution pH 6, air flow rate 3 L/min, air gap 2 mm, dye volume 1500 mL, 50 g/L NaCl electrolyte and silver	51
Figure 4.11: Effect of air flow rate on the degradation efficiency (experimental conditions: applied voltage 25V, peak voltage 7.8 kV, MB concentration 5 mg/L, solution pH 6, MB volume 1500 mL, 50 g/L NaCl electrolyte, air gap 2 mm, silver electrode and running time 60 minutes	52
Figure 4.12: Effect of electrolyte on decolourization efficiency (experimental conditions: applied voltage 25V, peak voltage 7.8 kV, MB concentration 5 mg/L, solution pH 6, air gap 2 mm, air flow rate 3 L/min, MB volume 1500 mL, silver electrode and running time 60	53
Figure 4.13: Effect of applied voltage on the degradation efficiency (experimental conditions: MB concentration 5 mg/L, solution pH 6, air gap 2 mm, air flow rate 3 L/min, dye volume 1500 mL, 50 g/L NaCl electrolyte, silver electrode and running time 60 minutes)	53
Figure 4.14: Effect of electrode type on decolourization efficiency (experimental conditions: MB concentration 5 mg/L, solution pH 6, applied voltage 25 V, peak voltage 7.8 kV, air flow rate 3 L/min, dye volume 1500 ml, 50 g/L NaCl electrolyte and running time 60 min	54
Figure 4.15: Effect of silver electrode size on the decolourization percentage of MB solution (experimental conditions: MB concentration 5 mg/L, solution pH 6, dye volume 1500 mL, applied voltage 25, peak voltage 7.8 kV, air gap 2 mm, air flow rate of 3 L/min, 50 g/L.....	55
Figure 4.16: Evolution of hydrogen peroxide and ozone concentrations with time (experimental conditions: MB concentration 5 mg/L, solution pH 6, dye volume 1500 mL, applied voltage 25, peak voltage 7.8 kV, air flow rate of 3 L/min, air gap 2 mm, 50 g/L NaCl electrolyte, 0.5 mm silver electrode	56

Figure 4.17: Effect of time and concentration on MB decolourization efficiency at the following experimental conditions: applied voltage 25 V, Peak voltage 7.8 kV, pH (various), air flow rate 3 L/min, air gap 2 mm, MB volume 1500 mL, 50 g/L NaCl electrolyte and 0.5 mm silver electrode	59
Figure 4.18: Methylene blue structure	60
Figure 4.19: Ultra violet – Visible Spectra of untreated and treated MB solutions at different times at the following experimental conditions: applied voltage 25 V, Peak voltage 7.8 kV, pH (various), air gap 2 mm, air flow rate 3 L/min, MB volume 1500 mL, 50 g/L NaCl electrolyte.	60
Figure 4.20: Intensity Vs time of MB degradation showing progressive degradation of MB over time (using UV-vis data)	61
Figure 4.21: FTIR Spectra of deionised water, deionised water + MB and that of treated MB solution	62
Figure 4.22: Pathway of MB decomposition (Houas et al., 2001).....	65
Figure 4.23: Decolourization efficiency of MB at normal and optimum conditions.....	68
Figure 4.24: New constructed EHD reactor.....	70
Figure 4.25: Isometric wireframe view of reaction vessel.....	71
Figure 4.26: Front and left hand wireframe view of reaction vessel.....	71
Figure 4.27: New power supply and AC convertor to drive the EHD reactor	72
Figure 4.28: Mass percentage of immobilised TiO ₂ obtained by various decomposition temperatures and holding times using the 8% PAN/DMF/TiO ₂ sol gel solution coating method.....	73
Figure 4.29: XRD pattern of 8% (PAN/DMF/TiO ₂) decomposed TiO ₂ at 50°C/min and different holding temperatures for 2 h: Samples (TT4.1B), (TT4.2B), (TT4.3B) and (TT4.4B).....	74
Figure 4.30: HRSEM micrographs of 8% (PAN/DMF/TiO ₂) sol gel solution coated stainless steel mesh calcined at 300 °C with the heating rate of 50 °C/min and different times, where [A] = 1 h, [B] = 2 h, [C] = 3 h, [D] = 4 h, [E] = 5 h and [F] = 6 h.	75
Figure 4.31: (TT4.2) 8% (PAN/DMF/TiO ₂) sol gel solution coated stainless steel mesh calcined at 400°C with heating rate of 50 °C/min and holding times of [A] = 1 h, [B] = 2 h, [C] = 3 h and [D] = 4 h.....	76
Figure 4.32: 8% (PAN/DMF/TiO ₂) sol gel solution coated stainless steel mesh was calcined at 500 °C with heating rate of 50 °C/min and holding times were [A] = 1 h, [B] = 2 h, [C] = 3 h and [D] = 4 h.....	77
Figure 4.33: HRSEM of samples made with 8% (PAN/DMF/TiO ₂) sol gel solution coated on stainless steel mesh calcined at 600 °C with heating rate of 50 °C/min and holding times [A] = 1 h, [B] = 2 h, [C] = 3 h and [D] = 4 h.	78
Figure 4.34: HRTEM image for the TiO ₂ nanocrystals (TT4.2) formed after decomposing by heating at 50°C/min and holding at: 400°C for 2 h, B = SAED pattern of 400°C for 2 h.....	79
Figure 4.35: FTIR of sample (TT4.2) prepared at 400 °C for 2 h	79

Figure 4.36: Degradation of MB for 30, 60 and 90 min using the carbonized supported TiO₂ nanocrystals prepared by heating at 50°C/min to 400°C for 1 h, 2 h, 3 h or 4 h (TT4.2) 80

Figure 4.37: Evolution of *E. coli* optical density recorded within 60 minutes at room temperature and stirring speed of 50 rpm..... 82

Figure 4.38: Effect of DBD reactor on *E. coli* sterilization. Experimental conditions (Applied voltage 25 V, peak voltage 7.8 kV, *E. coli* volume 1500 mL, NaCl electrolyte concentration 50 g/L, 1.5 mm silver electrode, treatment time 60 minutes)..... 83

LIST OF TABLES

Table 2.1: Classification of plasma.....	5
Table 2.2: Plasma properties of atmospheric discharge schemes Nehra et al. (2008)	6
Table 3.1: Standard concentrations vs Absorbance.....	24
Table 3.2: Inner and outer tube dimensions of reactors 1, 2 and 3.....	29
Table 3.3: Experimental conditions for each synthesis	36
Table 4.1: Absorbance of MB solution sampled within 60 minutes	39
Table 4.2: Degradation efficiencies of MB at different concentrations (increment 10 mg/L).....	42
Table 4.3: Rate of decolourization of MB solution from 10 to 50 mg/L at increment 10	44
Table 4.4: Absorbance of samples withdrawn every 10 minutes within 60 minutes at MB concentration ranging from 0.5 to 10 mg/L at the following EHD experimental conditions: applied voltage 25 V, Peak voltage 7.8 kV, pH (various), air gap 2 mm, air flow rate 3 L/min,	50
Table 4.5: Concentrations of H ₂ O ₂ and O ₃ estimated using de Beer's law at the following experimental conditions: applied voltage 25 V, Peak voltage 7.8 kV, air flow rate 3 L/min, air gap 2 mm, MB volume 1500 mL, 50 g/L NaCl electrolyte and 0.5 mm silver electrode.....	55
Table 4.6: Decolourization efficiency of samples withdrawn every 10 minutes within 60 minutes at concentration ranging from 0.5 to 10 mg/L with increment 0.5 (experimental conditions: applied voltage 25 V, Peak voltage 7.8 kV, pH (various), air flow rate 3 L/min, air gap 2 mm, 0.5 mm silver electrode.....	58
Table 4.7: Ecological parameters of untreated and treated MB solution	64
Table 4.8: EHD experiment at normal conditions (Applied voltage 25 V, peak voltage 7.8 kV, [MB] = 5 mg/L, V= 1500 mL, air flow rate 3 L/min, 0.5 mm silver electrode, 50 g/L NaCl electrolyte, air gap 2 mm and running time of 60 minutes)	67
Table 4.9: EHD experiment at optimum conditions (Applied voltage 25 V, peak voltage 7.8 kV, [MB] = 5 mg/L, V= 1500 mL, air flow rate 3 L/min, 1.5 mm silver electrode, 50 g/L NaCl electrolyte, air gap 2 mm and running time of 60 minutes)	67
Table 4.10: COD, TOC and pH value before and after flocculation/EHD treatment	69
Table 4.11: Optical density/absorbance of <i>E. coli</i> recorded within 60 minutes at room temperature and a stirring speed of 50 rpm	82
Table 4.12: Absorbance/optical density of <i>E. coli</i> solution sampled within 60 minutes of DBD experiment at room temperature. Experimental conditions (Applied voltage 25 V, peak voltage 7.8 kV, <i>E. coli</i> volume 1500 mL, NaCl electrolyte concentration 50 g/L, 1.5 mm silver	83

ACRONYMS & ABBREVIATIONS

AC	Alternating current
AP	Atmospheric pressure
APPJ	atmospheric pressure plasma jet
AR88	Acid Red 88
BOD	Biochemical Oxygen Demand
COD	Chemical Oxygen Demand
DBD	Dielectric Barrier Discharge
DBP	Disinfection By-Products
DC	Direct Current
DMF	N, N-Dimethylformamide
DRS	Diffuse Reflectance Spectroscopy
<i>E. coli</i>	<i>Escherichia coli</i>
EC	Electrical Conductivity
EHD	Electrohydraulic Discharge
FE-DBD	Floating-Electrode Dielectric-Barrier Discharge
FTIR	Fourier Transform Infrared Spectrometer
HRFEGSEM	High Resolution Field Emission Gun Scanning Electron Microscope
HRSEM	High Resolution Scanning Electron Microscope
HRTEM	High-Resolution Transmission Electron Microscopy
MB	Methylene Blue
MHCD	Micro Hollow Cathode Discharge
NTP	Non-Thermal Atmospheric Plasma
PAN	Polyacrylonitrile
ROS	Reactive Oxygen Species
SAED	Selected Area Electron Diffraction
SEM	Scanning Electron Microscope
TDS	Total Dissolved Solids
TEM	Transmission Electron Microscopy
TOC	Total Organic Carbon
TSS	Total Suspended Solids
UV-Vis	Ultraviolet-Visible Spectroscopy
XPS	X-Ray Photoelectron Spectrometer
XRD	X-Ray Diffraction Spectrometer

CHAPTER 1: BACKGROUND

1.1 INTRODUCTION

The global demand for fresh and clean water keeps increasing on a daily basis. This is due to geometrical population growth coupled with high industrial expansion. Aside from this, the quantity of wastewater generated through anthropogenic activities has doubled recently. This has put pressure on the limited available clean water in water stressed countries. In order to have sustainable water resources, there is a need to treat, re-use and recycle wastewater. Wastewater treatment is a complex process due to composition of different constituents such as heavy metals, micropollutants, inorganic pollutants and high concentrations of dissolved organic dyes.

Conventional wastewater treatment facilities have long been employed as method to remove physical, chemical and biological contaminants that pose a threat to human health and the environment. However, the effectiveness of these treatment techniques has become a source of worry in the last few years. For instance, biological treatments such as aerobic and anaerobic categories cannot completely mineralise biologically recalcitrant toxic organic pollutants into innocuous substances due to chemical resistance to biological degradation. Other treatment methods such as coagulation/flocculation or activated carbon adsorption only change the pollutants phases without necessarily removing or degrading them completely (Gultekin and Ince, 2007; Tsai et al., 2009). Precipitation methods also produce sludge/flocs upon the addition of polymer coagulators or inorganic coagulants. Other methods such as reverse osmosis, nanomembrane, sedimentation and filtration are costly, and generate toxic by-products which need safe storage (Gaya and Abdullah, 2008). Shortcomings of the filtration techniques include filter fouling as well as disposal of concentrated retentate that requires more energy, time and extra costs to dispose safely. Chlorination technology, which is widely used for disinfection purposes, often accumulates disinfection by-products, that are mutagenic and carcinogenic affecting public health (Yang and Cheng, 2007; Lu et al., 2009; Chong et al., 2010). This means that no single conventional method manages to remove or treat all contaminants in drinking water. A combination of treatment processes that will augment the conventional method is required to effectively treat water.

Advanced oxidation technologies involving the use of corona discharge was recognized as one of the best alternatives to treat wastewater. The application of non-thermal plasmas in water has been studied for two decades because of its practical applications in drinking water and wastewater treatment, as well as, potentially, in environmentally benign chemical processes (Krause et al., 2009; Zhang et al., 2013; Jiang et al., 2014). Ever since then, several laboratory studies and review articles by different research groups have indeed focussed on the applications of electrical energy to water treatment (Locke et al., 2006; Malik, 2010; Bruggeman and Locke, 2013; Jiang et al., 2014) . There are different categories of electrical discharge systems for water treatment depending on the relative magnitude of applied energy in the system. The

efficiency or reactivity of the plasma generation systems vary with respect to reactor configuration, energy yield, and furthermore depend on the input energy, liquid properties and excitation voltage (Malik, 2010; Jiang et al., 2014). Electrohydraulic discharge involves passage of high energy electron voltage through electrodes immersed in polluted water to produce plasma. The plasma has strong oxidizing impacts on the pollutants and that makes the technique more unique than conventional wastewater treatment technologies, since contaminants are degraded, not just moved from one phase to another. Plasma processes are extensively applied to generate ozone, hydrogen peroxide, and ultraviolet (UV) in wastewater treatment applications (Bruggeman and Locke, 2013). The combination of generated reactive species has been reported to degrade biological and chemical pollutants in water. The process is considered highly efficient with greater energy saving, high speed, use of few or no expensive chemicals and non-destructive impacts upon the ecosystem.

Despite all these advantages, the most challenging task is the optimization of the electrohydraulic discharge system. Apart from this, detection and quantification of free reactive species is also difficult due to the short-lived nature of the species. Therefore, this report encompasses the results obtained from the optimization studies and free reactive species detection and quantification.

1.2 PROJECT AIMS

This project was designed to achieve the following aims:

- To generate plasma directly in water which will produce radicals from water ionisation
- Optimisation of the reactor configuration using copper wire electrodes, and then replacement of the initial conventional electrodes and study synergetic effects of advanced oxidation processes (AOP) on water treatment
- Identify and quantify the cocktail of chemicals species production, such as OH radicals, ozone and hydrogen peroxide which can target and attack the pollutants in the water without adding chemicals
The integration of innovations in nanophotocatalysts in the proposed electrohydraulic system to maximally utilize the UV radiation produced in the reactor
- To design and construct a new reactor system based on corona discharge principals using multiple electrodes to avoid corrosion on electrohydraulic mode, which will promote chemical oxidation reactions in the liquid phase, and produce a cocktail of oxidants.
- Copper electrodes will be replaced with arrays of nanowires either as free form structures or embedded in a polymer matrix. It is envisaged that the nanostructured electrodes may reduce the total power consumption of the system, or improve the energy efficiency of the discharges
- Microbial confirmation of destruction of indicator organisms such as pathogenic organisms, parasites and viruses, comparison to SANS241

1.3 SCOPE AND LIMITATIONS

The replacement of copper electrodes with arrays of nanowires could not be wholly achieved because preliminary experiments showed that nanowires embedded in polymer matrix decomposed due to free radical attack, and as such the EHD system needs a dielectric material such as quartz. Instead, other metal electrodes such as silver electrodes were tested. Adhesion to quartz of either TiO₂ nanocrystals or metal nanowires has not been successful yet thus is not reported although various studies have been performed. With regards to the inactivation of microorganisms by the EHD system, only *E. coli* was used as a model microbial contaminant.

CHAPTER 2: LITERATURE REVIEW

2.1 INTRODUCTION

It is important to highlight that water is not only an economical factor but also a significant sanitation parameter in social life. Healthy and prosperous life requires the use of safe water supply which is unfortunately not equally accessible around the globe. The growth of human activities has exposed communities to chemical, microbial and biological pollutants as well as to micro pollutants resulting from chemistry-related industry, common household or agricultural applications. Pollution control and prevention requires innovative, cost effective and resourceful methods for environmental protection and effluent discharge into the environment which could affect human health, natural resources and the biosphere, (Huang et al., 1993; Legrini et al., 1993). To solve pollution problems, various conventional techniques of treating contaminated waters have been developed. These include chlorination, wet oxidation and electrical discharges, etc. Conventional treatment methods have proven to exhibit a complete operational efficacy but the amount of toxins in waters is problematic. Recently, a new generation of procedures for water/wastewater treatment has been established and proved to be potent not only in degradation of organic pollutants but in their total mineralization as well. These new techniques are termed advanced oxidation processes (AOPs). This chapter therefore gives a review of advanced oxidation technology used for wastewater treatment, physical and chemical characteristics of plasma and the degradation of organic pollutants from water/wastewater using EHD as a typical advanced oxidation process.

2.2 PLASMA TECHNOLOGY

Plasma is often categorised as the fourth state of matter besides solid, liquid and gas that are commonly known (Kaunas, 2012). Plasmas are generally ionized gases that consist of electrons, positive and negative ions and neutral species (Kaunas, 2012). These gases either ionise completely (100%) or are somewhat ionised (with low values between 10^{-4} - 10^{-6}). Moreover, Sturrock (1994) identified two other groups of plasmas such as low temperature plasmas ($\leq 50\ 000$ K), and high-temperature or fusion plasmas ($50\ 000$ - 10^6 K). Nehra et al. (2008) equally classified plasmas into two categories. The first category is the one in which the active species (electrons, ions and neutrals) have the same temperature and is usually referred to as thermal equilibrium plasmas, in the case of fusion plasma ($T_e \approx T_i \approx T_n > 10^6$ K). Whereas in the second category known as non-thermal/equilibrium plasma, the aforementioned species have different temperatures in such a way that electrons are considered to have a higher temperature (10,000-50,000 K) than that of heavy ions and neutrals, hence ($T_e \gg T_i$, with $T_i \approx T_n$). Furthermore, the authors emphasised that plasma can be classified based on pressure. Based on this, Kaunas wrote that the gas discharge plasmas can be classified into local thermodynamic equilibrium (LTE) and non-LTE plasmas. As for LTE plasma, the high pressure induces many collisions in the plasma and therefore leads to a significant energy interchange between the plasma species. On the other hand, the low gas pressure in non-LTE plasma leads to few

collisions and hence different temperatures of plasma species due to poor energy exchange. As earlier mentioned, in equilibrium plasma, electron temperature (T_e) is generally equal to ion temperature (T_i) or thermodynamic gas temperature (T_g). However, in non-equilibrium plasma, (T_e) largely exceeds (T_g) and the temperature of heavy particles. Kauna (2012) also stated that in non-equilibrium plasma, the electron density (n_e) is often reasonable in the bulk region of plasma and becomes significant toward the centre of the dense volume. Based on this background information the plasma concepts are briefly summarised and presented in Table 2.1.

Table 2.1: Classification of plasma

<i>Plasma</i>	<i>State</i>	<i>Example</i>
Low temperature plasma		
Thermal plasma (Quasi-equilibrium plasma)	$T_e \approx T_i \approx T_g \leq 2 \times 10^4 K$ $n_e \geq 10^{20} m^{-3}$	Arc plasma, plasma torches, RF inductively coupled discharges
Non-Thermal plasma (Non-equilibrium plasma)	$T_e \gg T_i \approx T_g = 300 \dots 10^3 K$ $n_e \approx 10^{10} m^{-3}$	Glow, corona, direct barrier discharge, atmospheric pressure plasma jets, hollow cathode discharges, electron beams, microwave and etc.

(Source: Kaunas, 2012)

A few years ago, Nehra et al. (2008) argued that low pressure discharge plasmas play a significant role in fundamental research, microelectronic industry and material technology. The use of air to generate these plasmas in numerous configurations makes these technologies extremely expensive and time consuming. Apart from this, the amount of their corresponding activated particles is small. Therefore there is an urgent need to develop new plasma sources which could maintain the properties constant and operate unchangeably at atmospheric pressure. Non-thermal plasma (NTP) generated at 1 atm presents operational and economic advantages which have led to the development of multiple plasma sources that have been employed in industry. Based on these claims, great attention has been attributed to NTPs due to their substantial industrial advantages compared to low-pressure discharge. A decade ago, Mark et al. (2001) reported that non-thermal atmospheric plasma offers a number of advantages for environmental control and protection such as dry cleaning operations as well as processing of chemical waste streams. Apart from these advantages of NTP highlighted by Mark and colleagues, Nehra et al. (2008) recalled that non-thermal atmospheric plasma may be obtained by a variety of electrical discharges including: micro hollow cathode discharge (MHCD), corona discharge, atmospheric pressure plasma jet (APPJ), one atmospheric uniform glow discharge, dielectric barrier discharge (DBD), plasma needle and gliding arc discharge presenting crucial technological applications.

The common characteristics of these plasma sources based on plasma properties have been summarised by Nehra et al. (2008) and are presented in Table 2.2.

Table 2.2: Plasma properties of atmospheric discharge schemes Nehra et al. (2008)

Parameters	Corona discharge	DBD	APPJ	Atmospheric glow MHCD
Method and type	Sharply pointed electrode	Dielectric barrier cover on electrodes	RF capacitively coupled	DC glow with micro hollow cathode electrode
Excitation	Pulsed DC	AC or RF	RF 13.5 MHz	DC
Pressure (bar)	1 bar	1 bar	760 torr	1 bar
Electron energies, eV	5 variable	1-10	1-2
Electron density, cm ⁻³	10 ⁹ -10 ¹³ variable	~10 ¹² -10 ¹⁵	10 ¹¹ -10 ¹²
Breakdown voltage, kV	10-50	5-25	0.05-0.2
Scalability & flexibility	No	Yes	Yes	Yes
Tmax Temp, T (K)	Room	Average gas temperature (300)	400	2000
Gas	N ₂ + O ₂ + NO + Rare gas/Rare gas halides	Helium, Argon	Rare gas/Rare gas halides

Over the last few years, plasma treatment has widely attracted scientists' attention as an alternative method of cleaning water. This is due to the production of ultra-violet (UV) radiation, shock waves and mostly highly reactive species such as O₃, H₂O₂, ·OH, etc. that oxidize the pollutant and mineralize it into CO₂, H₂O and simpler inorganics. Besides, electrode configurations in the aforementioned electrical discharge reactors also play a crucial role in the treatment of polluted water. In fact most electrode arrangements in these water/wastewater technologies have failed to meet the expectations of significantly cleaning polluted water. Therefore, electrode configuration is a key parameter to differentiate electrical discharges from one another. For instance, several electrode configurations summarised by Gupta, (2007) and presented in Figures 1 and 2 have been explored in corona electrohydraulic discharge reactors. In these configurations, the powered tipped anode is directly in contact with the discharged gas and the polluted liquid. This usually results in electrode etching and corrosion. In addition, in corona discharge active species result from streamers produced at the tip of the conductive anode. This could therefore slow down/limit the production of oxidizing species responsible for the degradation of organics and microbes.

Therefore, the development of a novel reactor configuration with different electrode arrangements is of great importance to overcome the water pollution dilemma. The choice of dielectric barrier discharge (DBD) over corona discharge and other types of electrical discharges lies in plasma properties proposed by Nehra et al. (2008) and presented in Table 2.2. In addition, the presence of one or two dielectric barriers in DBDs facilitates a fair distribution/dispersion of high energetic electrons (charges) on the surface of the whole electrode and therefore increasing micro discharge density along the anode surface. Other than the plasma generated inside the discharge zone, UV, shock waves as well as ozone is produced. In DBD, the charges are dispersed along the anode rod. This increases the yield of reactive species in the DBD reactor which improves the rate of decomposition of the pollutant. Based on these benefits of DBDs, various DBD reactor/electrode configurations have been developed. The most common DBD configurations employed in literature are introduced in the following paragraphs showing the structure and description of the DBD. In Figure 2.2 the reactor was positioned vertically and the dead volume in the chamber was eliminated by a cylindrical Teflon block on the bottom and an oil paraffin layer on the top to avoid electrical breakdown in air.

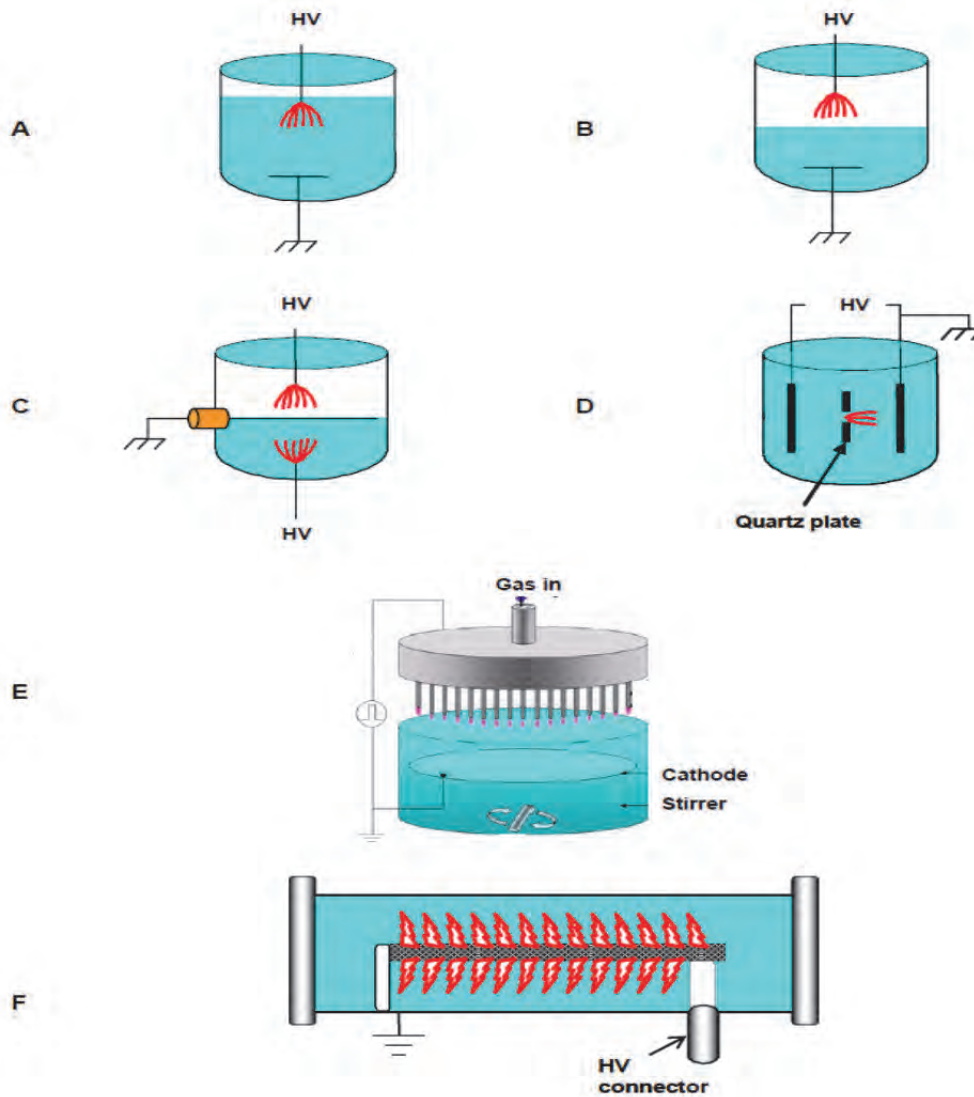


Figure 2.1: Different configurations for the initiation of streamer discharges in water. [A] Point plane geometry for liquid phase corona discharges. [B] Point-plane geometry for glow discharge initiation in the gas plenum above the water. [C] Hybrid geometry (Gupta, 2007)

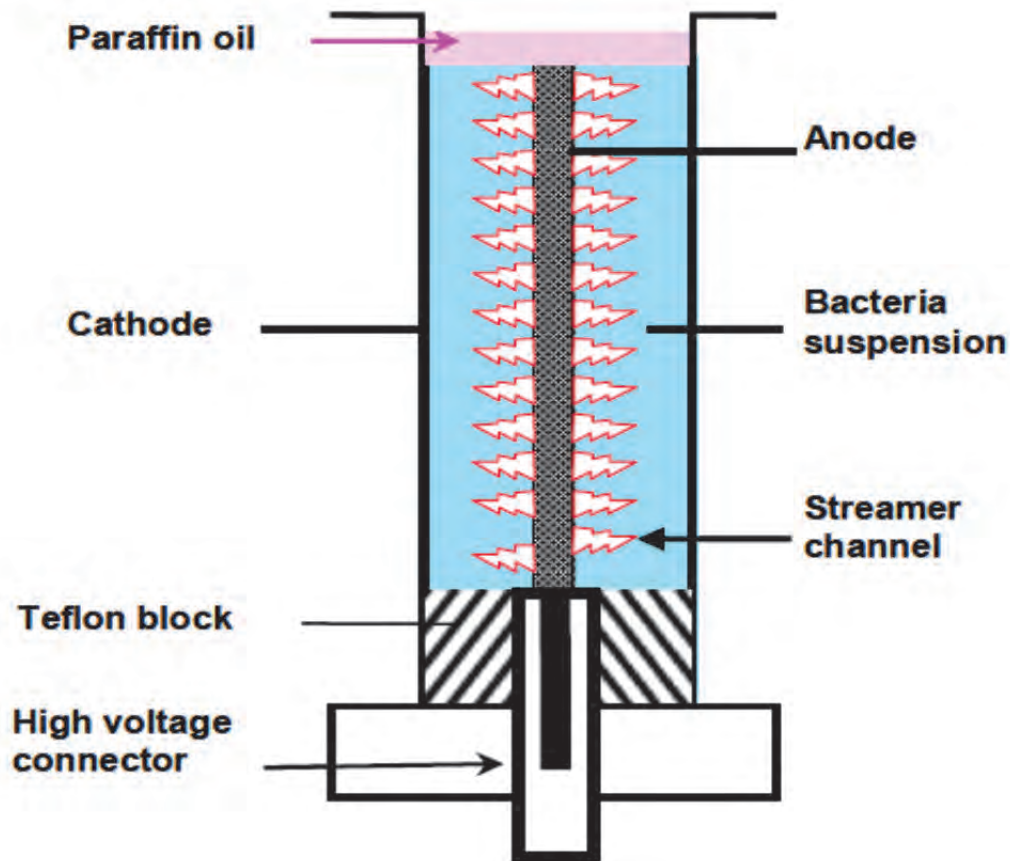


Figure 2.2: Schematic of the modified corona reactor for microbiological studies (Gupta, 2007)

2.3 STRUCTURE AND CHARACTERISTICS OF THE DIELECTRIC BARRIER DISCHARGE

Mark et al. (2001) characterised dielectric barrier discharges (DBDs) as specific and silent AC electrical discharges providing durable thermodynamic, non-equilibrium plasma at reasonable atmospheric temperature and pressure. Based on the discharge properties and the various possibilities in configurations, different DBDs names such as barrier discharge, silent discharge, ac-discharge, normal pressure glow discharge, ozonizer discharge and display discharge are often used to denote DBD (Kaunas, 2012). Their studies highlighted that DBDs are usually formed in configurations consisting of two electrodes (anode and cathode) whereby one or both metal electrodes are normally protected with layers having a high insulating (dielectric) constant such as pyrex, quartz, ceramic, etc., that separates them from a gas layer (single dielectric). Otherwise the dielectric can also be positioned between electrodes to separate two gas layers (double dielectric). Kaunas, (2012) also proved that DBD is a non-equilibrium discharge that can be operated at ambient conditions with the main goal being the long term generation of ozone. In this regard, Nehra et al. (2008) proposed that the difference between a traditional and a DBD discharge relies on the fact that in traditional discharge, electrodes are directly in contact with the discharge gas and plasmas. This consequently leads to premature electrode etching and corrosion during the discharge process. However, in DBDs the electrode (anode and cathode) is separated from the discharge gas by one or more dielectric layers and hence reducing or eliminating electrode etching and corrosion as presented in Figures 2.3 to 2.6.

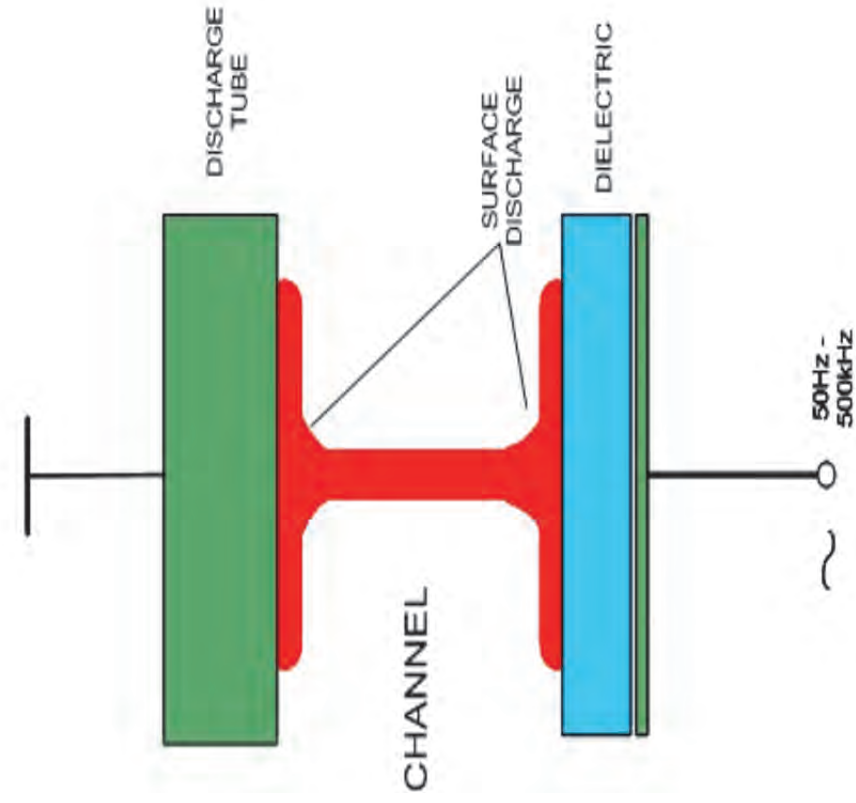


Figure 2.3: Double planar dielectric electrode configuration, (Lopez, 2008):

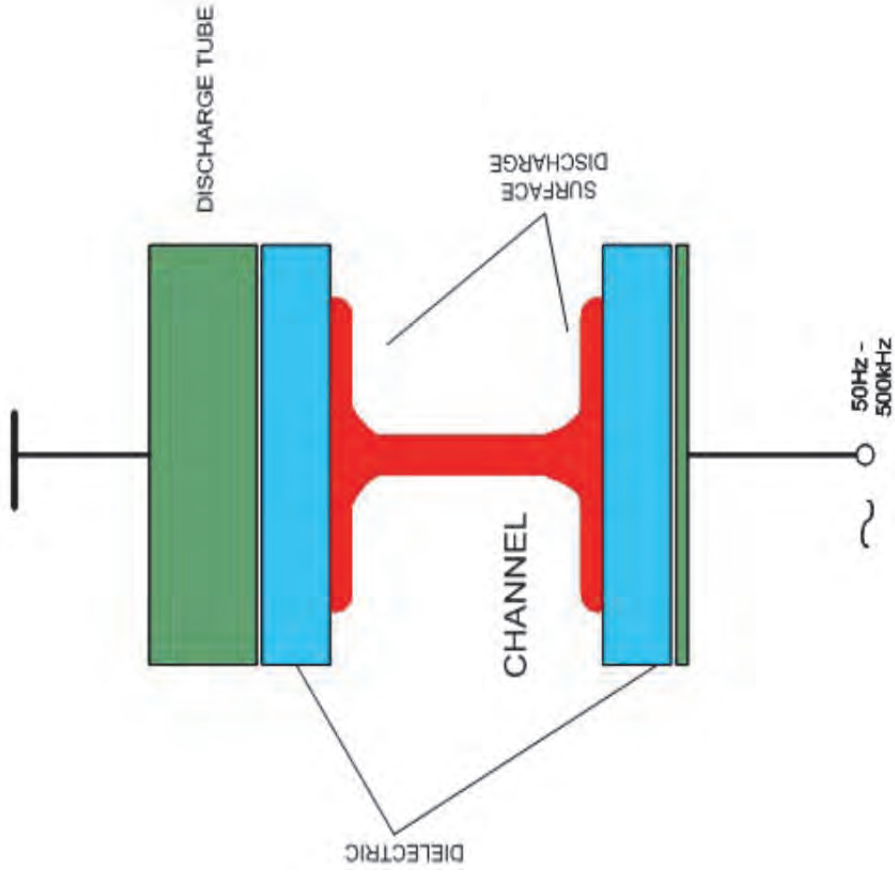


Figure 2.4: Single planar dielectric electrode configuration, (Lopez, 2008)

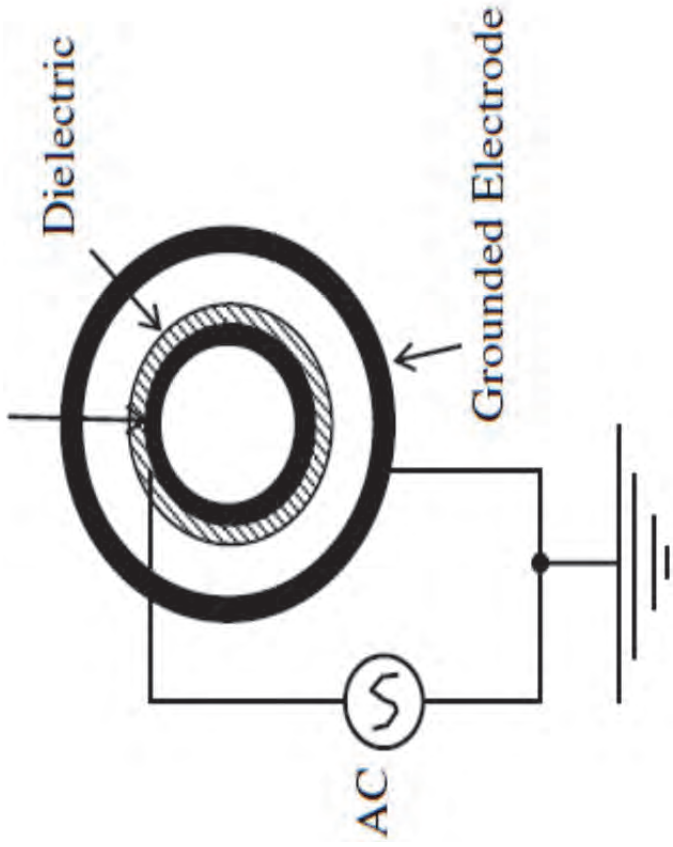


Figure 2.5: Cylindrical single dielectric electrode arrangement (Source: Nehra et al., 2008)

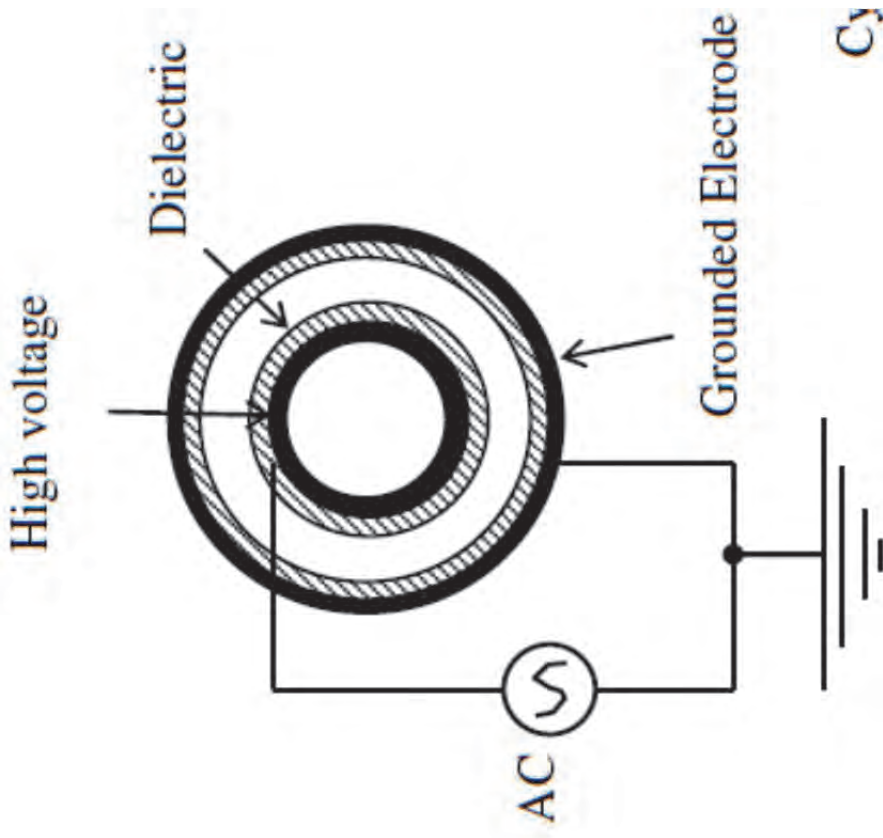


Figure 2.6: Cylindrical double dielectric electrode arrangement, (Source: Nehra et al., 2008)

In addition, glass, quartz, ceramics and polymers are usually used as common dielectric materials. The distance between electrodes (gap) varies noticeably from a few millimetres to several centimetres. Furthermore Lopez (2008) and Kaunas (2012) recalled that the dielectric limits the amount of charges transported by a single micro discharge (micro plasma) over the entire electrode surface area. Furthermore, Konelschatz et al. (1997) claimed that non-equilibrium plasma conditions of DBD are presented in a simpler way compared to those of other types of discharges such as electron beam, low pressure discharges and pulsed high pressure corona discharges. This aspect therefore gives DBD a possibility of being scaled up from the laboratory scale to industrial conditions. According to Lopez (2008) and Nehra et al. (2008), DBD cannot be performed using direct current (DC) but can be operated at high voltage alternating current (AC) due to the capacitive coupling of dielectric which requires an alternating voltage to drive a displacement current.

A decade ago, Kogelschatz et al. (2003) demonstrated that ionization of the discharged gas, also called breakdown, occurs in the region between the two electrodes in a DBD reactor at a sufficient high voltage. In this process, the charges accumulated on the surface of the dielectric layer discharge somewhere else on the exterior of the insulator. Hence, plasma generation is maintained if the continuous energy source delivers a corresponding degree of ionization preventing the recombination route that leads to the destruction of the discharge. During the discharge of the accumulated particles, an energetic photon, whose frequency and energy correspond to the type of gas used is emitted and fills the discharge gap. Kogelschatz and colleagues also showed that numerous configurations can be used to induce DBD. Some of these include parallel plates (planar) separated by a dielectric or cylindrical and coaxial plates with a dielectric tube between them. The common DBD configurations reported in literature are presented in Figure 2.7.

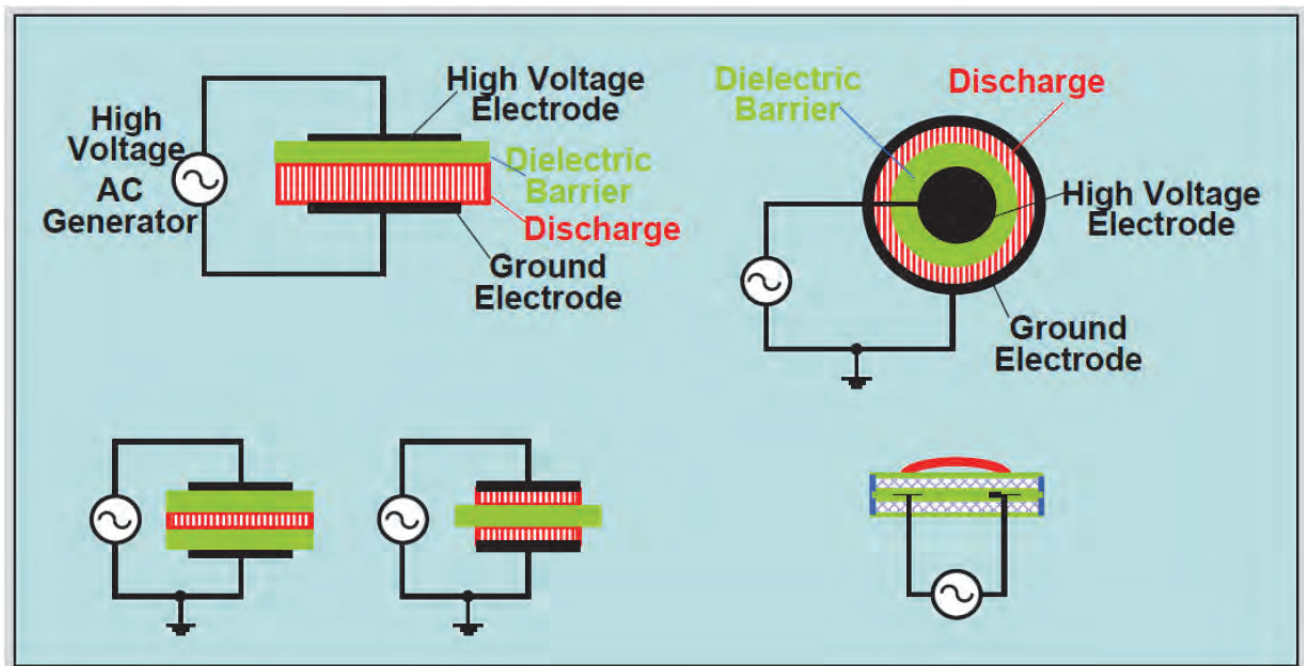


Figure 2.7: Common dielectric barrier discharge configurations with one or two dielectric barriers (Kogelschatz et al., 2003)

Furthermore, Mark and colleagues clarified that the creation of DBDs is characterized by the production of a huge amount of short lifetime micro discharges induced by the continuous current flow in the system. The study also proved that the dielectric barrier conformation supplies a self-ending electrical discharge regardless of the applied voltage wave shape. Their paper also highlighted that in the absence of a barrier/insulator, gas pressures of about one atmosphere and a gas discharge gap of limited millimetres, only a few localized intense arcs would develop in the gas gap between the powered metal electrodes. However, in the presence of the dielectric layer between the conductive electrodes with an AC voltage of about 1-100 kV and a frequency of a few or several Hz, a significant amount of plasma is created by an important number of micro discharges in the gas discharge zone, (Nehra et al., 2008; Mark et al., 2001). Whereby, each micro discharge is regarded as a source of non-thermal plasma characterised by energetic electrons that produce extremely reactive free species in the plasma region. As earlier mentioned, in non-thermal plasma, species such as electrons, ions and neutrals have different temperatures and hence different kinetic energies. Thus in the case of DBD, electrons having the highest energy, initiate the formation of active species such as O₃, H₂O₂ and mostly free radicals including O(1D), O(3P), OH•, and H• from the gaseous feeds such as O₂, air, etc. which free radicals are immediately used to decompose the contaminants.

2.4 WASTEWATER TREATMENT BY DIELECTRIC BARRIER DISCHARGE SYSTEM

Safe drinking water, a very important source for human survival, has become inaccessible in various developing countries (Hernández-Arias et al., 2012). The growth of anthropogenic activities has exposed humans to chemical, microbial and biological pollutants as well as to micro pollutants resulting from chemistry-related industry, common household or agricultural applications (Mastanaiah et al., 2013). The presence of toxins in water portends great danger to human health, natural resources and the biosphere (Huang et al., 1993). Therefore, various conventional techniques for water disinfection such as thermal sterilization, chemical sterilization and irradiation of UV and gamma rays have been developed. In addition to this, dry heat sterilization, pressurized steam sterilization, boiling, chlorine dioxide, bromine chloride, ethylene oxide (EO), formaldehyde, ozone, ultraviolet light, and ultrasonic have been widely used in water treatment technologies (Chen et al., 2009; Sato et al., 2008; Zhang et al., 2006). However, for the past few years, plasma based technologies have gained much attention for biological sterilization and have been widely applied in water treatment compared to conventional methods. According to Yue et al. (2008), this is due to the fact that conventional water disinfection and sterilization methods exhibit some drawbacks. For example, it was reported that UV and gamma irradiations generate energetic photons which can potentially destroy DNA and are hence extremely harmful to the human body. In addition to this, conventional sterilization methods are operated in closed systems and the sterilization process takes time to complete.

Furthermore, Yue et al. (2008) emphasised that some polymer based instruments such as endoscopes which are costly, are degraded by UV light. Some of the chemical substances such as ethylene oxide, or formaldehyde used in the disinfection process are not only toxic to humans but also pollute the environment. Moreover, chlorination for instance, which is considered as one of the traditional water treatment disinfection approaches, has been used worldwide and appears as an effective disinfectant against a large number of

enteric bacteria. However, Koivunen and Heinonen-Tanski (2005) reported that the use of chlorination has declined due to toxic, mutagenic and/or carcinogenic disinfection by-products (DBP) and chlorine residuals formed during the disinfection process. Hence, its use is being limited. Nevertheless, Hernández-Arias and colleagues (2012) mentioned that implementation of various water treatment techniques has shown a significant impact upon severe health hazards responsible for waterborne diseases. A few years later, Fisher et al. (2008) stated that numerous wastewater technologies for bacteria inactivation in aqueous medium are being developed without the use of hazardous chemicals. Advanced oxidation processes have attracted great attention in the removal of organic contaminants from water and waste water streams. Yet the scale up of these technologies has been a great challenge due to the cost and insufficient information about the composition of effluents (Gilmour 2012). The inactivation of microorganisms by gas plasma, especially dielectric barrier discharge is being noted by many researchers. In that regard, Suresh et al. (2011) proved that non-thermal atmospheric pressure plasma such as dielectric barrier discharge (DBD) also called silent or cold plasma, is being widely studied as a disinfection technique in Biology and Medicine. The effectiveness of DBD as a suitable sterilization technique was proved by Joshi et al. (2010). In their study, Joshi et al. (2010) showed that bacteria such as *Escherichia coli*, *Staphylococcus aureus*, and methicillin-resistant *Staphylococcus aureus* taken in both their planktonic form and in biofilms were quickly inactivated by non-thermal DBD plasma using a floating-electrode technique. Indeed, the huge amount of charged particles, reactive oxygen species and the UV produced in the plasma process significantly damages the bacteria cell and hence induces inactivation or mutation of the microorganism (Chen et al., 2009; Sato et al., 2008; Zhang et al., 2006).

The study performed by Paunikar and co-workers in 2014 also highlighted that protein denaturalization, enzyme deactivation and DNA mutation are some biochemical impacts usually observed during inactivation of microorganisms. Their study also indicated that the destruction of the cell membrane of *Escherichia coli* by plasma treatment results in cell lysis. Chen et al. (2009), Sato et al. (2008) and Zhang et al. (2006) independently reported that plasma sterilization of microorganisms such as *Escherichia coli* could be classified into three mechanisms, which include the attachment of hydroxyl radicals to unsaturated fatty acids inducing lipid peroxidation, oxidation of DNA caused by oxygen radical and oxidation of amino acids followed by protein oxidation. However, their paper reported that, up to date, the effect of plasma treatment on bio macromolecules such as cell walls and membranes composed of polysaccharides and membrane-bound proteins remains unclear. In this regards, the cell lysis and death, as well as mutation processes need to be investigated with care in order to understand the impact of plasma on the inactivation of microorganisms. Even though the effect of DBD reactor sterilization has been widely studied on vegetative bacteria, viruses, bacterial spores and protozoan, most of these studies involved the use of *Escherichia coli* (*E. coli*) as a model microorganism (Chen et al., 2009; Sato et al., 2008; Zhang et al., 2006). Suresh et al., (2011) confirmed that *E. coli* is one of the micro-organisms widely explored in laboratory as one of the commonly used Gram-negative bacterial contaminants.

The deactivation of *E. coli* by DBD has been investigated by many researchers. For example, Suresh et al. (2011) investigated the inactivation of *Escherichia coli* which involved the oxidative DNA damage and membrane lipid peroxidation using plasma-induced non-thermal dielectric-barrier discharge. Their study

supported that oxidative stress resulting in membrane lipid peroxidation leads to products triggering different levels of oxidative modifications in the cell. In the study conducted by Suresh and co-workers (2010), atmospheric air was utilized in a floating-electrode dielectric-barrier discharge (FE-DBD) configuration to inactivate contaminants among which *E. coli*. Their study also highlighted that the lipid peroxidation process is mostly initiated by reactive oxygen based species. Therefore, silent plasma (DBD) has gradually been used for surface contaminant inactivation. Similarly, Mastanaiah et al. (2013) utilized DBD to reduce the level of *Geobacillus stearo thermophiles* as well as vegetative bacteria and yeast cells. They report that within 4 minutes and 20 minutes of plasma discharge, the log reduction in the concentration of vegetative bacteria and yeast cell was greater than 6 respectively. This was ascribed to the differences in temperature and acidification value according to the authors. In addition, Pavlovich et al. (2013) investigated the ozonation of *E. coli* in a plane DBD reactor configuration using air as a feeding gas. In their study, reactive species that formed in the solution during plasma treatment were measured. The antimicrobial efficiency of the reactor was assessed by varying parameters such as power densities, treatment time and the composition of the buffer solution. The results of their study showed that the sterilization of *E. coli* was related to ozone concentration. The interpretation of these results suggested that ozone generated during the plasma process was the main oxidizing species responsible for the inactivation of the *E. coli*. After showing that their results correlated with those of previous studies, they demonstrated that the inactivation rates of *E. coli* were significant. In addition, the study proved that based on the low solubility of ozone, the antimicrobial effect of the system was highly dependent of the gas-liquid mixing ability.

Furthermore, the study conducted by Pavlovich and colleagues in 2013 showed that different results on the inactivation of microorganisms by plasma treatment could be obtained. This might be due to the complexity of non-thermal atmospheric plasma, their design and operation modes. Similarly, Choi et al. (2006) analysed the sterilization effect by pulse dielectric barrier discharge. During their study, they confirmed that nearly all categories of bacteria could be sterilized by atmospheric pressure (AP) plasma. This is due to the diversity of highly reactive species, and UV radiations generated during plasma process, thus making it a selective method for cleaning and sterilization. Their study aimed at assessing the germicidal effect of pulsed plasma system in air using dielectric barrier discharge (DBD) as a specific type of reactor configuration. In their study, *E. coli*, *Bacillus subtilis* and *Pseudomonas aeruginosa* bacteria were used as model microorganisms in the sterilization process. The results of their study showed that sterilization percentage of *E. coli*, 99.99% was reached within 70 s and was related to the concentration of ozone that was the dominant germicidal species in the treatment process. From their results, it was concluded that sterilization of bacteria by pulsed DBD system is very effective.

2.5 DEGRADATION OF ORGANIC POLLUTANTS USING DBD PLASMA-AN OVERVIEW

The aforementioned advantages of DBD over the conventional plasma technologies have attracted a wide attention in various studies. Very recently, Reddy et al. (2014) used a cylindrical single dielectric barrier catalytic non-thermal plasma reactor (Figure 2.8) for mineralization of endosulfan in aqueous medium for the treatment of pesticide contaminated water. Indeed, in their study an advanced oxidation process was

developed by combining non-thermal plasma with cerium oxide catalysts for the mineralization of a model pesticide endosulfan from aqueous medium. The single dielectric electrode configuration presented in Figure 2.8 shows that the endosulfan solution was mixed with air in the gas discharge gap and therefore exposed to micro discharge plasmas generated on the inner electrode (first dielectric quartz).

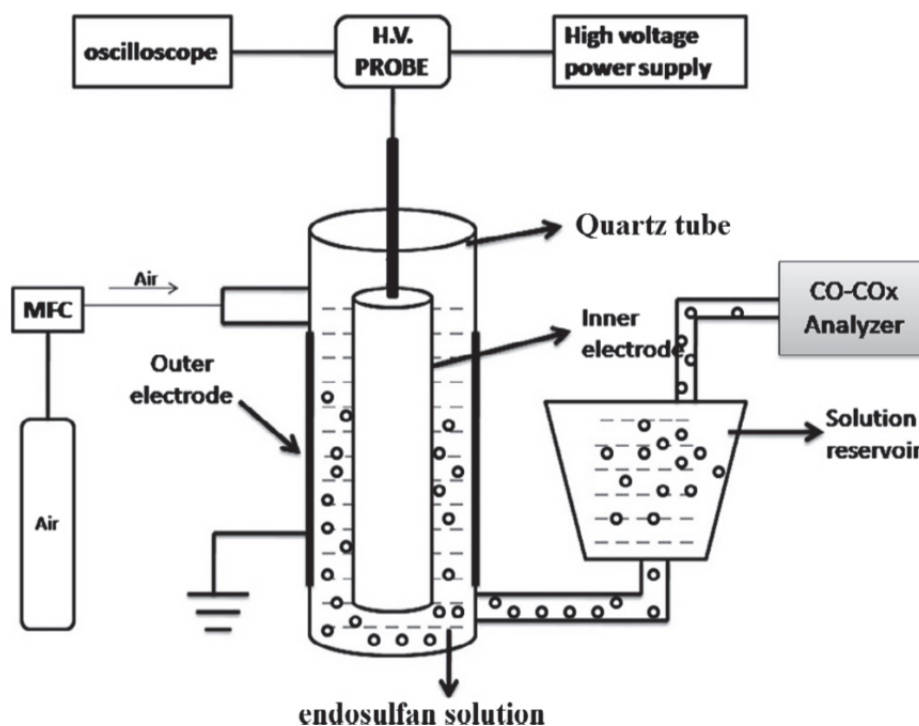


Figure 2.8: Single dielectric barrier discharge experimental setup for the treatment of endosulfan in aqueous medium (Reddy et al., 2014)

The results of their study showed that incorporation of cerium oxide catalysts into the DBD reactor significantly improved not only the conversion but also increased the mineralization efficiency of the pollutant. This was evidenced by total organic carbon and infrared spectroscopy analysis. Various similar studies on treatment of water/wastewater using single dielectric electrode configuration have been conducted. Joshi et al. (2010) reported that oxidative stress induces membrane lipid peroxidation, which leads to the production of detrimental substances causing oxidative modification in cells. Based on this claim, Joshi et al. (2011) successfully applied non-thermal plasma using a floating-electrode dielectric-barrier discharge (FE-DBD) technique for rapid inactivation of bacterial contaminants in normal atmospheric air. The study proved that reactive oxygen species (ROS) such as singlet oxygen and hydrogen peroxide-like species were the main regulator oxidative species in oxidative stress process. These oxidising agents were also suspected to be responsible for the lipid peroxidation in *Escherichia coli*. In the same vein, Reddy et al. (2013) investigated plasma-induced methylene blue degradation using dielectric barrier discharge. In their study, dielectric barrier discharge at the gas water interface was used as an advanced oxidation process for the oxidative degradation of dye contaminated wastewater.

Mark and Schluep (2001) proved that DBD can be used to degrade volatile organic compounds (VOCs) as their emission into the atmosphere causing photochemical smog formation can cause adverse effects on human health. In that regard, Mark and Schluep (2001) used a single DBD to generate gas-phase free radicals such as O (1D), O(3P), OH, etc. at low temperature (293 K) to decompose pollutants, such as benzene. The results showed that a near complete decomposition of benzene (> 99%) was reached in both wet and dry gas streams. Apart from environmental and industrial applications, DBD has also been employed in the medical sector. For example, Arjunan et al. (2012) recalled that vascularization is very important for tissue engineering and wound healing. They highlighted that non-thermal plasma principally DBD as a source of reactive oxygen species (ROS), has been frequently used for medical applications such as sterilization, malignant cell apoptosis and blood coagulation. Based on these DBD applications, Arjunan and colleagues (2012) conducted the treatment of liquids and porcine aortic endothelial cells with a non-thermal dielectric barrier discharge plasma in vitro. The successful outcomes of their study showed that endothelial cells treated with a plasma dose of 4.2 J cm⁻² had 1.7 times more cells than untreated samples 5 days after plasma treatment. In addition, Mastanaiah et al. (2013) claimed that sterilization by plasma is faster, less toxic and more multipurpose compared to traditional sterilization methods. By using low temperature, atmospheric, single dielectric barrier discharge surface plasma generator, the authors achieved high sterilization rates (elimination of different bacteria) in short periods of time compared to conventional sterilization techniques.

Apart from the single DBD, double DBD has also been used in several different fields such as the environmental, industrial and health sectors. In the double dielectric configuration, the two conductive electrodes are protected by two insulating layers (dielectrics). The discharge zone between the inner and the outer dielectric quartz is a source of highly reactive species produced via the interaction of air gas and the highly energetic electrons widely dispersed on the surface of the anode in the inner quartz tube. The resulting free radicals in the air gap are directly circulated into the polluted solution to induce oxidation process. In the same way the single dielectric barrier discharge has been explored in various fields. Several experiments have also been performed with the double dielectric barrier discharge. For instance, Rong et al. (2014) applied a cylindrical double dielectric barrier discharge reactor (Figure 2.9) as an advanced oxidation process for the degradation of diclofenac in aqueous medium. The outcomes of their study showed that at specific conditions (power 50 W and a pH of 6.15) a 10 mg/L diclofenac was completely removed within 10 minutes. These authors also affirmed that the presence of Fe²⁺ in the liquid phase promoted the decomposition of diclofenac.

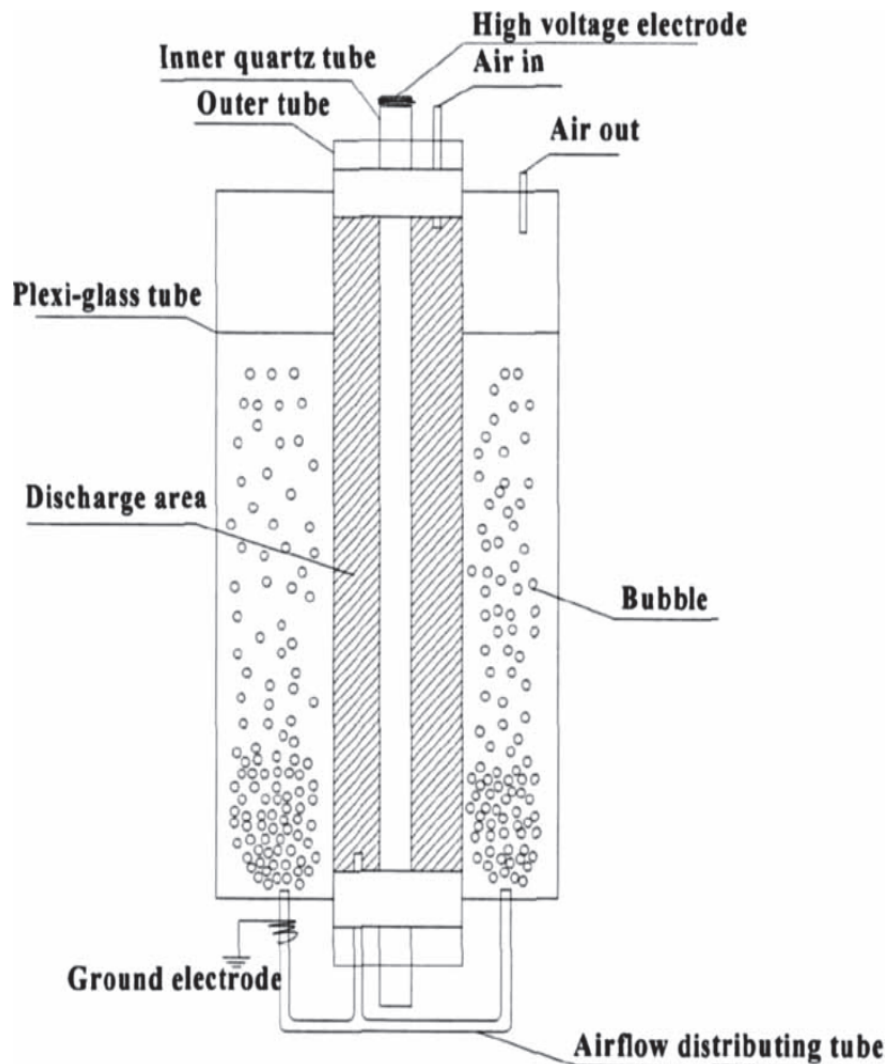


Figure 2.9: Cylindrical double DBD experimental setup (Source: Rong et al., 2014).

As for medical applications, Deng et al. (2008) investigated bacterial inactivation by atmospheric pressure dielectric barrier discharge plasma. In their experiment, *Bacillus subtilis* and *E. coli* planted in two media (agar and filter papers) were exposed to after-glow plasma generated by a double dielectric barrier discharge (DBD) plasma jet generator in open air at a temperature between about 30 to 80°C. For the bacteria planted in agar medium, the results showed that after 5 min of treatment, the effective area of inactivation was much larger than the plasma jet and increased with the plasma treatment time. In the case of the bacteria seeded on the filter paper, the results indicated that significant inactivation was obtained when adding reactive gases such as oxygen and hydrogen peroxide vapour compared to noble gases. By comparison, the current DBD (Figure 2.9) reactor used in this study is similar to the double dielectric used by Rong et al. (2014). However, in the actual DBD reactor used, the inner and outer dielectric tubes are made of quartz while in Rong's reactor the inner insulator tube was made of quartz but the outer dielectric layer was a plexi-glass tube. In addition to the tube material, the configuration used by Rong and colleagues had two air flow distribution

tubes. This might be beneficial for even distribution of bubbles in the bulk solution, but the configuration design would be very complex and short-lived reactor species may be lost during distribution.

Contrary to this configuration, the DBD reactor used in this study has a single air outlet distributing pathway that circulated bubbles directly into the simulated water. With the aid of a sparging outlet, the generated bubbles are uniformly distributed to achieve a considerable oxidation of the target pollutant. Moreover, the reactor tube in the current DBD configuration can be placed and moved out of the treatment vessel. This means that the double dielectric configuration can easily be scaled up to treat the desired volumes of the pollutants. As earlier mentioned in sections based on the structure and description of the DBD, electrode/reactor configuration is a very crucial parameter for treatment of effluents. The literature cited in the paragraphs above showed that the cylindrical single dielectric configuration can be employed in various applications. Likewise, the cylindrical single and double barrier has also been widely utilised in water/wastewater treatment technologies. In this project, the cylindrical double DBD electrode/reactor configuration was used as one of the advanced oxidation processes to treat wastewater at room temperature and ambient pressure. Methylene blue was particularly used as a model target contaminant in simulated wastewater.

2.6 TiO₂ PHOTOCATALYSIS

Titanium dioxide (TiO₂) or titanium (IV) oxide often referred to as titania, titanium white, titanic anhydride, or titanic acid anhydride occurs naturally as an oxide of titanium. It exists in three different polymorphs namely rutile, anatase and brookite phases. These three crystal structures differ appreciably from one another through the distortion of the bond angle of the octahedral chains. Among the three polymorphs, anatase and rutile are photocatalytically active, though rutile is the most thermodynamically stable phase among them. Anatase sometimes is mixed with rutile to help reduce the recombination rate of the electron-hole pair. The use of TiO₂ as photocatalyst started since 1971 by Fujishima and Honda. These authors explored the feasibility of using a photoelectrochemical cell made up of a rutile titania anode and inert cathode to split water. This remarkable achievement served as a turning point in the history of heterogeneous photocatalysis. Ever since then scientist all over the world have conducted extensive research in trying to understand the fundamental processes and also enhancing the photocatalytic efficiency of TiO₂. Titanium dioxide (TiO₂) is generally considered to be one of the best semiconductor photocatalysts available, due to its high photoactivity, photodurability, chemical and biological inertness, mechanical robustness and low cost (Chong et al., 2010). The photocatalytic process is otherwise called an advanced oxidation process (AOP) and is suitable for oxidizing a wide range of organic pollutants. Among AOPs, heterogeneous photocatalysis have been widely used to degrade organic pollutants probably due to its tendency to generate hydroxyl radicals responsible for the mineralization of recalcitrant organic compounds to harmless products (Gaya and Abdullah, 2008; Choi et al., 2010; Chong et al., 2010; Foo and Hameed, 2010; Byrne et al., 2011).

The photocatalytic degradation technology is presently being used and is highly efficient at moderate temperature and pressure. Zhou et al. (2008) and Martinez-Huitle and Brillas, 2009 reported the effectiveness of the photocatalytic oxidation of organic compounds. The photocatalytic process involves the absorption of photoenergy ($h\nu$) by the photocatalysts such as TiO₂ to produce electron excitation shown in equations 1 and 2.



The pairs of mobile charges produced by the semiconductor in UV light reach the surface of the semiconductor particle and initiate a reduction and oxidation process. This later produces the reactive species such as OH^\bullet and $\text{O}_2^{\bullet-}$ that may act as strong oxidants with a high potential to decompose and mineralize a wide range of organic compounds (Martinez et al., 2011). The mechanism for the formation of electron-hole pairs on the surface of these semiconductor, photocatalytic, metal oxides through a series of redox reactions are well reported and documented in the literature (Figure 2.10) (Ahmad et al., 2010; Akpan and Hameed, 2009; Chong et al., 2010). Since photocatalytic reactions mainly take place on the surface of the catalyst, a high surface-to-volume ratio is of significance for increasing the transformation rate. Although a lot of progress has been achieved in this area, the low contact areas for two dimensional films of nanoparticles are still challenges for their commercial applications (Lomoră et al., 2011).

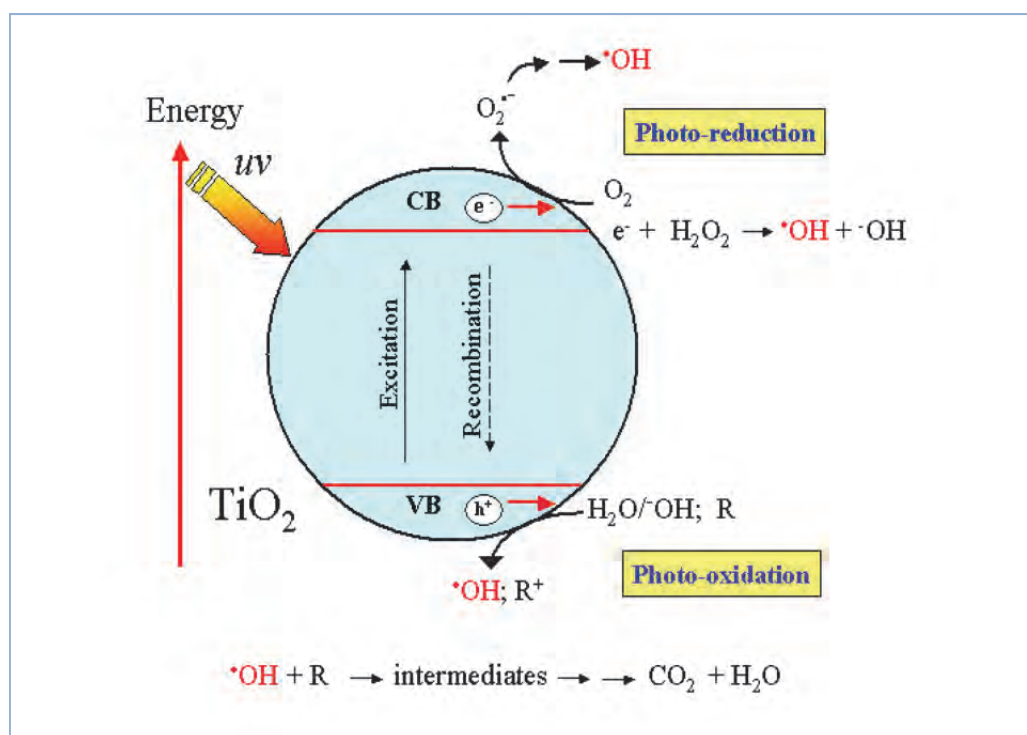


Figure 2.10: Scheme showing some photochemical and photophysical events that might take place on an irradiated semiconductor particle (Source: Chong et al., 2010).

Two dimensional nanocrystalline TiO₂ films have already shown very high photocatalytic activity. However, most findings revealed that particulate titania semiconductor crystals offer the best results with regard to degradation of organic contaminants (Blake et al., 1999) and these organic contaminants are totally degenerated and converted into CO₂, H₂O, N₂ and other harmless inorganic anions. Suffice to mention that chlorination, ozonation, and germicidal lamps such as low pressure mercury vapour lamps emitting UV at 254 nm are the most used earlier methods to purify water in developed countries. The other reported techniques such as disinfection rely on chemical or photochemical induced damage or physical removal by filtration (Blake et al., 1999), which is still being used today. But, available information from literature revealed that TiO₂ nanocrystals offer a very useful way of detoxifying wastewater contaminated with persistent, recalcitrant, toxic and non-biodegradable pollutants.

Several studies have been conducted on the use of titania photocatalyst or immobilized forms of titania to degrade and mineralize organic compounds, some of these studies are highlighted below. Anatase titania nanocrystals were obtained from decomposed nanofibres through the interaction of nanopolymer and the titanium precursor in an electrospun process (Hu et al., 2007). The electrospun process was used to spin fibres with the aid of an electric field to sub-micron level diameters. Anatase titania nanocrystals were prepared with a high activity, which was related to grain size, morphology, specific surface area, surface state, and porosity (Chuangchote et al., 2009). Chen & Mao (2007) reported that a large surface area catalyst with a constant surface density of adsorbents leads to faster surface photocatalytic reaction rates. Therefore, the larger the specific surface area of the catalyst, the higher the photocatalytic activity. Girginov et al. (2012) studied the photocatalytic efficiency of Ag doped TiO₂ photocatalyst for methyl orange degradation and it was found that the addition of Ag onto TiO₂ nanoparticle surface increased the photocatalytic activity in comparison to the standard titania. In a related development, Naik et al. (2012) synthesised and characterized nanocrystalline TiO₂, Ag immobilized TiO₂ and TiO₂-SBA-15 nanocomposites for the removal and degradation of methyl orange solution, using a simple aqueous solution-based chemical method. The characterization of the synthesised materials were done using thermal analysis, powder X-ray diffraction method, surface area and porosimetry analysis, diffuse reflectance analysis and transmission electron microscopy. The photocatalytic potential of the synthesised materials were reported as a function of sunlight exposure and monitored by UV-visible spectrophotometry. The obtained results showed that crystallite size of the crystalline phase were dependent on calcination temperature and the Ag-doped TiO₂ exhibited enhanced photocatalytic activity when compared to undoped TiO₂.

Furthermore, Behnajady et al. (2008) used liquid impregnation and photodeposition methods to synthesize Ag doped TiO₂ nanoparticles for the degradation of Acid Red 88 (AR88). The characterization results by surface analytical technique such as scanning electron micrographs (SEM) and X-ray diffraction (XRD) showed that silver immobilized TiO₂ was more effective at degrading AR88 photocatalytically than undoped TiO₂. The difference was ascribed to the ability of silver to trap electrons. The AR88 decomposition with Ag doped titania synthesised using a photodeposited method was faster and higher than that deposited using other methods. Ag doped TiO₂ was also prepared by photodeposition process, characterised and then applied for photocatalytic oxidation of methyl orange. The performance of Ag-TiO₂ in terms of complete mineralization was better than the prepared TiO₂ (Nainani et al., 2012). In addition, Ag-TiO₂ nanoparticles

were prepared and characterized for the degradation of methylene blue. The characterization was done using X-ray diffraction (XRD), scanning electron microscope (SEM), X-ray photoelectron spectroscopy (XPS), BET surface area analysis and UV-vis diffuse reflectance spectroscopy (DRS) and the findings revealed that the Ag loading effect was responsible for the changing of the anatase titania to rutile. Li et al. (2011) observed that with an increasing Ag-loading, the wavelength of Ag-TiO₂ shifted but the band gap energy decreased.

The photocatalytic activity of Ag-TiO₂ for methylene blue (MB) degradation was found to increase with the molar ratio of Ag-doped from 0 to 0.8%, but however, declined despite further increase of the molar ratio to 2.0%. The commendable visible photoactivities of the nanocomposites were attributed to the activity of Ag deposits that sometimes act as electron trappers that help in the MB adsorption. Ubonchonlakate et al. (2012) opined that TiO₂-Ag composites films produced by a sol-gel method for the photocatalytic reaction against *P. aeruginosa* bacteria had disinfection efficiency of 57% to 93% within 15 min during UV irradiation treatment compared to TiO₂. The disinfection ability of TiO₂-Ag was ascribed to the co-existence of Ag⁺ that pave the way for trapping electrons thus preventing electron-hole pair recombination and enhancing the photodisinfection activity.

Despite the enormous potential associated with TiO₂ nanoparticles regarding elimination of refractory non-biodegradable organic pollutants from wastewater, there exist some shortcomings that researchers are still trying to rectify. Among others is the inactivity of TiO₂ within the visible region caused by high band gap energy, as well as the short-lived electron-hole carriers linked to lower photon quantum efficiency. Not only these, there is difficulty in light penetration of a solution containing suspended, particulate titania nanocomposites. There is also a post separation problem to remove the suspended TiO₂ nanoparticles after the treatment process, because such post separation processes are time consuming and expensive.

CHAPTER 3: EXPERIMENTAL DESIGN AND METHODOLOGY

3.1 INTRODUCTION

This chapter provides the detailed experimental and analytical procedures used to achieve the outlined aims and objectives of the project.

3.2 UV-VIS SPECTROSCOPY

UV-vis spectroscopy technique was used to determine unknown concentrations of MB samples.

3.2.1 Sample preparation

An initial model solution of 100 mg/L methylene blue was prepared as follows: About 0.2 g of powered methylene blue was weighed and quantitatively transferred into a 2000 mL volumetric flask and made up to the mark with deionised water. Other concentrations (10; 20; 30; 40 and 50 mg/L) were prepared by serial dilutions. Each of these solutions was separately used to perform the degradation of methylene blue using electro hydraulic discharge.

3.2.2 Experimental set up for UV Vis spectroscopy

In the experimental set up for UV-Vis spectroscopy, Hellma precision cells made of quartz Suprasil were used to run UV-vis of all samples. The quartz Suprasil had characteristic specifications as follows: cuvettes 2, Type No. 110-QS, light path nm: 10nm and match.c: 284, as shown in Figure 3.1 below. In addition, Figure 3.2 below shows a GBC UV/VIS 920 spectrometer set up that was used to analyse dye samples as described in the UV/vis procedure below.



Figure 3.1: Cuvettes pieces used in UV-vis analysis of samples



Figure 3.2: UV/Vis spectroscopy set up

3.2.2.1 Procedure

First, the two quartz Suprasil cuvettes were washed and filled up with deionised water. Then the cuvettes were placed in the UV machine for base line analysis considering deionised water as a reference solution. After the base line run, one cuvette was removed from the instrument and the other was left as reference. The removed cuvette was washed with deionized water and filled up with the sample of interest and placed back into the machine. All the samples were run at a fixed wavelength of 665.00 nm. Wavelength, absorbance and other parameters of these samples could be obtained from UV-vis instrument. In order to determine the corresponding concentration of each of these absorbance values, absorbance of standards solutions (from 10 to 50 mg/L) of methylene blue were obtained from UV-vis spectrometer and presented in Table 3.1 below. Results showed that the absorbance of samples increased linearly with an increase of dye concentration.

Table 3.1: Standard concentrations vs Absorbance

<i>Standard concentrations (mg/L)</i>	<i>Absorbance</i>
10	1.28
20	2.4
30	3.498
40	4.54
50	5.75

The obtained absorbance of standard dye solutions were used to plot a calibration curve as shown in Figure 3.3. Likewise absorbance of samples taken in the time scale of 60 minutes at various MB concentrations was extrapolated on the calibration curve to find unknown concentrations of MB samples. The absorbance of MB solutions sampled between 0 and 60 minutes decreased as dye concentration was decreasing during degradation. This trend indicated that MB dye was being degraded as the experimental running time increased. That is, absorbance of the solution sampled after 10 minutes for example was greater than that of the one taken after 20 minutes and so forth.

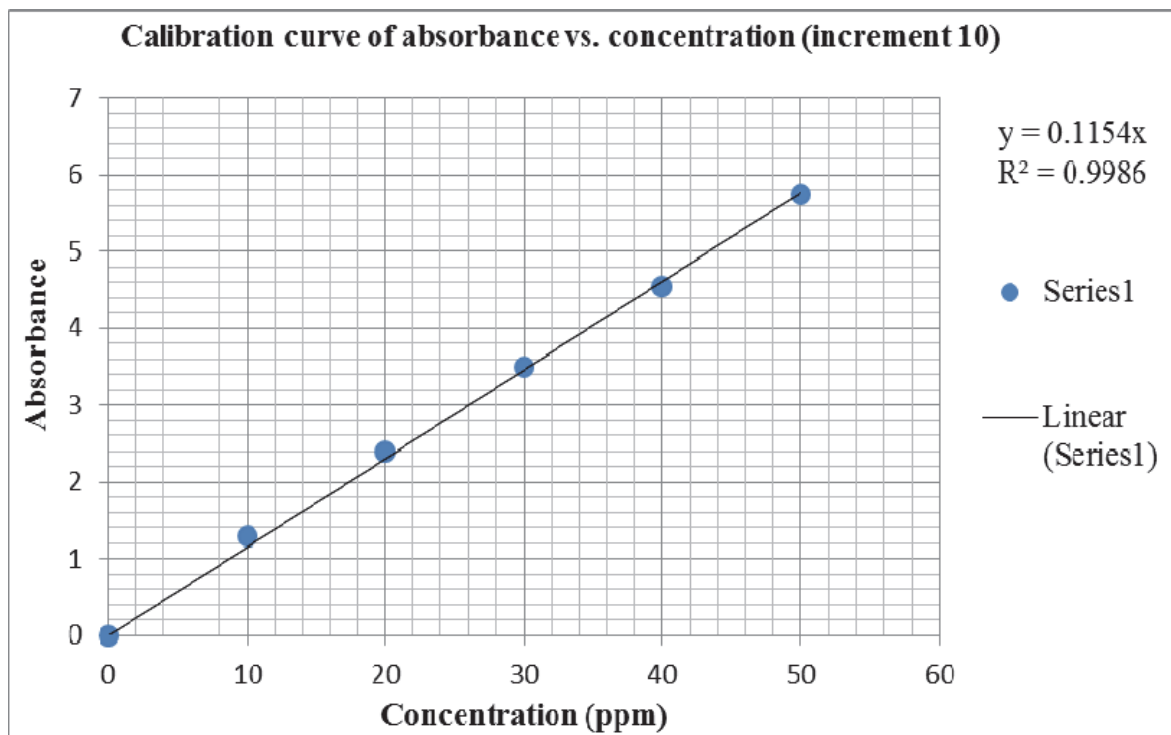


Figure 3.3: Calibration curve of absorbance vs. concentrations of methylene blue at $t = 0$ minute

Since the calibration curve was a straight line passing through the origin, it therefore obeyed the following equation: $y = mx$, where y represents absorbance values, m the slope of the line and x the unknown concentration that needed to be determined. According to the calibration curve above the equation of the line was given by $y = 0.1619x$, where $m = 0.1619$ and y any absorbance value on the y -axis.

So the desired x (concentration) could be calculated as follows:

Since $Y = 0.1154x$, therefore $X = Y/0.1154$

Therefore, unknown concentrations of methylene blue samples taken after 10, 20, 30, 40, 50 and 60 minutes were estimated using this formula. A second possibility of assessing unknown dye concentrations involved using known absorbance values of samples on the y -axis. Once the absorbance value is identified on the y -axis and by using a ruler, the value can be extrapolated on the straight line. Therefore, deducing the corresponding value of x , thus measuring the inferred concentration. This procedure could be applied to all solutions of unknown concentrations. Decolourization efficiency could be referred to as the effectiveness of colour removal of dye methylene blue by electro hydraulic discharge. Recently Kumar Reddy et al. (2013), studied the degradation and mineralization of methylene blue by dielectric barrier discharge non-thermal plasma reactor. In that study, methylene blue degradation efficiency also called degradation percentage or decolourization efficiency and was calculated using the formula presented in Equation (1):

$$\text{Degradation percentage (\%)} = [(C_o - C_t) / C_o] \times 100 \dots \dots \dots (1)$$

Where C_o and C_t are the initial and the final concentrations of MB solution respectively. So in the current study, the formula highlighted above could also be used to evaluate methylene blue degradation percentage at the given initial and final concentrations.

3.3 PREPARATION OF METHYLENE BLUE STANDARD SOLUTIONS

The initial model solutions of 100 mg/L MB were prepared as follows: About 0.2 g of powered MB was weighed and quantitatively transferred into a 2000 mL volumetric flask and made up to the mark with deionised water. Other concentrations (10; 20; 30; 40 and 50 mg/L) were prepared by serial dilution. Each of these solutions was separately used to perform the degradation of MB using electrohydraulic discharge. Based on the EHD experimental procedure explained in the following section, a series of EHD experiments at concentrations taken from 10 to 50 mg/L with increments of 10 were performed.

3.4 EHD EXPERIMENTAL PROCEDURE

The current DBD (Figure 3.4) reactor used in this study has some similarities to the double dielectric used by Rong et al. (2014) as described in the literature review. In this project, the cylindrical double DBD electrode/reactor configuration was used as one of the advanced oxidation processes to treat wastewater at room temperature and ambient pressure. Methylene blue was particularly used as a model target contaminant in simulated wastewater. A power supply set at 25 V, delivering a current of 3 A and a power of 80 W, was directly connected in series to a transformer that steps the AC voltage up to a DC peak voltage of ~8 kV directly delivered into the system. A 0.5 mm silver (or as otherwise specified) electrode that was directly connected to the high voltage (output of the transformer), was immersed in a 50 g/L (or as specified) of electrolyte solution of sodium chloride placed in the inner tube of a single cell reactor (Figure 3.2). This latter was placed in 1.8 L beaker containing 1.5 L of MB solution. An air pump with a high and low flow speed switch was connected to an air flow meter that was directly connected to the single cell reactor tube for air (mostly oxygen) production. The air pump had a maximum flow rate of 4.8 L/min but was varied as further specified. The electrical discharge values mentioned above as well as dye volume and air flow were kept constant or varied as specified in the experiments.

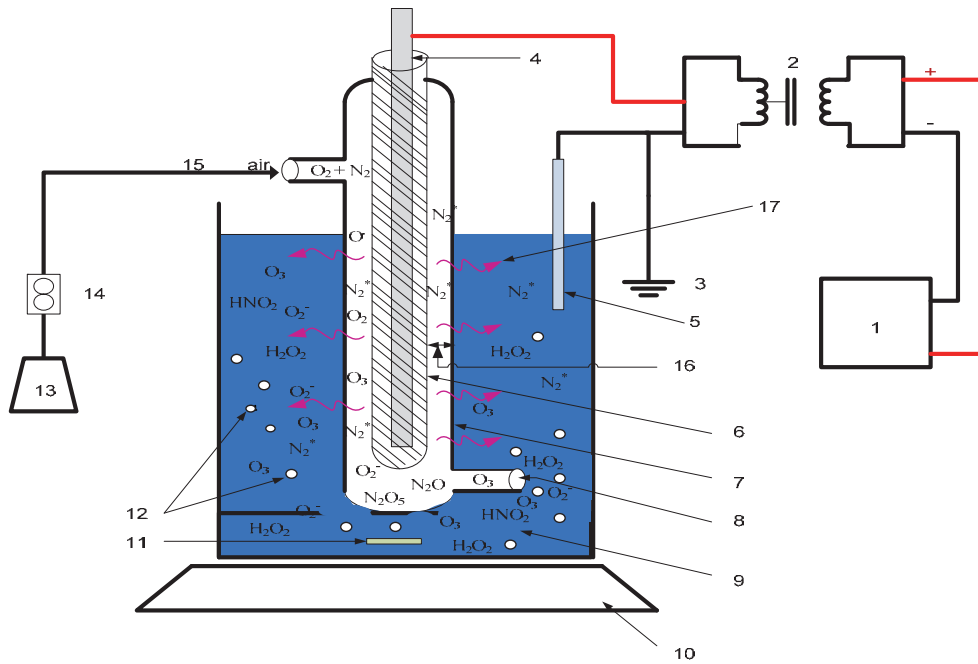


Figure 3.4: Actual DBD electrode/reactor arrangement.

Where:

- | | |
|----|---------------------------------|
| 1 | Power supply |
| 2 | Step up transformer |
| 3 | Ground (earth) |
| 4 | High voltage electrode |
| 5 | Copper foil |
| 6 | First quartz dielectric tube |
| 7 | Second quartz dielectric tube |
| 8 | Gas outlet |
| 9 | Methylene blue solution |
| 10 | Magnetic stirring base |
| 11 | Stirring rod |
| 12 | Bubbles formed (active species) |
| 13 | Air pump |
| 14 | Flow meter |
| 15 | Air inlet |
| 16 | Discharge/air gap |
| 17 | UV radiations |

The reactor consisted of an inner and outer tube. The diameter of the inner tube was approximately equal to 1 mm and that of the outer tube was 7 mm. The reactor was 23 cm long with an inlet and outlet for air circulation. The air gap was about 2 mm but was varied as specified. The ground electrode was submerged into the MB solution in the beaker to complete the circuit and also grounded to the Earth to avoid any electrocution (Figure 3.5).



Figure 3.5: Electro hydraulic experimental set up

An electrode directly connected to the high voltage (output of the transformer) was immersed in the electrolyte solution of sodium chloride placed in the inner tube of the single cell reactor. An air pump with a high and low switch was connected to an air flow meter that was directly connected to the single cell reactor tube for air (mostly oxygen) production.

Methylene blue solution of specified concentrations was sampled at the time $t = 0, 10, 20, 30, 40, 50$ and 60 minutes, pH and electrical conductivity of methylene blue samples at these time scales were measured. Methylene blue samples, collected at $0, 10, 20, 30, 40, 50$ and 60 minutes of each experiment were further analysed using UV-vis in the range of $600-700$ nm. Absorbance values of these samples obtained at a fixed wavelength of 665.0 nm were recorded. Therefore using the initial concentrations and their corresponding absorbance, a calibration curve of absorbance vs. dye concentration was plotted to estimate the unknown concentration of methylene blue samples. Finally having initial and final concentrations, the decolourization efficiency of dye was calculated. Thus the rate of decolourization of Methylene blue was also studied.

3.4.1 Effect of air gap between the outer and inner tubes of the EHD reactor

3.4.1.1 Procedure

Besides the effect of electrode type and diameter, the amount of air flowing between the outer and the inner tubes is believed to impact on the decolourization/degradation of the pollutant. This was supported by Zhang et al. (2008) and others researchers who highlighted that the air gap in electrical discharge reactors might impede the degradation (% removal) of organic pollutants. Therefore, three reactor tubes/cells were designed at different air gaps of $2, 4$ and 6 mm and were used in the EHD system to investigate the effect of the air gap on MB degradation efficiency at the following experimental conditions: MB concentration 5 mg/L, pH 6 , applied voltage 25 V, peak voltage 7.8 kV, dye volume 1500 mL, air flow rate 3 L/min, 50 g/L NaCl electrolyte, a 0.5 mm silver electrode and a contact time of 60 minutes at 25 °C. The absorbance of MB solutions treated with each reactor at a specific air gap was measured. The MB solution was sampled every 10 minutes. The unknown concentrations of MB samples and their degradation efficiencies were estimated

and presented in order to compare the performance of the three reactor configurations. The UV results of these data were plotted and based on these results, the reactor tube with air gap 2 mm was used for all further experiments. The dimensions of reactor configurations and air gap varied in EHD experiment are presented in Table 3.2 and the schematic representations of DBD reactor tubes used in this section are presented in Figures 3.6-3.8, respectively.

Table 3.2: Inner and outer tube dimensions of reactors 1, 2 and 3

Reactors	Inner tube		Outer tube		Air gap (mm)	Reactor length
	ID (mm)	OD (mm)	ID (mm)	OD (mm)		
Reactor tube 1	2	3	5	7	2	20 cm
Reactor tube 2	2	4	8	10	4	20 cm
Reactor tube 3	3	5	11	13	6	20 cm

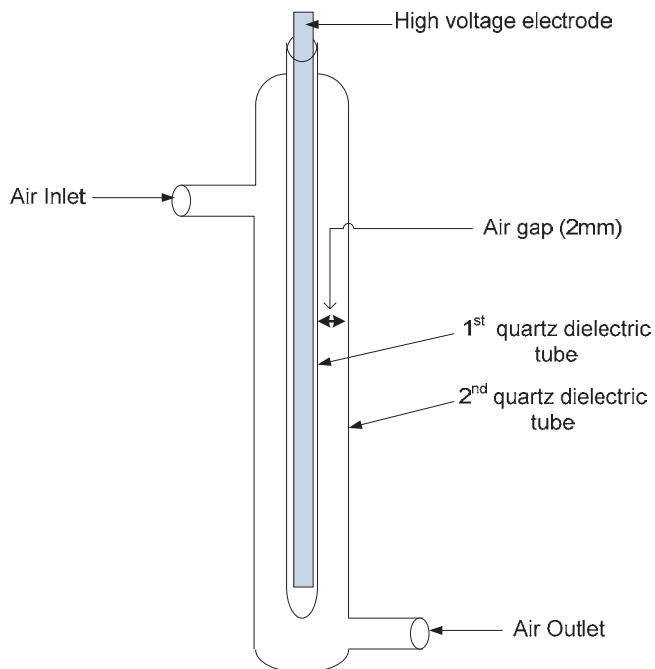


Figure 3.6: Schematic representation of the DBD reactor (tube)1 (air gap =2 mm)

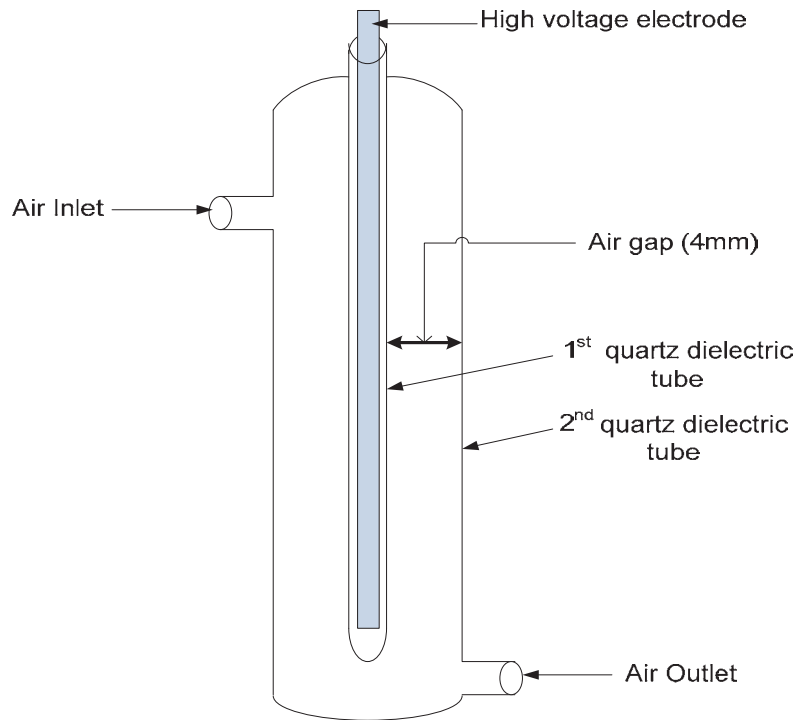


Figure 3.7: Schematic representation of the DBD reactor (tube) 2(air gap =4 mm)

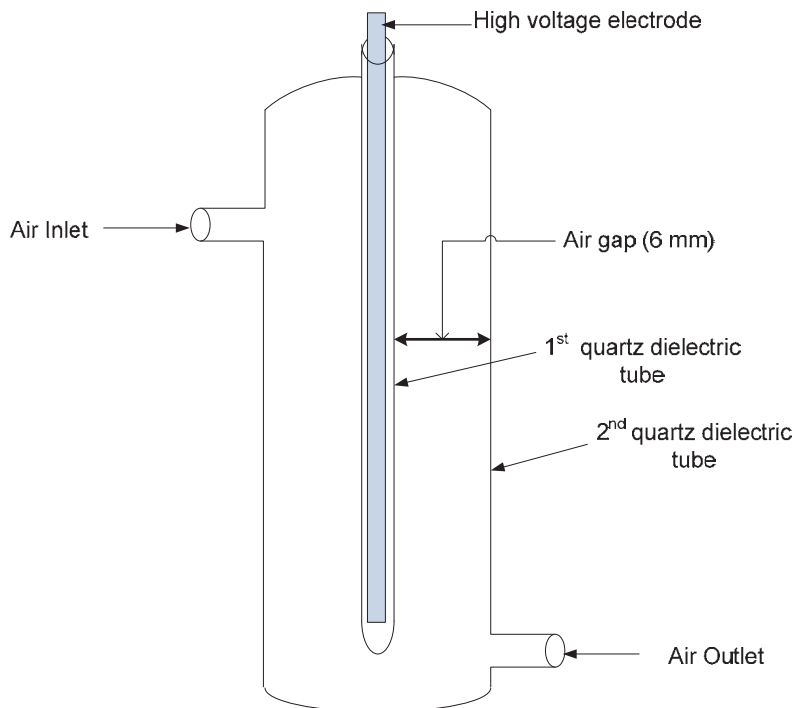


Figure 3.8: Schematic representation of the DBD reactor (tube) 3(air gap =6 mm)

3.4.2 The effect of pH on decolourization efficiency of MB

A few drops of either concentrated H₂SO₄ or NaOH were carefully diluted in separate beakers containing approximately 400 mL of deionised water. About 1500 mL of 5 mg/L MB solution was placed in a 200 mL beaker in which a pH/conductivity probe was immersed. The pH of MB solution was varied from 2.5 to 10.5 and was adjusted to the desired value by adding a reasonable amount of diluted H₂SO₄ and NaOH drop wise using 10 ml syringes. During this process the solution was continuously swirled with pH/conductivity meter probe to get the pH value needed. The monitored solution was further used in the electrohydraulic discharge experiment at the following experimental conditions: Applied voltage 25 V, Peak voltage 7.8 kV, air flow rate 3 L/min, air gap 2 mm, 0.5 mm silver electrode and 50 g/L of NaCl for 60 minutes.

3.4.3 The effect of solution conductivity on decolourization efficiency of MB

About 1500 mL of MB solution was placed in a 2000 mL beaker. With the aid of a pH/conductivity meter, MB conductivity was adjusted from 5 mS/min to 20 mS/min by drop wise addition of diluted HNO₃/NaOH in the beaker and swirling the solution with the pH/conductivity probe until the desired conductivity value was obtained. Furthermore MB solution at a fixed conductivity value was then used as model sample pollutant to which electrohydraulic discharge was applied for 60 minutes while the following parameters were kept constant: applied voltage 25 V, peak voltage 7.8 kV, air flow rate 3 L/min, air gap 2 mm, MB concentration 5 mg/L, solution pH 6, 50 g/L NaCl electrolyte and 0.5 mm silver electrode. The sampled solutions were analysed using a UV-vis spectrophotometer. Absorbance of these samples was used to determine unknown concentrations. These values were used to calculate the decolourization efficiency of methylene blue.

3.4.4 The effect of MB volume on the degradation efficiency

A 100 mg/L methylene blue stock solution was prepared by dissolving 0.1 g of powder MB in deionised water in a 1 L volumetric flask which was then filled up to the mark with deionised water. Different volumes of 500, 1000, 1500 and 2000 mL of 5 mg/L solution of methylene blue were prepared by serial dilutions. The following parameters were then applied during EHD experiments using these solutions: Voltage 25 V; peak voltage 8 kV; air flow rate of 3 L/min, air gap 2 mm, MB concentration 5 mg/L, pH 6 and 50 g/L NaCl electrolyte were kept constant, using electrohydraulic discharge experimental procedure described in the previous section. The experiment was repeated four times by varying methylene blue volume (500, 1000, 1500 and 2000 mL). For each experiment, a single reactor tube (23 cm) was immersed in a 2000 L beaker. Methylene blue degradation efficiency was evaluated when increasing the dye volume. The sampled solutions were analysed using UV-vis spectrophotometer. Absorbance of these samples was used to determine unknown concentrations. These later were used to calculate the decolourization efficiency of Methylene blue.

3.4.5 The effect of air flow rate on MB decolourization efficiency

Using the EHD system as described in the previous section, most parameters were kept constant (applied voltage 25V, peak voltage 7.8 kV, MB concentration 5 mg/L, solution pH 6, 50 g/L NaCl electrolyte and MB volume 1500 mL, air gap 2 mm) while the air flow rate was altered from 2, 3 to 4 L/min. In total 3 experiments were performed in the same way during a period of 60 minutes whilst sampling every 10 minutes. The sampled solutions were analysed using a UV-vis spectrophotometer. Absorbance of these samples was used to determine unknown concentrations. These later were used to calculate the decolourization efficiency of methylene blue.

3.4.6 The effect of NaCl electrolyte on MB decolourization efficiency

In order to evaluate the effect of sodium chloride electrolyte solution on decolourization efficiency of MB dye, the following procedures were followed. 10 g, 30 g and 50 g of granulated sodium chloride (NaCl) was weighed respectively and transferred into three separate 1000 mL volumetric flasks. The granulated NaCl was then dissolved by continuous shaking and filled up to the mark with deionised water. The obtained solution at different concentrations; 10 g/L, 30 g/L and 50 g/L was used as electrolyte in the central electrode compartment of the electrohydraulic discharge system under the following conditions: applied voltage 25V, peak voltage 7.8 kV, MB concentration 5 mg/L, solution pH 6, air flow rate 3 L/min, air gap 2 mm, 50 g/L NaCl electrolyte and MB volume 1500 mL using silver electrode. About 8-10 ml of the specified concentration of sodium chloride solution was put into the central electrode compartment of the electrohydraulic discharge reactor as electrolyte. Though sodium chloride solution is a good conductor of electricity, it was mostly used in this system to avoid sparking between the high voltage electrode and reactor tube walls during electrohydraulic discharge reactions.

3.4.7 The effect of electrical parameters: Applied voltage on decolourization efficiency of MB

In this section the applied voltage was varied between 20 V, 22 V to 25 V, corresponding to the peak voltage of 6.4 kV, 6.8 kV and 7.8 kV respectively delivered by the power supply and step up transformer. The following parameters were kept constant: [MB] concentration 5 mg/L, solution pH 6, air flow rate 3L/min, air gap 2 mm, 50 g/L NaCl electrolyte and dye volume 1500 mL and silver electrode. In total three electrohydraulic discharge experimental reactions were performed by altering the applied voltage between 20 V to 22 V and 25 V as indicated above. The experiment was performed over 60 minutes and MB solution was sampled every 10 minutes.

3.4.8 The effect of electrode type on MB percentage removal

Besides various chemical and physical parameters that have been inspected in this study, it was also believed that the type of electrode used would have an effect on MB removal. Several studies on EHD have used different types of electrodes such as graphite, stainless steel and copper using different EHD reactors. However different results have been reported. To verify this parameter and select the most suitable electrode

for the current EHD reactor tube, three types of electrodes: copper, silver and stainless steel (25 cm long and 1 mm diameter) were selected and used in the EHD system. The rest of the parameters including MB concentration 5 mg/L, solution pH 6, applied voltage 25 V, peak voltage 7.8 kV, air flow rate 3 L/min, air gap 2 mm, 50 g/L NaCl electrolyte and dye volume 1500 ml were maintained constant while varying the electrode type. Using the same EHD procedure as previously described, three EHD experiments were carried out. Each experiment was run for 60 minutes. MB solution was sampled every 10 minutes. The samples were analysed using UV-absorption spectroscopy. The recorded absorbance values were used to calculate unknown concentrations as well as the colour removal percentage of MB.

3.4.9 Optimization of the diameter of the electrode

Electrical energy in conductive material may sometimes depend on their length and diameter. That necessitates the investigation of the different diameters of silver electrode on MB colour removal percentage. In this case, EHD procedure remained the same. The following parameters were applied: MB concentration 5 mg/L, solution pH 6, dye volume 1500 mL, applied voltage 25, peak voltage 7.8 kV, air gap 2 mm and air flow rate of 3 L/min, 50 g/L NaCl electrolyte and silver electrode were retained constant during the experiments while silver electrode diameter was changed from 1 mm to 1.5 mm. Therefore two experiments in total were performed within 60 minutes, whilst sampling every 10 minutes.

3.4.10 Procedure of the EHD performed at optimal conditions

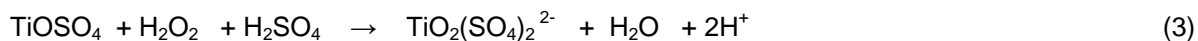
In order to test the efficacy of the optimized electrohydraulic discharge (EHD) system, two EHD experiments at normal and optimum conditions were carried out. The experimental normal conditions included: applied voltage 25 V, peak voltage 7.8 kV, [MB] = 5 mg/L, V = 1500 mL, air flow rate 3 L/min, 0.5 mm silver electrode, 50 g/L NaCl electrolyte, air gap 2 mm and running time of 60 minutes. As for the optimum parameters, the following: applied voltage 25 V, peak voltage 7.8 kV, [MB] = 5 mg/L, V = 1500 mL, air flow rate 3 L/min, 1.5 mm silver electrode, 50 g/L NaCl electrolyte, air gap 2 mm and running time of 60 minutes were used.

3.5 QUANTIFICATION OF ACTIVE SPECIES AT OPTIMUM CONDITIONS IN THE BULK SOLUTION

3.5.1 Quantification of H₂O₂

For the quantification of H₂O₂ the concentration of the yellow-coloured peroxotitanyl complex was determined by UV absorption spectroscopy at 410 nm (Uher et al., 1991). The absorbance at this wavelength was directly proportional to the initial hydrogen peroxide concentration. Approximately 2.4 g of titanyl sulfate (hydrate) was weighed and mixed with 100 mL (20%) H₂SO₄ in a volumetric flask. The remaining volume of the flask was made up to 500 mL with Millipore water. After specific time intervals during electro hydraulic discharge treatment, 3 mL of the treated water was sampled from the EHD reactor

and mixed with 0.3 mL of the prepared titanylsulphate solution in a cuvette (flask). From the absorbance measured with a photo spectrometer the H₂O₂ concentration can be derived.



3.5.2 Detection of ozone in the liquid phase

Ozone, being one of the active species produced in underwater streamer discharges was detected and quantified using the indigo method as described by Bader et al. (1981). Indigo has a strong absorbance at 600 nm ($\epsilon = 20000 \text{ L mol}^{-1} \text{ cm}^{-1}$). One molecule of ozone could decolourise one molecule of the indigo dye. The decolorized products hardly consumed further ozone. The amount of ozone scavenged could be determined from the decolourisation of the reagent measured at 600 nm. During measurement, no interference with OH radicals was expected after pulsing of the reactor. This had been earlier demonstrated by Bader et al. (1981) that the presence of hydrogen peroxide does not interfere with the measurement of OH radicals. Indigo reagent was prepared as follows:

Solution-A: About 0.5 mL of phosphoric acid was mixed with 310 mg of indigo trisulfanate in a volumetric flask and filled up to 500 mL with Millipore water.

Solution-B: 14 g of sodium dihydrogen phosphate was mixed with 17.5 g of H₃PO₄ together in a volumetric flask and filled up to 500 mL with Millipore water.

2 mL of each solution (A and B) were mixed together in a volumetric flask and filled up to 25 mL with Millipore water. The absorbance of this solution was measured and recorded as a reference [blank absorbance count]. To determine the ozone concentration dissolved in the water, again 2 mL volumes of each reagent were mixed together in a 25 mL volumetric flask and the rest of the volume filled up with treated water. Then the absorbance of the solution was measured and recorded as the sample absorbance. As described beforehand, the O₃ concentration was calculated from the differences in absorbance between the initial indigo solution and that of the solution exposed to ozone.

3.6 PRELIMINARY EXPERIMENTS ON REAL TEXTILE WATER

Real textile water was obtained from a textile manufacturing company. The collected wastewater samples supplied by the textile manufacturing company, Cape Town, was odoriferous and dark in colour. The effluent was characterized for pH, electrical conductivity (EC), Total Suspended Solids (TSS), Total Dissolved Solids (TDS), Biochemical oxygen demand (BOD), Total organic carbon (TOC), and Chemical Oxygen Demand (COD). All the parameters were measured in accordance with "Standard methods for treatment of water and wastewater". The following chemicals were used; Al₂(SO₄)₃, Ca(OH)₂, FeCl₃ and FeSO₄.7H₂O.

3.6.1 Experimental set-up

The wastewater sample was subjected to gravitational settling for 30 minutes due to the presence of a substantial quantity of suspended solids. But, it was found that the suspended solids were poorly settled within 30 minutes. Thus, a coagulation-flocculation study was undertaken. The study was performed by varying the mass of Al₂(SO₄)₃, Ca(OH)₂, FeCl₃, FeSO₄·7H₂O, and Fe-Mn oxide from 0.2-1.0 g. Firstly, 500 ml each of wastewater sample was added to five beakers to which were added various mass of the respective coagulant and flocculants (see Table 21). Thorough mixing was performed for 1 min at 100 rpm, then flocculation was carried out at a speed of 20 rpm for 20 min. Finally, the wastewater content in the beaker was allowed to settle for 40 minutes and the supernatant was collected for analysis. The parameters measured for the supernatant were COD, TOC and pH.

3.6.2 Electrohydraulic discharge treatment

The effluents, as well as the supernatants after flocculation of the textile water, were further subjected to electrohydraulic discharge (EHD) treatment. The EHD experiment was conducted for 1 hour and a sample of process water was taken every ten minutes. The sample was analysed for TOC, COD and pH. The results of the process water analysed after 60 minutes of EHD treatment are shown in the results section.

3.7 MATERIALS AND PREPARATION FOR SUPPORTED TiO₂ PHOTOCATALYSTS

The titanium tetrachloride (TiCl₄) 99% pure and polyacrylonitrile (PAN) were purchased from (Sigma Aldrich) and dimethylformamide (DMF) was purchased from B & M Scientific. 3 g of the polyacrylonitrile (PAN) and 34.5 g of N, N-dimethylformamide (DMF) were weighed out and added together, making up 37.5 g of PAN and the DMF. The PAN was dissolved in DMF at room temperature (25 °C) over night (12 hour) in a sealed vessel ensuring that the entire polymer was dissolved making up the 8% PAN/DMF clear solution. This solution was slightly viscous. Then 6 g of 99% concentrated TiCl₄ was weighed out and added to the 8% PAN/DMF solution drop by drop while stirring with a magnetic stirrer at room temperature making up the 8% (PAN/DMF/TiO₂) sol gel solution (Table 3.3). This experiment was undertaken in the fumehood as the TiCl₄ released white fumes of HCl. During the addition of the concentrated TiCl₄ the solution turned yellow and released heat, so the reaction occurring was exothermic.

Table 3.3: Experimental conditions for each synthesis

Unique name	Solution	Method	Decomposition
TT4.1	8% (PAN/DMF/TiO ₂) sol gel solution	Manual Coating	50°C/min to 300°C in air holding time = (1 h, 2 h, 3 h, 4 h, 5 h or 6 h)
TT4.2	8% (PAN/DMF/TiO ₂) sol gel solution	Manual Coating	50°C/min to 400°C in air holding time = (1 h, 2 h, 3 h or 4 h)
TT4.3	8% (PAN/DMF/TiO ₂) sol gel solution	Manual Coating	50°C/min to 500°C in air holding time = (1 h, 2 h, 3 h or 4 h)
TT4.3	8% (PAN/DMF/TiO ₂) sol gel solution	Manual Coating	50°C/min to 600°C in air holding time = (1 h, 2 h, 3 h or 4 h)

3.7.1 Coating the 250 mm² stainless steel mesh support with the 8% PAN/DMF/TiO₂ sol gel solution

The 250 mm² stainless steel mesh was coated manually with 0.5 mL 8% (PAN/DMF/TiO₂) sol gel solution drawn from a glass vessel containing 50 mL of the 8% (PAN/DMF/TiO₂) sol gel solution (Section 3.8 and 3.9) placed on a magnetic stirrer to ensure that the (PAN/DMF/TiO₂) sol gel solution was homogeneous. The 0.5 mL (~0.1965 g) of the sol gel solution was deposited as a zig zag pattern on the 250 mm² stainless steel mesh and the (PAN/DMF/TiO₂) sol gel solution was spread evenly throughout the stainless steel mesh manually. As soon as the stainless steel mesh was coated with (PAN/DMF/TiO₂) sol gel solution, the solution colour on the stainless steel mesh changed from yellow to a violet colour. The coated mesh was then placed on a ceramic boat and left for 10-15 minutes in the fumehood to dry at room temperature after which it was calcined according to the following procedure. The coated samples were calcined in air by heating within the temperature range between 300°C to 600°C at a heating rate of 50°C/min and holding the temperature at the final temperature for 2 h. The time required for heating was calculated as follows subtracting the the room temperature (25°C): 600°C – 25°C = 575°C and the time as: 575°C ÷ 50°C/min = 11.5 min

3.7.2 Characterization of supported TiO₂ materials

The synthesized PAN/DMF/TiO₂ supported nanocrystals were characterized using these characterization techniques: XRD, HRSEM, EDS, HRTEM, SAED, FTIR and UV-visible to study the physical and chemical properties of the synthesized decomposed supported PAN/DMF/TiO₂ nanocrystals. X-ray diffraction (XRD) was used for phase identification of the crystalline material. This characterization was done on the instrument called D8 Advance from Bruker AXS, for the identification of the TiO₂ nanocrystalline phases. The high resolution scanning electron microscope (HRSEM) was used to observe the external morphology texture, crystalline structure and the orientation of materials making up the sample. The characterization was done using a high resolution field emission gun scanning electron microscope (HRFEGSEM), using an Auriga Gemini FEG SEM.

The energy-dispersive spectroscopy (EDS) separates the characteristic x-rays of different elements into an energy spectrum and also analyses the energy spectrum in order to determine the abundance of specific elements. This characterization was carried out using the HRSEM. The samples were transferred to the EDS for qualitative identification of the different elements contained by the sample. High resolution transmission electron microscopy was used to observe modulations in chemical identity, crystal orientation, as well as the regular absorption based imaging. The instrument used was a Technai, G2 F20 X-Twin MAT, to analyse the surface morphology of samples and the crystal distribution. Selected area electron diffraction (SAED) was used to determine the crystal structure and the crystallographic orientation of the sample. This instrument was used with HRTEM; the sample that was analyzed by the HRTEM then was transferred to the SAED detector to do the analysis.

Fourier transform infrared spectroscopy (FTIR) was used to determine the molecular structure and chemical bonding of materials and identify the unknown materials. This characterization was done with a Perkin Elmer 100 FT-IR spectrometer. The powdered sample was placed on the attenuated total reflectance (ATR) cell which was the sample holder. Ultraviolet-visible spectroscopy (UV-Vis) was used for qualitative and quantitative analysis of effluent samples. The instrument was used for the characterization of the methylene blue samples to determine the concentration of the methylene blue dye before and after photocatalytic degradation. The reference sample, deionized water, was analysed first and the baseline check was done, to subtract the interferences. The samples were analysed over the range of 400-800 nm wavelength as this was the visible region.

3.8 DISINFECTION OF BACTERIAL USING DIELECTRIC BARRIER DISCHARGE

This section provides detailed experimental and analytical procedures used to achieve the disinfection of bacterial using dielectric barrier discharge. In this section, three fundamental experiments were covered: the inoculation of the bacteria (*E. coli*), the stirring of the *E. coli* in the absence of the DBD reactor and finally the sterilization of *E. coli* by DBD system at the applied conditions.

3.8.1 Preparation of *E. coli*

The *E. coli* populations required by the study were inoculated in 5 mL of nutrient broth and incubated for 24 h at 37 °C and continuously stirred (overnight culture) in order to promote bacterial growth. After the incubation, the culture was centrifuged for 10 min at 50 rpm twice. The bacteria were put in a 5 mL suspension of distilled and sterilized water and the monoculture was taken at 0.5 of their optical density in the log phase.

3.8.2 Experiment performed with blank solution of *E. coli*

After the micro-organisms (*E. coli*) were inoculated, the monoculture was taken at 0.5 of their optical density in the log phase. The purpose was to confirm the growth of bacteria in that range and investigate whether

they could die by only stirring their solution with a magnetic stirrer for 60 minutes. About 1500 mL of the inoculated *E. coli* bacteria was placed in a 200 mL beaker. A magnetic stirrer was placed in the solution. The solution was then stirred on a magnetic stirrer plate set at 50 rpm for 60 minutes at atmospheric conditions of temperature and pressure. The *E. coli* solution was sampled every 10 minutes. The optical density of the sampled solution was recorded as absorbance using a UV-spectrophotometer.

3.8.3 Disinfection of *E. coli* using Dielectric barrier discharge

After the *E. coli* growth was confirmed in their log phase, it was then necessary to evaluate the killing effect of the DBD reactor using the inoculated solution of *E. coli*. Therefore, a DBD experiment was carried out using the prepared *E. coli* solution as described below. However, the DBD process in this study was performed in a number of steps as described in the following paragraphs. The untreated and treated *E. coli* samples were analysed by UV-vis spectrophotometer to measure their optical density (absorbance).

3.8.3.1 DBD experimental procedure

The cylindrical double DBD electrode/reactor configuration was used in this study as one of the advanced oxidation processes to treat the contaminated water at room temperature and ambient pressure. *E. coli* was particularly used as a model target contaminant in water. The schematic representation of the actual DBD system is presented in Figure 3.4.

3.8.3.2 Procedure for E. coli inactivation

An electrode directly connected to high voltage (output of the transformer) was immersed in the electrolyte solution of sodium chloride placed in the inner tube of the single cell reactor. This latter was placed in a 1800 mL beaker containing 1.5 L of *E. coli* solution of specified concentrations. An air pump with a high and low switch was connected to an air flow meter that was directly connected to the single cell reactor tube for air (mostly oxygen) production. *E. coli* solution was sampled at the time $t = 0, 10, 20, 30, 40, 50$ and 60 minutes during the experiment. *E. coli* samples collected at 0, 10, 20, 30, 40, 50 and 60 minutes of each experiment were further analysed using UV-vis in the range of 600-700 nm. The optical density (absorbance) values of these samples obtained at a fixed wavelength of 665.0 nm were recorded in order to show the decline of the optical density of *E. coli* with time, as an indicator of cell disintegration.

CHAPTER 4: RESULTS AND DISCUSSION

4.1 INTRODUCTION

This chapter presents results of the optimization of physico-chemical parameters of the EHD system; as well as the optimization of supported TiO₂ photocatalysts incorporated into the EHD reactor.

4.2 EFFECT OF AIR GAP BETWEEN THE OUTER AND INNER TUBES OF THE EHD

Three different reactor configurations were designed and tested for MB decolouration efficiency. The aim was to evaluate the impact of the distance between the inner and the outer quartz tube (air gap) on MB degradation. The air gap was varied from 2, 4 and 6 mm as presented in Table 4.1. EHD experiments on degradation of MB solution were performed using the three configurations. Each experiment was carried out within 60 minutes and sampled every 10 minutes. Absorbance of MB solution sampled within 60 minutes using reactors with air gap 2, 4 or 6 mm is shown in Table 4.1. While the air gap was varied, the following conditions were kept constant: MB concentration 5 mg/L, applied voltage 25 V, Peak voltage 7.8 kV, pH (various), dye volume 1500 mL, air flow rate 3 L/min, 50 g/L NaCl el.

Table 4.1: Absorbance of MB solution sampled within 60 minutes

Experiment	Time (minutes)	Absorbance (nm)	Concentration (mg/L)	Degradation (% removal)
Absorbance of MB solution sampled within 60 minutes using reactor 1 with air gap 2 mm	0	1.023	5	0
	10	0.423	3.665	26.7
	20	0.200	1.733	65.34
	30	0.096	0.832	83.36
	40	0.045	0.389	92.22
	50	0.016	0.138	97.24
	60	0.000	0.000	99.999
Absorbance of MB solution sampled within 60 minutes using reactor 2 with air gap 4 mm	0	1.077	5	0
	10	0.553	4.792	4.16
	20	0.304	2.634	47.32
	30	0.116	1.005	79.9
	40	0.062	0.537	89.26
	50	0.042	0.364	92.72
	60	0.025	0.2166	95.68
	70	0.008	0.069	98.62
	80	0.000	0.000	99.999

Table 4.1 (continued): Absorbance of MB solution sampled within 60 minutes

Experiment	Time (minutes)	Absorbance (nm)	Concentration (mg/L)	Degradation (% removal)
Absorbance of MB solution sampled within 60 minutes using reactor 3 with air gap 6 mm	0	1.059	5	0
	10	0.58	5	0
	20	0.57	4.94	1.2
	30	0.467	4.05	19
	40	0.335	2.903	41.94
	50	0.224	1.941	61.18
	60	0.149	1.291	74.18
	70	0.080	0.693	86.14
	80	0.049	0.426	91.48
	90	0.033	0.286	94.28
	100	0.020	0.173	96.54
	110	0.008	0.069	98.62
120	0.000	0.000	99.999	

Table 4.1 shows that the amount of air circulating in the dielectric region, which is the space between the inner and the outer quartz tubes of the EHD reactor had an effect on dye decolouration. From the calibration curve previously described in Chapter 3 of this study and by using de Beers law, unknown concentrations of samples were calculated. Having the initial and final concentrations of MB samples, decolourization efficiency of this dye with time was estimated and results obtained and were plotted in Figure 3.4. The results obtained (Figure 4.1) showed that complete decolouration of MB in reactor 1 with a 2 mm air gap was achieved within 60 minutes. However, with reactor 2, MB was totally decolourized after 80 minutes and 120 minutes in reactor 3. These results clearly demonstrate that the shortest decolouration time of MB was achieved with reactor 1 having an air gap of 2 mm, closely followed by reactor 2 and reactor 3. This showed that the air gap has a direct impact upon the efficiency. At a particular experimental time, for example after 20 minutes of experiment, about 65.34% of MB was decolourized with reactor 1 compared to 47.32% with reactor 2 and 1.2% with reactor 3. This trend was also observed after 10 minutes of experiment whereby 26.7% of dye decolourisation was achieved with reactor 1, 4.16% with reactor 2 and 0% with reactor 3. Based on these air gap dimensions and results presented in Figure 4.1, it could be inferred that degradation efficiency of MB significantly decreased with an increase in air gap. This could be explained by the fact that the small air gap in reactor 1 for instance, might have induced a strong electric field leading to high electron energy around the inner tube. These electrons might have increased the length and number of streamers that dissociated oxygen molecules quickly into singlet atomic oxygen which probably reacted back with oxygen to generate ozone and other active species such as hydrogen peroxide. These active species were then bubbled directly into a MB solution.

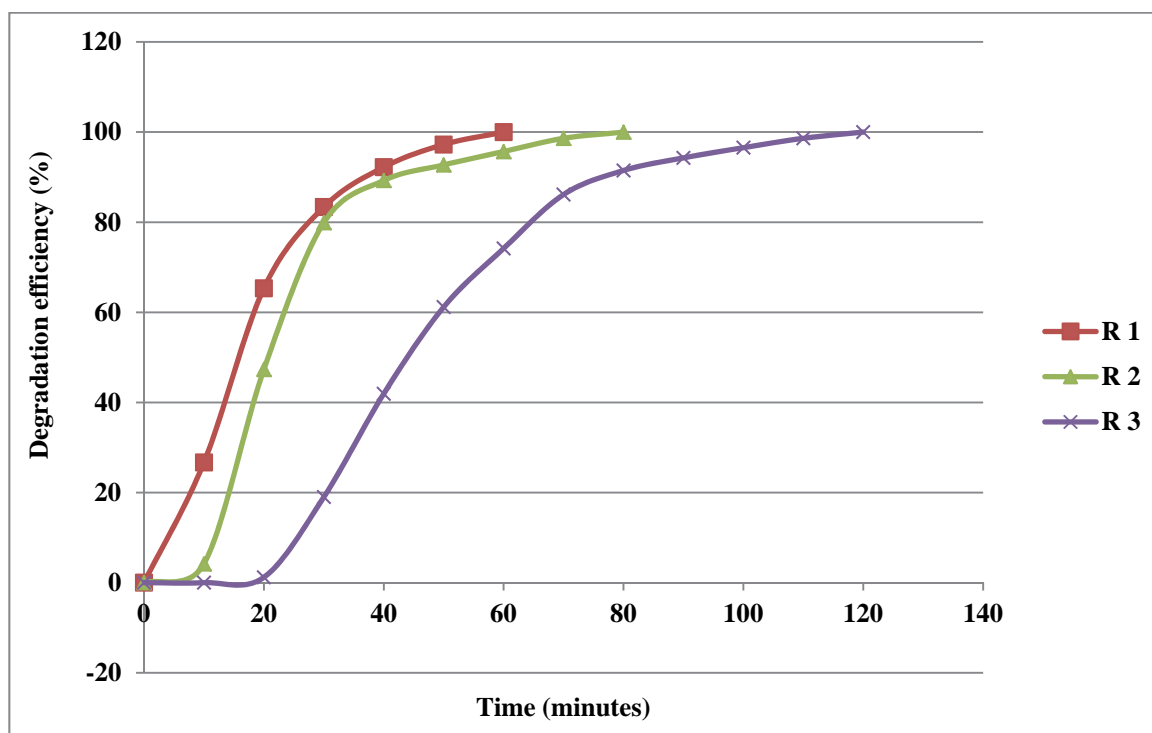


Figure 4.1: Effect of reactor configurations on MB degradation percentage. Varied parameters applied: air gap, [from 2 mm (R1), 4 mm (R2) and 6 mm (R3)]. Fixed parameters: MB concentration 5 mg/L, solution pH (various), air flow rate of 3 L/min, dye volume 1500 mL

The interaction of these species with dye could have resulted in the formation of other powerful and non-selective oxidants like OH^\cdot contributing to the quick decolourization of MB solution. Based on these observations, it was obvious that the increase of air gap in reactors 2 and 3 reduced the length and number of streamers as well as electron energy induced around the inner tube of the reactor as well as changed the flow rate of air. This eventually resulted in the decrease of oxygen molecules dissociation. Hence the decrease of active species formation that led to the diminution of MB degradation efficiency. Therefore reactor 1 was the optimum configuration used further for the current EHD system. Another aspect that might have lowered MB decolouration in reactors 2 and 3 could be the decrease of UV radiation intensity. In fact UV radiations also called photons generated in corona discharge have been proved to decompose water molecules into hydroxyl radicals and other species (Prendiville et al., 1986). Since the air gap in reactors 2 and 3 were enlarged, this might have weakened and reduced the intensity of these radiations. Therefore the energy of photons reaching the bulk solution was weak and could not dissociate water molecules as expected. This reduced the formation of reactive species and thus dramatically contributed to decrease of MB decolouration efficiency. From analysis of results presented in Figure 4.1, it was concluded that the dielectric region or air gap had an impact on the MB decolouration efficiency as colour removal percentage of MB decreased with an increase of air gap. This finding correlates with Zhang et al. (2008) observations, hence Reactor 1 was chosen as the optimum configuration for further experiments varying other parameters for MB decolouration in this study. As mentioned in literature in water/wastewater treatment technology, reactor configuration remains one of the most critical parameters.

4.3 CALCULATION OF DECOLOURIZATION EFFICIENCY USING INITIAL AND FINAL METHYLENE BLUE CONCENTRATIONS

Decolourization efficiency could be referred to as the effectiveness of colour removal of dye methylene blue by electro hydraulic discharge. Recently Kumar Reddy et al. (2013), studied the degradation and mineralization of methylene blue by dielectric barrier discharge non-thermal plasma reactor. In that study, methylene blue degradation efficiency also called degradation percentage or decolourization efficiency was calculated using the following formula:

$$\text{Degradation percentage (\%)} = [(C_o - C_t) / C_o] \times 100.$$

where C_o and C_t are the initial and the final concentrations of MB solution respectively. So in the current study, the formula highlighted above can also be used to evaluate methylene blue degradation percentage at the given initial and final concentrations. In addition using literature information and having initial and final concentrations of methylene blue precisely given in Table 4.1, the degradation efficiencies of dye after 10, 20, 30, 40, 50 and 60 minutes were calculated and reported in Table 4.2 below.

Table 4.2: Degradation efficiencies of MB at different concentrations (increment 10 mg/L)

Initial MB concentration (mg/L)	Decolourization efficiency within 60 minutes (%)					
	10 min	20 min	30 min	40 min	50 min	60 min
10	62.74	78.42	93.76	99.74	99.98	99.99
20	62.09	89.21	96.7	98.92	99.61	99.87
30	56.61	79.98	91.97	96.53	98.35	99.11
40	62.93	83.2	93.22	94.67	97.33	98.33
50	64.68	84.71	91.32	95.6	97.69	98.53

Results obtained above, showed that decolourization efficiency of MB increased with an increase of time along each series. This trend is shown in the plots presented in Figure 4.2. Degradation efficiency over time of 50 mg/L MB is supposed to be smaller than that at 40 mg/L. However the values obtained appeared to be greater than that of 40 mg/L. This could be justified by the fact that secondary species may have formed during the reaction, because the solution colour obtained within 60 minutes was green. Therefore these species could have absorbed more UV radiation, thus increasing the solution absorbance resulting in an apparently higher concentration of decolourized dye at 50 mg/L within 60 minutes. This also could have affected the rate of degradation of MB. It was apparent in Figure 4.2 that the degradation efficiency of MB decreased slightly as its concentration increased from 10 to 40 mg/L. This trend was represented again in Figure 4.3 by serial plots of decolourization efficiency vs. dye concentrations.

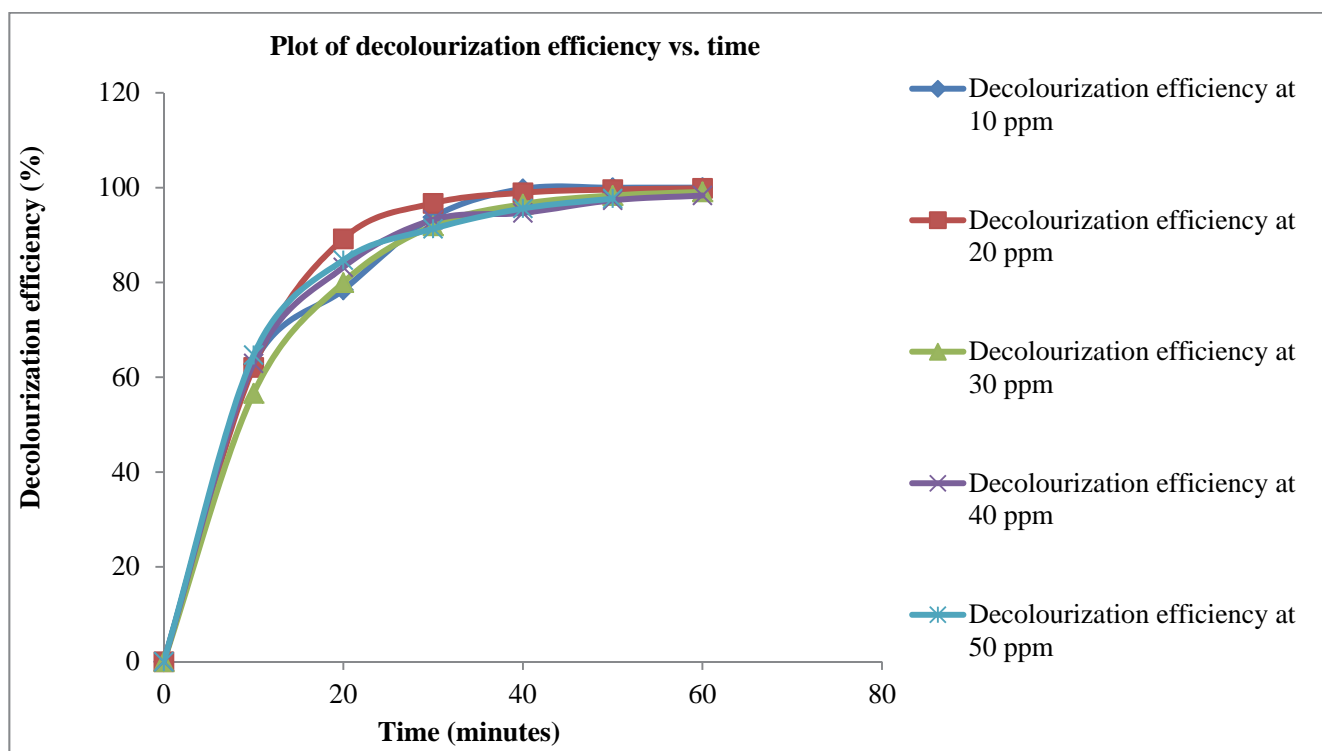


Figure 4.2: Decolourization efficiency (%) of MB of different starting concentrations vs. time

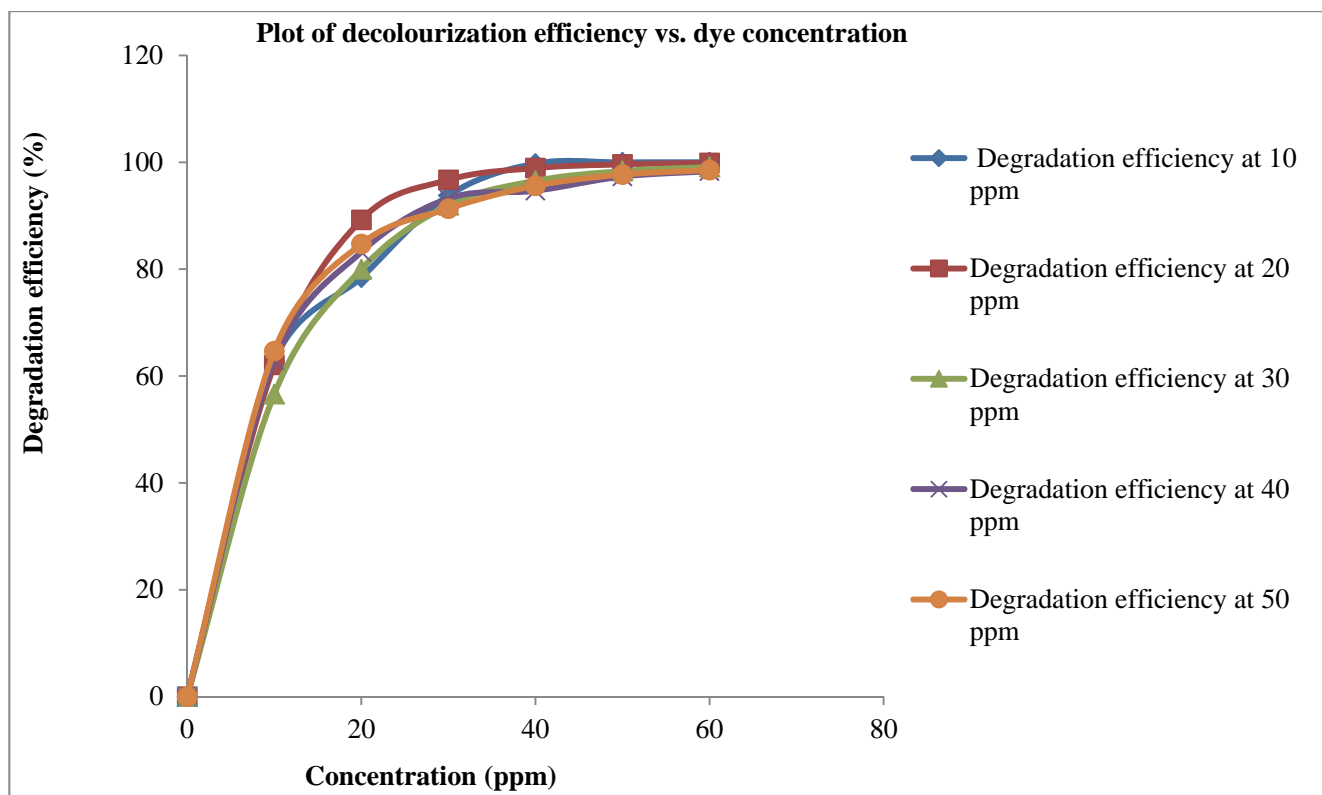


Figure 4.3: Decolourization efficiency vs. concentration of MB

4.4 RATE OF DEGRADATION

The rate of degradation of Methylene blue was one of the parameters that needed to be studied. This could give an idea of how Methylene blue degraded or decolourized not only with time but with dye concentration as well. By definition, the rate was defined as the change in concentration of Methylene blue Δ [MB] with time and given by: Rate = $-\Delta$ [MB] / time. Having the initial and final concentrations, the MB degradation rate at different sampling times was calculated (Table 4.3). Results obtained showed that as the concentration of dye increases, the rate of degradation decreased with time across the series. The second observation demonstrated that at a fixed time, the rate of degradation of MB increased along a period with an increase of concentration. All these observations are presented in Figure 4.4 below.

Table 4.3: Rate of decolourization of MB solution from 10 to 50 mg/L at increment 10

Initial concentrations (mg/L)	Rate of reaction (mg/L/min) Within 60 minutes					
	10 min	20 min	30 min	40 min	50 min	60 min
10	0.627	0.392	0.312	0.247	0.2	0.17
20	1.242	0.892	0.645	0.495	0.398	0.333
30	1.698	1.199	0.920	0.724	0.590	0.495
40	2.517	1.663	1.243	0.950	0.778	0.655
50	3.234	2.120	1.522	1.195	0.977	0.821

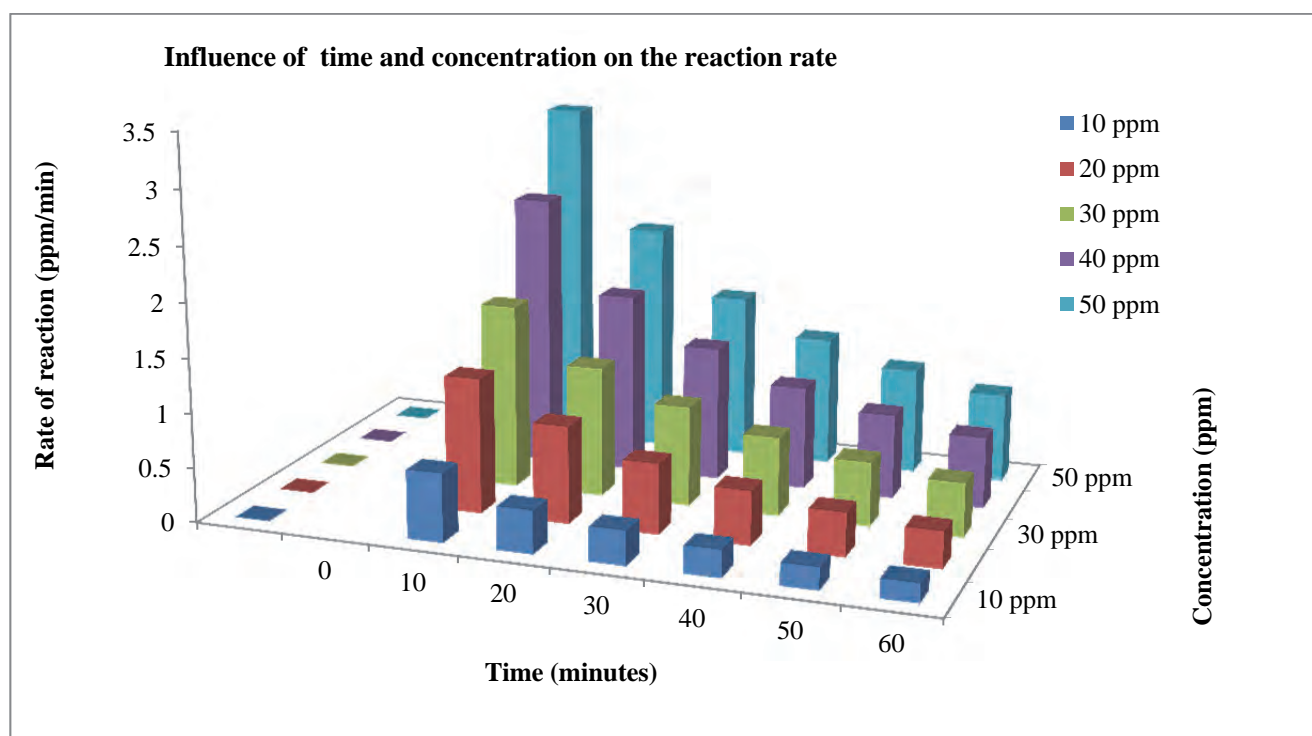


Figure 4.4: The influence of time and concentration on the reaction rate of methylene blue.

4.4.1 The effect of pH on decolourization efficiency of Methylene

The effect of the variation of pH on the decolourization efficiency of MB within 60 minutes is shown in Figure 4.5. The results obtained show that within 30 minutes under the applied conditions about 99.99% of MB colour removal was attained in all cases.

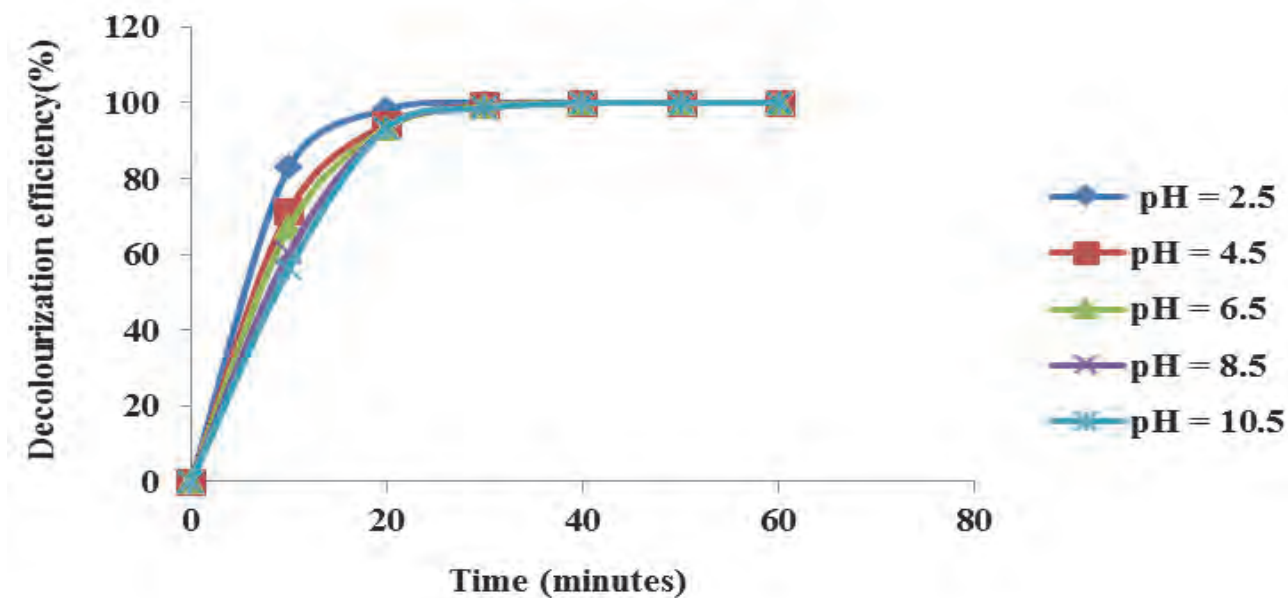


Figure 4.5: Effect of pH on decolourization efficiency of MB (experimental conditions: Applied voltage 25 V, Peak voltage 7.8 kV, air flow rate 3 L/min, air gap 2 mm, 0.5 mm silver electrode, 50 g/L of NaCl and running time 60 minutes)

In addition, Figure 4.6 below shows that within 20 minutes of the start of the experimental run, the percentage removal decreased with the increased in solution pH with an optimum removal observed at pH between 2-4. Figure 4.6 also confirmed that the best decolourization was accomplished at pH 2.5. This means that MB dye decolouration happened better in acidic conditions thus at pH less than 5. During EHD experiments, the decolourization efficiency of MB increased with decrease in solution pH. In other words, MB decolourization efficiency was higher at low pH. This was mostly due to the presence of various nitrate and sulphate by-products resulting from air and the decomposition of MB by the free reactive radicals. The existence of these inorganic acidic species was proven by nitrate and sulphate tests. Apart from this, other acidic organic residues such as carboxylic acids, etc. might also have evolved from the decomposition of MB dye in DBD system. This was supported by the decrease in TOC of the pollutant and further confirmed by the FT-IR analysis. Hence, effective decolourization of MB dye using the EHD process is pH dependent.

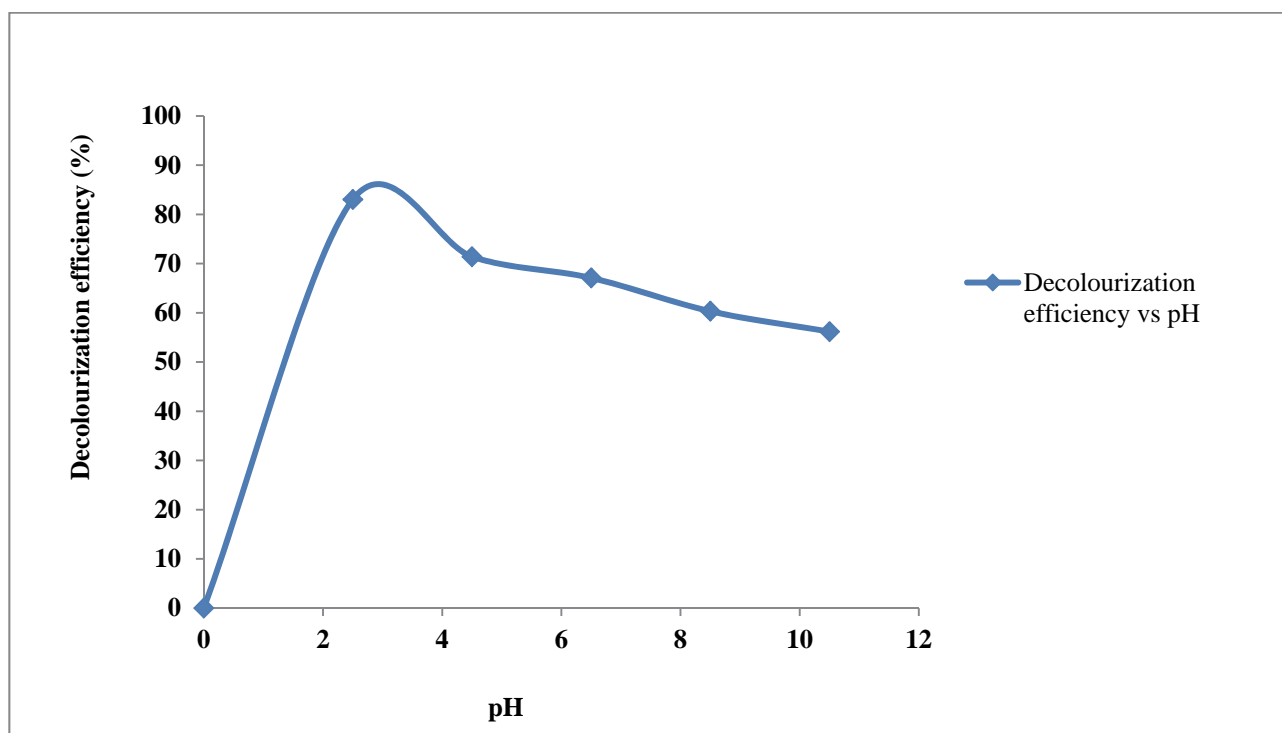


Figure 4.6: Effect of optimum pH on the decolourization efficiency of MB (experimental conditions: Applied voltage 25 V, Peak voltage 7.8 kV, air flow rate 3 L/min, 0.5 mm silver electrode, 50 g/L of NaCl and running time 20 minutes)

4.4.2 The effect of conductivity on percentage MB colour removal.

As for solution conductivity, this parameter was varied from 5 to 20 mS/cm using NaOH and HNO₃ solutions. The effect of conductivity which was varied from 5 to 20 mS/cm with increments of 5 mS/cm on the percentage MB colour removal at the applied conditions was plotted and results are presented in Figures 4.7 and 4.8 below. These figures, showed that complete decolouration of MB dye occurred within 30 minutes under the applied conditions. It was then observed that within 20 minutes of starting the experimental run, decolourization efficiency of MB increased with an increase of electrical conductivity. However the best decolouration percentage was achieved at an EC of 10 mS/cm. Since pH and electrical conductivity are inversely proportional, the impact upon one would affect the other. This also means that higher conductivity values led to low pH values. This therefore confirmed the trend observed in pH optimization which showed that good percentage removal was reached at low pH, therefore in acidic medium. Generally, the concentration of a given solution is directly related to the concentration of hydrogen (pH). For acidic solutions, the lower the pH value, the higher the concentration of hydrogen ions. At the same time, the concentration of MB in solutions sampled within 60 minutes reduces as the time increases whereas the pH decreases. This trend is consistent and agrees with Zhang et al. (2007) and Dojcinovic et al. (2011) who independently noticed a decrease in solution pH and an increase in conductivity during electrical discharges.

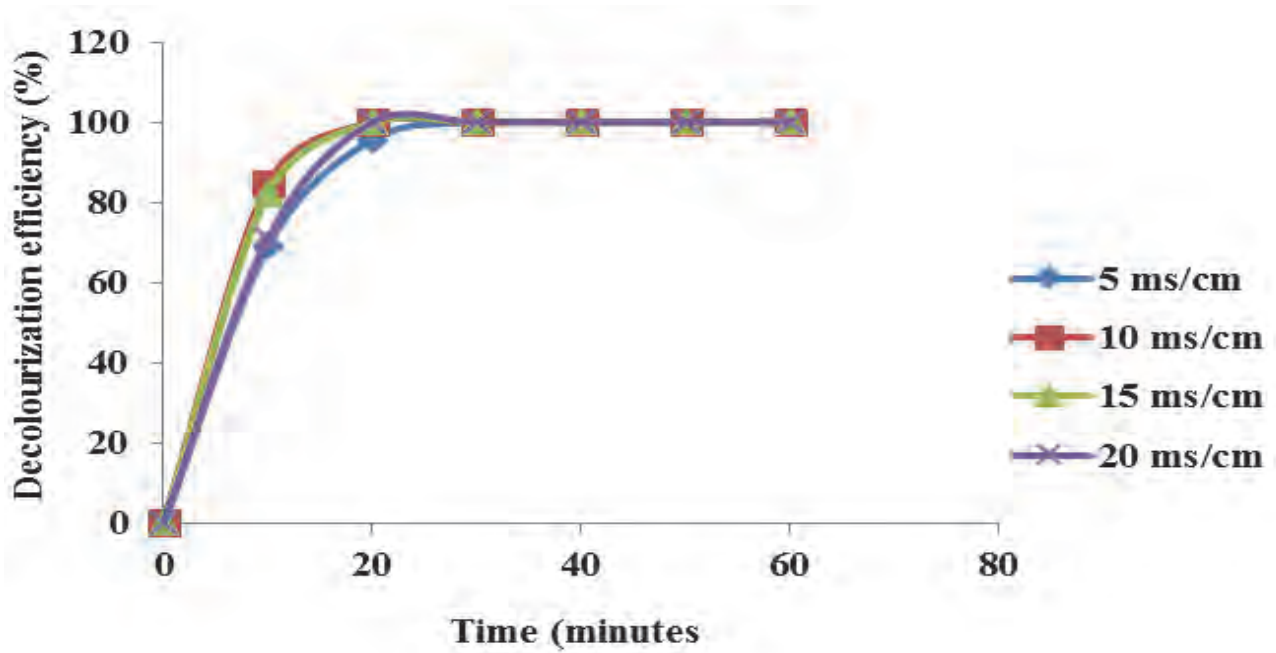


Figure 4.7: Electrical conductivity vs. time during degradation of methylene blue using electrohydraulic discharge (experimental conditions: applied voltage 25 V, peak voltage 7.8 kV, air flow rate 3 L/min, air gap 2 mm, MB concentration 5 mg/L, solution, pH 6, 50

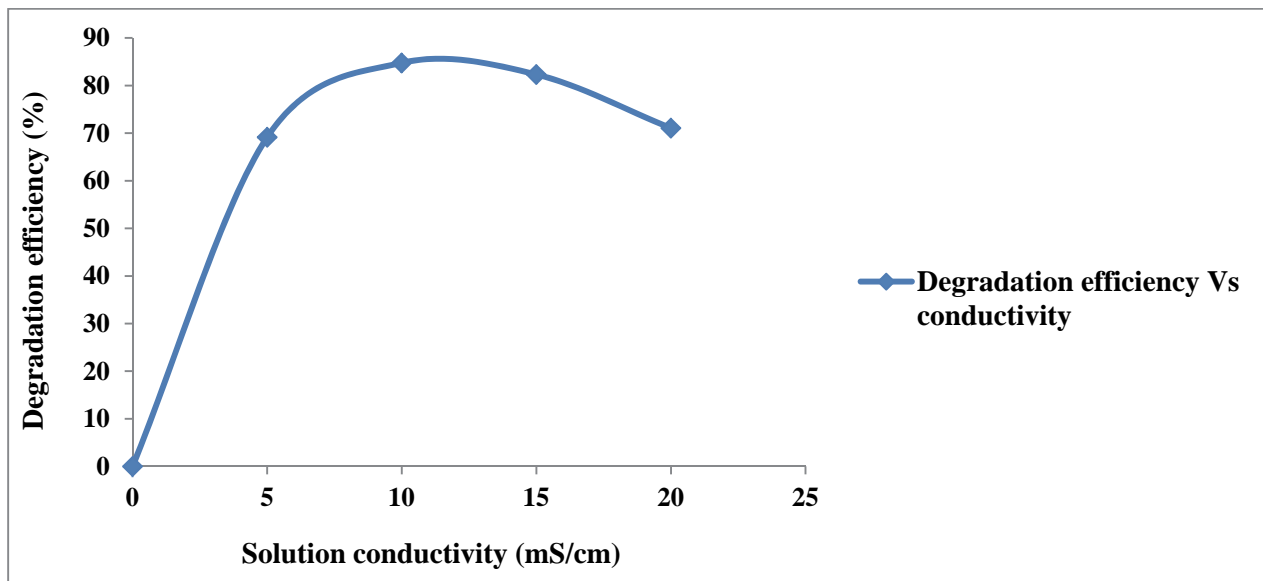


Figure 4.8: Effect of optimum electrical conductivity on degradation of methylene blue using electrohydraulic discharge (experimental conditions: applied voltage 25 V, peak voltage 7.8 kV, air flow rate 3 L/min, air gap 2 mm, MB concentration 5 mg/L, solution, pH 6

The same behaviour was also observed by Dang et al. (2008) in discharges generated directly in water. This was also corroborated from the findings of Monica Magureanu et al. (2013) on the pulsed corona discharge degradation of MB in water. The authors showed that after 15 minutes discharge, the pH of MB solution significantly decreased to 3.2 while the solution conductivity rose to 714 mS/cm. Based on these findings, it was evident that solution pH and conductivity are strongly related. In addition, concomitant with the decrease in pH and high electrical conductivity, a yellow-green colour became more intense. This was plausibly due to organic compounds resulting from the degradation of by-products in the solution depending on their concentrations or the formation of nitric and nitrous acids. According to Brisset et al. (2011) and Magureanu et al. (2013) the presence of acids might be ascribed to the formation of nitrogen oxides such as NO, NO₂, whose dissolution into liquid leads to nitrite (NO₂⁻) and nitrate ions (NO₃⁻) and ultimately forming nitric acid (HNO₃), nitrous acid (HNO₂) and peroxyxynitrous acid (ONOOH). Their formation is ascribed to the conversion of the N₂ component in the air feed. This was also observed by Manoj Kumar et al. (2013) in their study of reaction chains giving rise to the formation of intermediate organic and inorganic acids. The reactions pathway is presented below:



From these reactions, it could imply that nitrous oxides might have originated from air introduced into the system. However, the rise in electrical conductivity might have been caused by the presence of H⁺ and OH⁻ from the dissociation of water molecules as well as nitrate formation (Porter et al., 2009).

The results obtained during the variation of dye volume were plotted and presented in Figure 4.9 below. The results obtained show that complete decolourization of MB was achieved within 40 minutes irrespective of the volume of 5 mg/L solution of methylene blue used. For example at 30 minutes experimental time, 92.7% of MB colour removal was achieved with a volume of 500 mL. A similar trend was observed at 40 and 50 minutes under the applied experimental conditions. 97.58%, 99.3% and 99.48% removal were obtained with 1000 L, 1500 L or 2000 L volumes of 5 mg/L solution respectively. However, the degradation percentage varies and the decolourization efficiency of MB increased with an increase in solution volume. The reported trend could be justified by the fact that the 23 cm reactor tube was longer than the beaker, thus the generated UV radiations could not be effectively utilized as they were not completely focused in the solution for the smaller volumes used, showing that the reactor design needs optimization. Increasing dye volume led to the absorption of more of the UV radiation generated, thus enhancing the MB colour removal percentage.

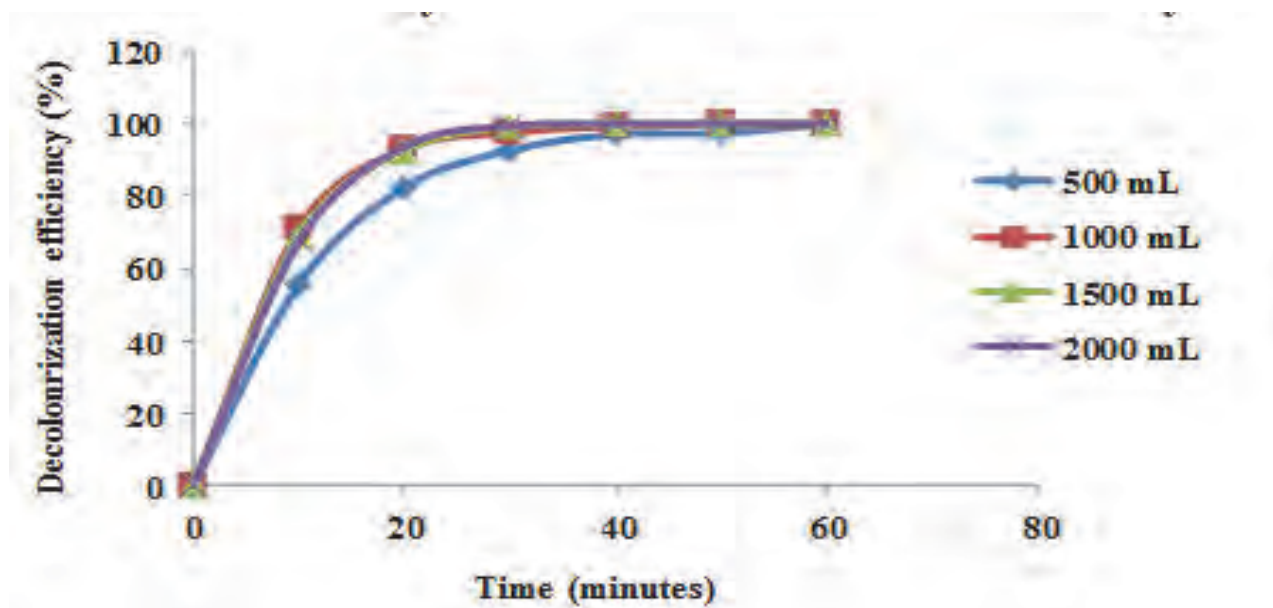


Figure 4.9: Effect of methylene blue volume on the degradation efficiency (experimental conditions: Voltage 25 V, peak voltage 8 kV, air flow rate of 3 L/min, air gap 2 mm, pH 6, MB concentration of 5 mg/L, 50 g/L NaCl electrolyte, silver electrode and running time 60 minutes)

In this experiment, 1500 mL was chosen as the optimum volume over 2000 mL because when air was passed through the system, an abundance of bubbles containing the reactive species were produced and had a longer path length in the larger volumes. However, excessive bubbles in the largest volumes used resulted in overloading of the system causing short-circuits. Even though a slight rise of MB degradation efficiency was noticed, it might be hard to generalize that dye volume has a significant effect on the decolourization achieved except to comment that the system showed no reduction in efficiency for larger volumes of the simulated waste solution. This can also be verified by the small difference between MB colour percentage removal mentioned above. Because the single reactor tube was applied, bubbles containing reactive species escaped the system, and a strong odour of ozone arose around the working system, indicating loss of ozone which could not be quantified. It is likely that other reactor configurations that sparge the bubbles more finely into the fluid, and utilize the reactive species more effectively when using and higher volumes will show an effective maximum removal depending upon the applied conditions. Currently a new reactor system is being implemented in the follow on project that will recirculate the fluid allowing better contact between reactive species in the gaseous phase and the liquid effluent to be treated.

4.4.3 Effect of initial concentration on MB decolourization BY EHD

The absorbance of the MB solution was measured within 1 hour at concentrations ranging from 0.5 to 10 mg/L with increment of 0.5 mg/L at the following EHD experimental conditions: applied voltage 25 V, Peak voltage 7.8 kV, pH (various), air gap 2 mm, air flow rate 3 L/min, were recorded and are presented in Table 4.4. From the results presented in Table 4.4, the absorbance of MB solution sampled within 1 hour of treatment in the EHD reactor showed that complete decolourization of MB was observed for 0.5 and 1 mg/L MB within 30 minutes.

Table 4.4: Absorbance of samples withdrawn every 10 minutes within 60 minutes at MB concentration ranging from 0.5 to 10 mg/L at the following EHD experimental conditions: applied voltage 25 V, Peak voltage 7.8 kV, pH (various), air gap 2 mm, air flow rate 3 L/min,

Initial conc (mg/L)	Absorbance within 60 minutes						
	0 min	10 min	20 min	30 min	40 min	50 min	60 min
0.5	0.087	0.029	0.002	0.000	0.000	0.000	0.000
1	0.161	0.007	0.000	0.000	0.000	0.000	0.000
1.5	0.323	0.031	0.009	0.002	0.000	0.000	0.000
2	0.415	0.053	0.014	0.002	0.00	0.000	0.000
2.5	0.418	0.084	0.014	0.003	0.001	0.000	0.000
3	0.485	0.060	0.009	0.005	0.000	0.000	0.000
3.5	0.453	0.040	0.009	0.007	0.003	0.000	0.000
4	0.619	0.119	0.025	0.009	0.006	0.002	0.002
4.5	0.701	0.181	0.037	0.014	0.006	0.004	0.003
5	0.742	0.194	0.004	0.020	0.009	0.004	0.004
5.5	0.707	0.167	0.029	0.010	0.005	0.002	0.000
6	0.752	0.156	0.026	0.010	0.005	0.000	0.000
6.5	0.842	0.220	0.053	0.024	0.011	0.005	0.003
7	0.862	0.287	0.077	0.026	0.011	0.006	0.005
7.5	0.896	0.232	0.060	0.023	0.015	0.009	0.006
8	0.914	0.265	0.049	0.013	0.006	0.000	0.000
8.5	0.957	0.279	0.041	0.010	0.001	0.000	0.000
9	0.996	0.198	0.044	0.016	0.010	0.005	0.005
9.5	1.036	0.319	0.113	0.046	0.016	0.009	0.005
10	2.476	1.254	0.589	0.290	0.124	0.073	0.034

Likewise from 0.5 to 5 mg/L of MB the final solution sampled within 60 minutes was clear whereas a different trend was noticed as MB concentration in solution was increased from 1.5 to 10 mg/L. The different colour changes of the final MB solution were photographed and shown in Figure 4.10. At concentrations above 5 mg/L, the colour of the solution withdrawn at 60 minutes varied from yellow to deep green as the concentration of MB increased as shown in Figure 28. Therefore the initial MB concentration had an effect on the decolourization rate by the EHD operated under the given conditions, which is as expected. This implies that 0.5 to 5 mg/L of MB is the optimum concentration range in which the current EHD system can operate perfectly in the given time frame, thus this concentration was used for further optimization of the system.

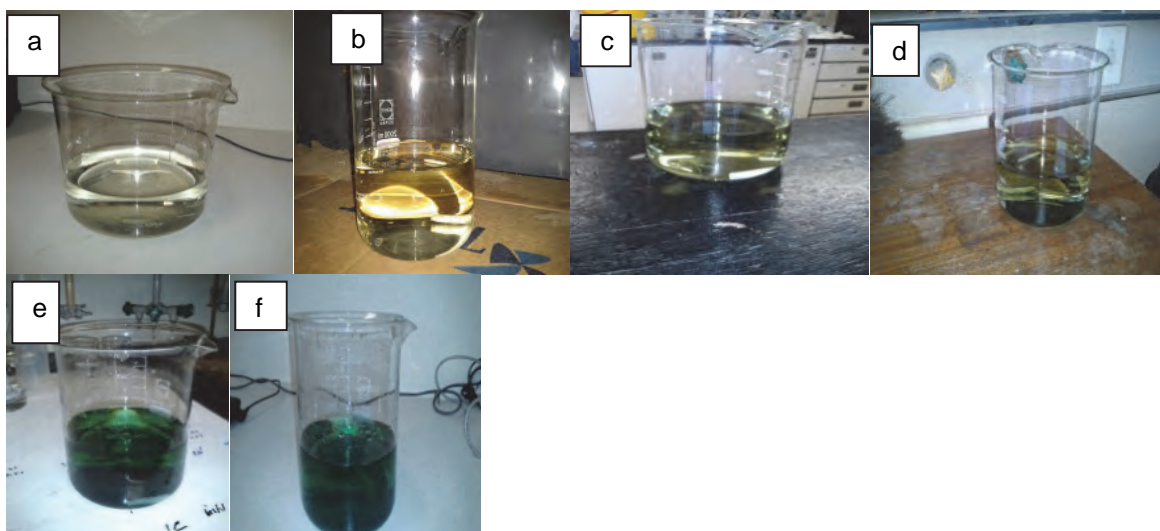


Figure 4.10: MB solutions obtained within 60 minutes at concentrations from: 0.5 to 5 mg/L (a) and above 5 mg/L (b, c, d, e and f) at the following experimental conditions: solution pH 6, air flow rate 3 L/min, air gap 2 mm, dye volume 1500 mL, 50 g/L NaCl electrolyte and silver

Similar studies on dye decolourization have been conducted by various researchers such as Inaloo et al. (2011) and Zhang et al. (2012) who also reported that dye decolourization decreases with an increase of its initial concentration. This observation was also supported by Inaloo et al. (2011) who showed that degradation efficiency of dye decreases with an increase of its concentration. In addition, Reddy et al. (2012) studied the degradation and mineralization of aqueous organic pollutants by discharge plasma. It was observed that dye colour removal was higher at low concentration because the performance of the technique used decreased with an increase of initial dye concentration. In this case it was important to assess the effect of initial concentration of MB decolourization for further optimization.

Aside from pH, electrical conductivity, and solution volume, the air flow rate is also a critical parameter in dye decolouration. So the effect of air flow rate on decolouration of MB was then studied. The results are presented in Figure 4.11. Results obtained show that the rate of dye decolourization increased with an increase in air flow rate. Theoretically, at sea level, air contains approximately 23.1% of oxygen (O₂) and 75.5% of nitrogen (N₂). Except for the fact that oxygen has unpaired electrons; it also plays an important biological role as an oxidizing agent. Therefore as more oxygen is provided, greater amounts of ozone are generated and by various chemical reactions, other active species such as hydroxyl radicals, ozone, hydrogen peroxide that facilitated dye decolourization were produced. As shown above, at 10 minutes under the applied conditions, decolourization of MB increased with an increase of air flow rate. Consequently, after 10 minutes, the maximum of 73.32% of MB colour removal was achieved. After 20 minutes 100% dye removal was observed in the case of the slower flow rates but the trend was not consistent, probably due to the residence time of gas bubbles in the liquid effluent. All further experiments were performed using 3 L/min of air which was chosen as the optimum air flow rate value for all experiments because in the results displayed above, 99.99% of colour removal was achieved at 3 L/min compared to 98.79 and 99.98 at 2 L/min and 4 L/min airflow respectively.

Also it was observed that when air flow rate was increased beyond 3 L/min, a lot of bubbles were formed leading to the solution being spilt and short-circuits occurring during electrohydraulic discharge. Apart from this, a sparking effect was also noticed which ultimately led to circuit shut down. As a consequence of this development, 3 L/min was the chosen as an optimum air flow rate for testing the current reactor configuration. The limits of the current reactor configuration will need to be evaluated and improved to provide sufficient mixing and circulation of the produced ozone without affecting the electrical circuitry.

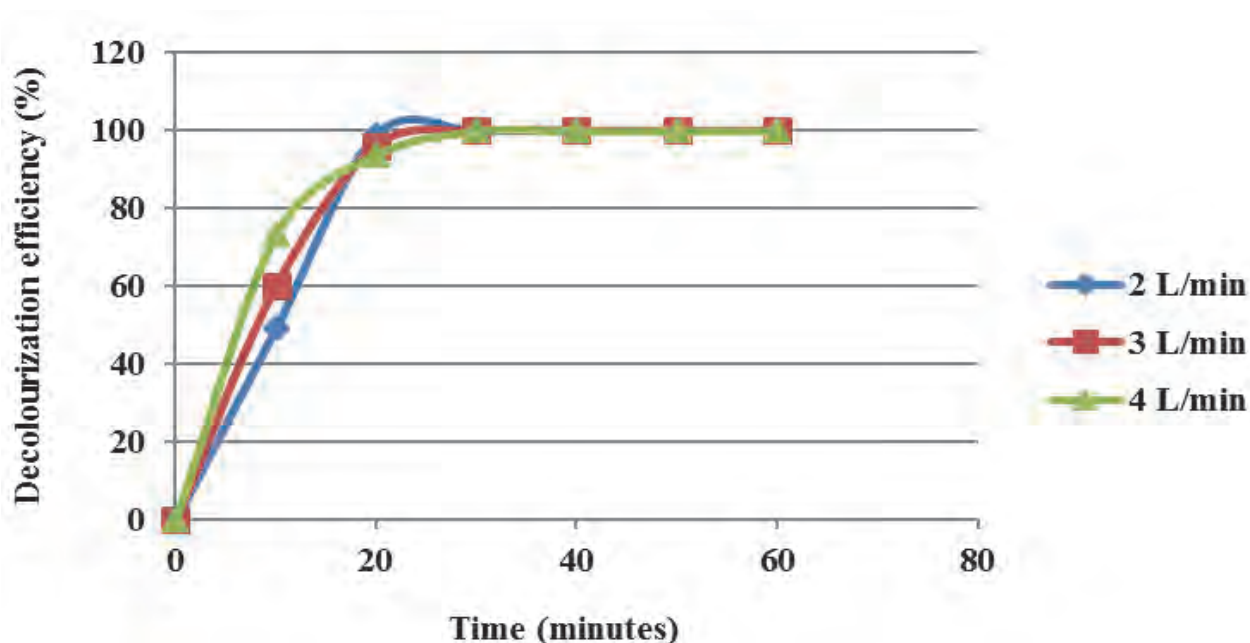


Figure 4.11: Effect of air flow rate on the degradation efficiency (experimental conditions: applied voltage 25V, peak voltage 7.8 kV, MB concentration 5 mg/L, solution pH 6, MB volume 1500 mL, 50 g/L NaCl electrolyte, air gap 2 mm, silver electrode and running time 60 minutes)

The effect of varying the NaCl electrolyte concentration in the electrode compartment on MB decolourization efficiency is shown in Figure 4.12. In this section, the NaCl electrolyte concentration in the electrode compartment experiment was repeated thrice. Results showed that there was no significant difference in methylene blue decolourization at concentrations of 10 g/L and 30 g/L of electrolyte sodium chloride. Whereas better MB colour removal was obtained when 50 g/L of sodium chloride was used as electrolyte as shown below (Figure 4.12). Since a clear trend on decolourization efficiency was not noticed when increasing electrolyte concentration, it was difficult to conclude that electrolyte concentration has an important effect on dye decolourization. Changing the type of electrolyte used may have a greater impact upon dye colour removal and should be further investigated.

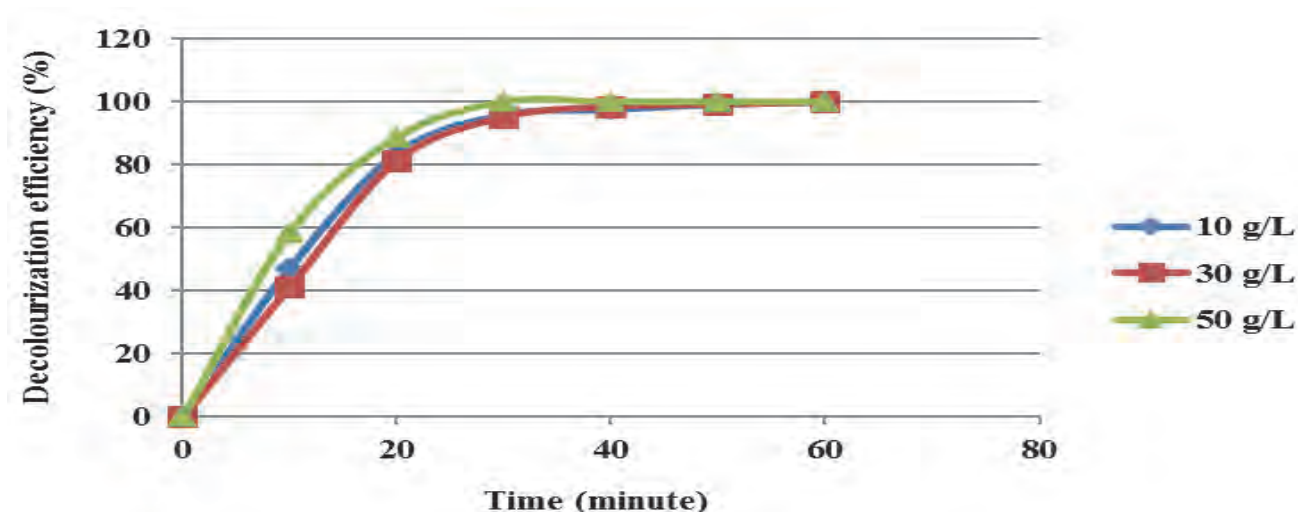


Figure 4.12: Effect of electrolyte on decolourization efficiency (experimental conditions: applied voltage 25V, peak voltage 7.8 kV, MB concentration 5 mg/L, solution pH 6, air gap 2 mm, air flow rate 3 L/min, MB volume 1500 mL, silver electrode and running time 60

The effect of the applied voltage on decolourization efficiency of Methylene blue is shown in Figure 4.13. Results obtained demonstrated that after 30 minutes under the applied experimental conditions, complete decolourization of MB was achieved at a voltage of 22 V and 25 V. After 10 minutes, 24.62% of colour removal was reached using 20 V. Likewise 40.22% and 58.58% were achieved at 22 V and 25 V respectively. This trend clearly shows that at a particular time degradation efficiency of MB increased with an increase of the applied voltage. The same trend could also be observed after 20 minutes.

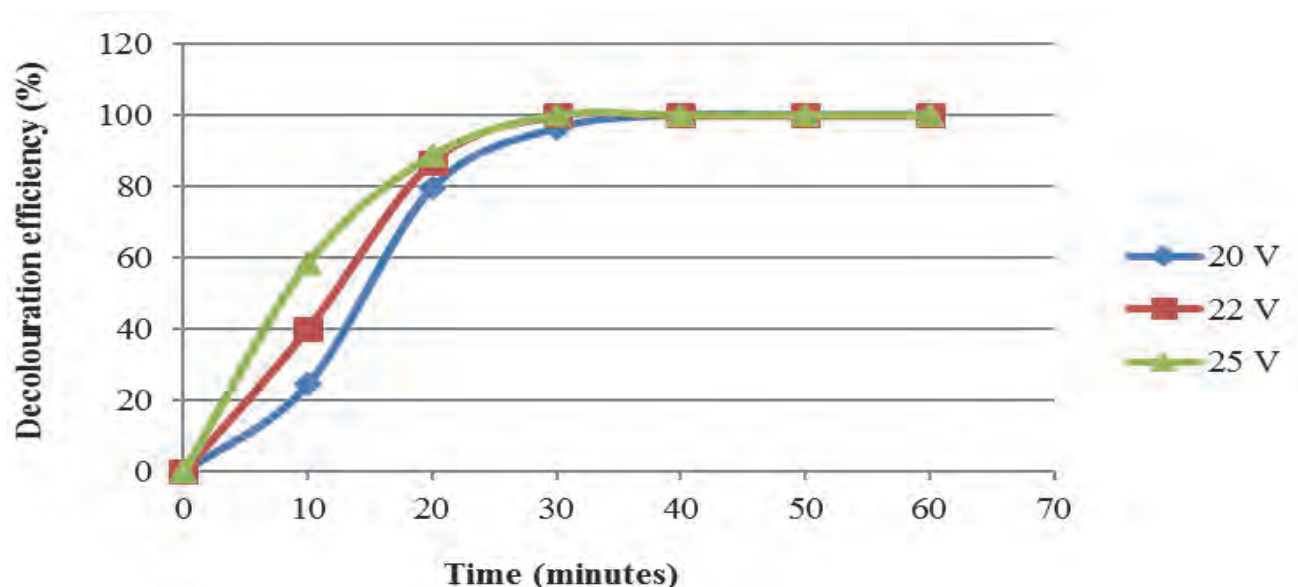


Figure 4.13: Effect of applied voltage on the degradation efficiency (experimental conditions: MB concentration 5 mg/L, solution pH 6, air gap 2 mm, air flow rate 3 L/min, dye volume 1500 mL, 50 g/L NaCl electrolyte, silver electrode and running time 60 minutes)

The results obtained based on the effect of the metal type used for the electrodes in MB decolourization efficiency were plotted and presented in Figure 4.14 below. From this figure, it was observed that after 30 minutes, decolourization of MB reached 99.84% and was complete after 40 minutes irrespective of the electrode composition. However, about 55.8% of colour removal of MB was obtained with the silver electrode, after 10 minutes under the applied conditions compared to 38.3% and 48.8%, obtained with copper and stainless steel electrodes respectively. The most rapid and highest methylene blue degradation was achieved with the silver electrode. Thus the composition of electrode has an impact on MB colour removal percentage.

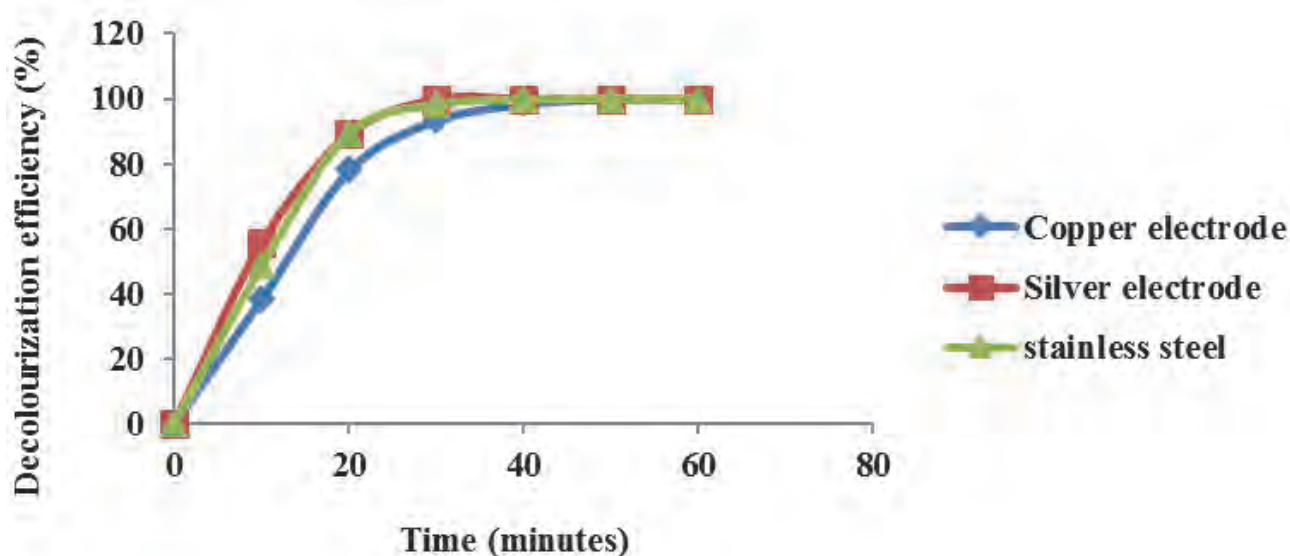


Figure 4.14: Effect of electrode type on decolourization efficiency (experimental conditions: MB concentration 5 mg/L, solution pH 6, applied voltage 25 V, peak voltage 7.8 kV, air flow rate 3 L/min, dye volume 1500 ml, 50 g/L NaCl electrolyte and running time 60 min)

The outcomes showing the impact of silver electrode diameter on MB colour removal percentage is presented in Figure 4.15. Results obtained show that complete decolouration of dye MB was achieved within 30 minutes for both silver electrode diameters investigated (0.5 and 1.5 mm). However after 10 minutes, 71.24% of colour removal was attained with the 1.5 mm diameter silver electrode compared to 55.8% achieved with the 1 mm diameter silver electrode of the same length. The same trend was observed after 20 minutes. From this analysis, it follows that the maximum decolourization of MB was reached with 1.5 mm diameter silver electrode. Thus the size of electrode can significantly affect dye colour removal.

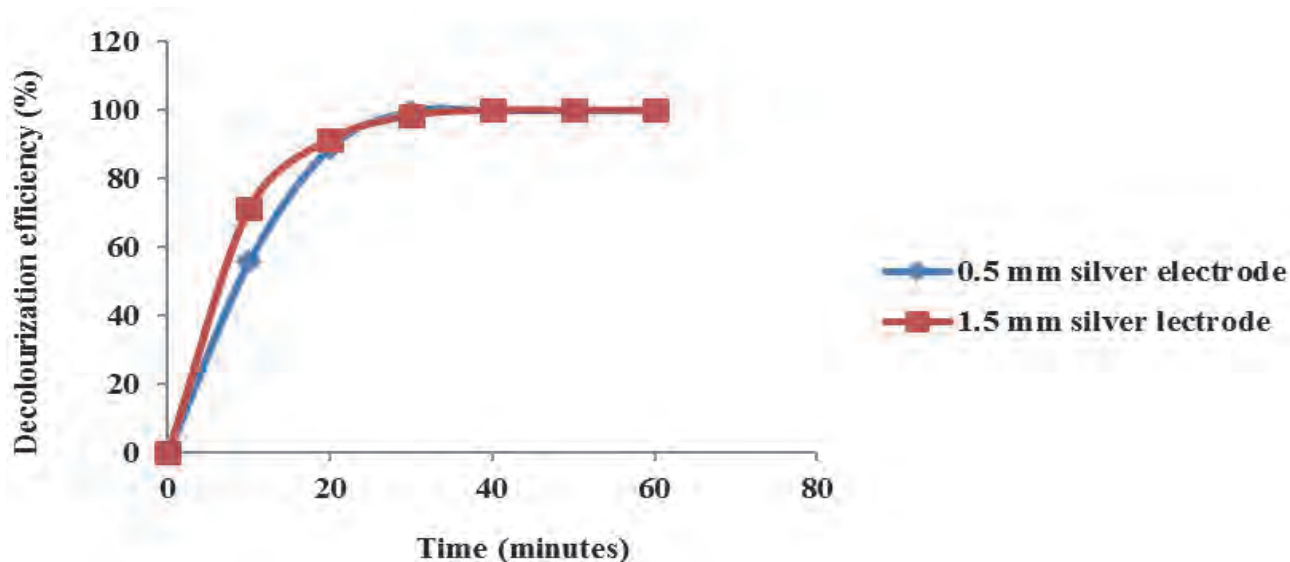


Figure 4.15: Effect of silver electrode size on the decolourization percentage of MB solution (experimental conditions: MB concentration 5 mg/L, solution pH 6, dye volume 1500 mL, applied voltage 25, peak voltage 7.8 kV, air gap 2 mm, air flow rate of 3 L/min, 50 g/L

4.4.4 Quantification and detection of free reactive species

In this section, two electrohydraulic discharge experiments were carried out at the following conditions, applied voltage 25 V, Peak voltage 7.6 kV, air flow rate 3 L/min, air gap 2 mm and MB concentration 5 mg/L, MB volume 1500 mL, 50 g/L NaCl electrolyte and 0.5 mm silver electrode. The concentration of hydrogen peroxide and ozone were detected and quantified after each 10 minute interval during the run time using Eisenberg (colorimetric) method and indigo method respectively. Results obtained are reported in Figure 4.16 below and the plots of ozone and hydrogen concentrations vs. time are presented in Table 4.5. From the above Table 4.5 and Figure 4.16, it could be observed that within the first twenty minutes, no significant amount of ozone was produced, whereas the concentration of hydrogen peroxide significantly increased and reached 6.05×10^{-7} mol/L after 10 minutes and then decreased to 4.76×10^{-7} mol/L after 20 minutes.

Table 4.5: Concentrations of H₂O₂ and O₃ estimated using de Beer's law at the following experimental conditions: applied voltage 25 V, Peak voltage 7.8 kV, air flow rate 3 L/min, air gap 2 mm, MB volume 1500 mL, 50 g/L NaCl electrolyte and 0.5 mm silver electrode.

Time (minute)	H ₂ O ₂ concentration ($\times 10^{-7}$ mol/L)	O ₃ concentration ($\times 10^{-7}$ mol/L)
10	6.05	0
20	4.76	0
30	5.4	0.5
40	4.32	0
50	3.67	1.15
60	2.8	0.65

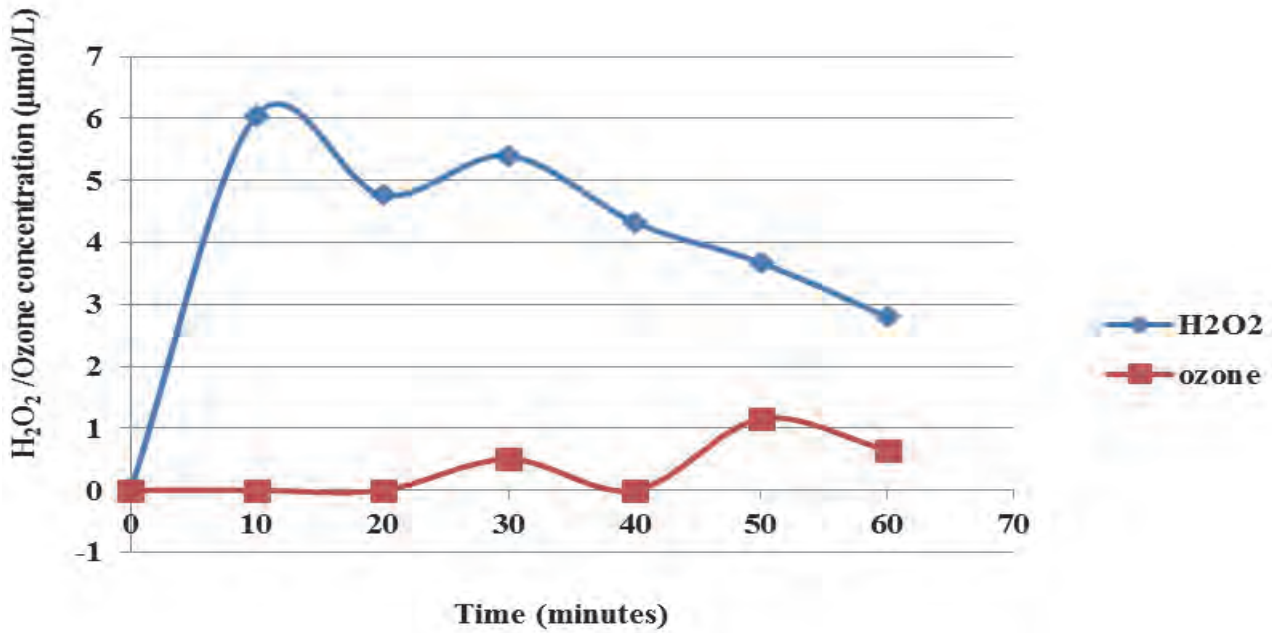
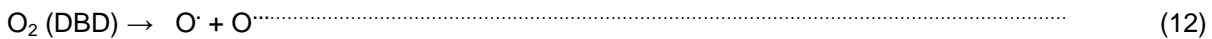


Figure 4.16: Evolution of hydrogen peroxide and ozone concentrations with time (experimental conditions: MB concentration 5 mg/L, solution pH 6, dye volume 1500 mL, applied voltage 25, peak voltage 7.8 kV, air flow rate of 3 L/min, air gap 2 mm, 50 g/L NaCl electrolyte, 0.5 mm silver electrode

This shows that hydrogen peroxide rather than ozone is the first species to be formed. Its high concentration after 10 and 20 minutes are thought to be mainly responsible for the MB degradation trend observed in the first stages of the experiment and were probably the result of various chemical reactions between ionic species and peroxide in the bulk solution. Active species such as hydroxyl radicals resulting from water molecule dissociation recombine to form hydrogen peroxide. Apart from this, hydro peroxide radicals (HO₂[·]) generated in the system via chemical processes induced in water might have reacted with atomic hydrogen (H[·]) to produce hydrogen peroxide. This could be further supported by equations highlighted by Tarr et al. (2003) as follows:



It is possible that ozone formation during the first 20 minutes was not significant because the oxygen dissociated into singlet atomic oxygen which reaction might have taken time to be completed. According to Prendiville et al. (1986) the produced atomic oxygen reacts with oxygen molecules to yield ozone as shown in the following chemical equations.



In addition, from 20 to 30 minutes, both the concentration of hydrogen peroxide and that of ozone showed a sharp increase until these species reached 4.5×10^{-7} mol/L and 0.5×10^{-7} mol/L respectively. The presence of these species after 30 minutes was followed by a slight decrease for 10 minutes. At 30 minutes, hydrogen peroxide and ozone might have reacted to generate hydroxyl radicals which are considered as powerful oxidants that attacked methylene blue dye and thus led to complete decolourization within 40 minutes. Beyond this time, the concentration of hydrogen peroxide decreased continuously while that of ozone continued to rise in a sinusoidal fashion. This could be explained by the fact that from 30 up to 60 minutes hydrogen peroxide was being used to generate other active species that certainly contributed to the formation hydroxyl radicals. Meanwhile the fluctuating production of ozone might be due to the recombination of those species as shown in chemical equations suggested by Tarr et al. (2003).



4.4.5 Effect of time on MB decolourization efficiency

The decolourization efficiency of MB (D %), was determined using the formula suggested in equation 3 by (Luís et al., 2011), given by:

$$D\% = [(A_0 - A_t) / A_0] \times 100 \dots\dots\dots (22)$$

Where A₀ and A_t stand for the absorbance at treatment time 0 and t, respectively. So the estimated MB decolourization efficiencies in 0.5-10 mg/L concentration range at specific time intervals was recorded and is shown in Table 4.6, and was plotted and is exhibited in Figure 4.17.

Table 4.6: Decolourization efficiency of samples withdrawn every 10 minutes within 60 minutes at concentration ranging from 0.5 to 10 mg/L with increment 0.5 (experimental conditions: applied voltage 25 V, Peak voltage 7.8 kV, pH (various), air flow rate 3 L/min, air gap 2 mm, 0.5 mm silver electrode

Initial concentrations (mg/L)	D%					
	10 min	20 min	30 min	40 min	50 min	60 min
0.5	66.66	97.7	99.999	99.999	99.999	99.999
1	95.65	99.999	99.999	99.999	99.999	99.999
1.5	90.4.	97.21	99.38	99.999	99.999	99.999
2	87.22	96.63	99.52	99.999	99.999	99.999
2.5	79.90	96.65	99.28	99.76	99.999	99.999
3	87.63	98.14	98.97	99.999	99.999	99.999
3.5	91.2	98.01	98.45	99.34	99.999	99.999
4	80.77	95.96	98.4	99.03	99.67	99.67
4.5	74.2	94.72	98.00	99.14	99.43	99.57
5	73.85	99.46	97.30	98.78	99.46	99.46
5.5	76.37	95.89	98.58	99.29	99.71	99.999
6	79.25	96.54	98.67	99.33	99.999	99.999
6.5	73.87	93.70	97.14	98.69	99.40	99.64
7	66.70	91.06	96.98	98.72	99.30	99.41
7.5	74.10	93.30	97.43	98.33	98.99	99.33
8	71.0	94.64	98.6	9.34	99.34	99.34
8.5	70.84	95.71	98.95	99.89	99.999	99.999
9	80.12	95.58	98.39	98.99	99.49	99.5
9.5	69.21	89.09	95.55	98.45	99.13	99.52
10	49.35	76.21	88.28	94.99	97.05	98.62

Since the tabulated trend between concentration, time and decolourization efficiency was not well observed in table form, decolourization efficiency at specific times such as those at 10, 30 and 60 minutes of the experiment were selected and plotted in Figure 4.17. The results obtained showed that after 10 minutes of the experiment, decolourization efficiency fluctuated with increasing MB concentration and tended to decrease with an increase of MB concentration. Degradation efficiency at 30 and 60 minutes also showed a slight decrease with an increase MB concentration over time. Hence the performance of the actual EHD reactor slightly decreased with an increase of dye concentration but adjusting the time could compensate for the decrease in efficiency at higher MB concentrations.

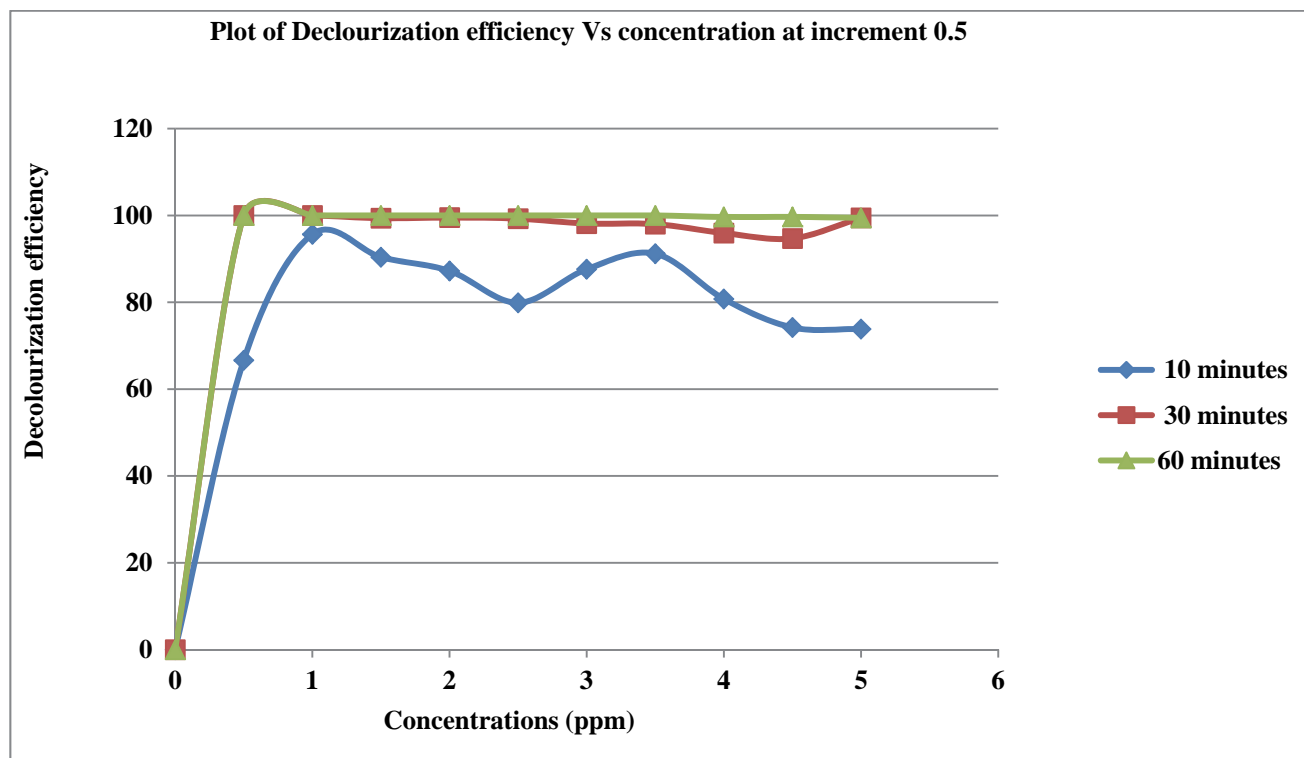


Figure 4.17: Effect of time and concentration on MB decolourization efficiency at the following experimental conditions: applied voltage 25 V, Peak voltage 7.8 kV, pH (various), air flow rate 3 L/min, air gap 2 mm, MB volume 1500 mL, 50 g/L NaCl electrolyte and 0.5 mm silver electrode

Although the current EHD system was proved to completely decolourize MB at 5 mg/L, this does not mean MB was also degraded and mineralized at that concentration. Therefore there was a need to investigate complete MB degradation using analytical techniques such as UV-vis, FT-IR, TOC, COD, etc. to characterise the final solution of treated MB. The characterization techniques used are covered in detail in the sections that follow.

4.5 ULTRA VIOLET – VISIBLE SPECTROSCOPY (UV-VIS)

UV-vis has been widely used to follow the degradation of the substance of interest. MB (Figure 4.18) was used as a model compound in water treated using the EHD system, which was applied for the decomposition of MB during plasma treatment. The UV-vis spectra obtained for untreated and treated MB are shown in Figure 4.19.

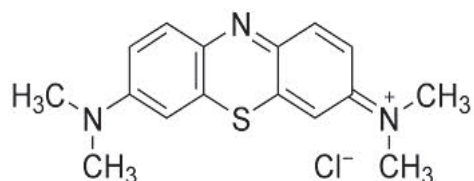


Figure 4.18: Methylene blue structure

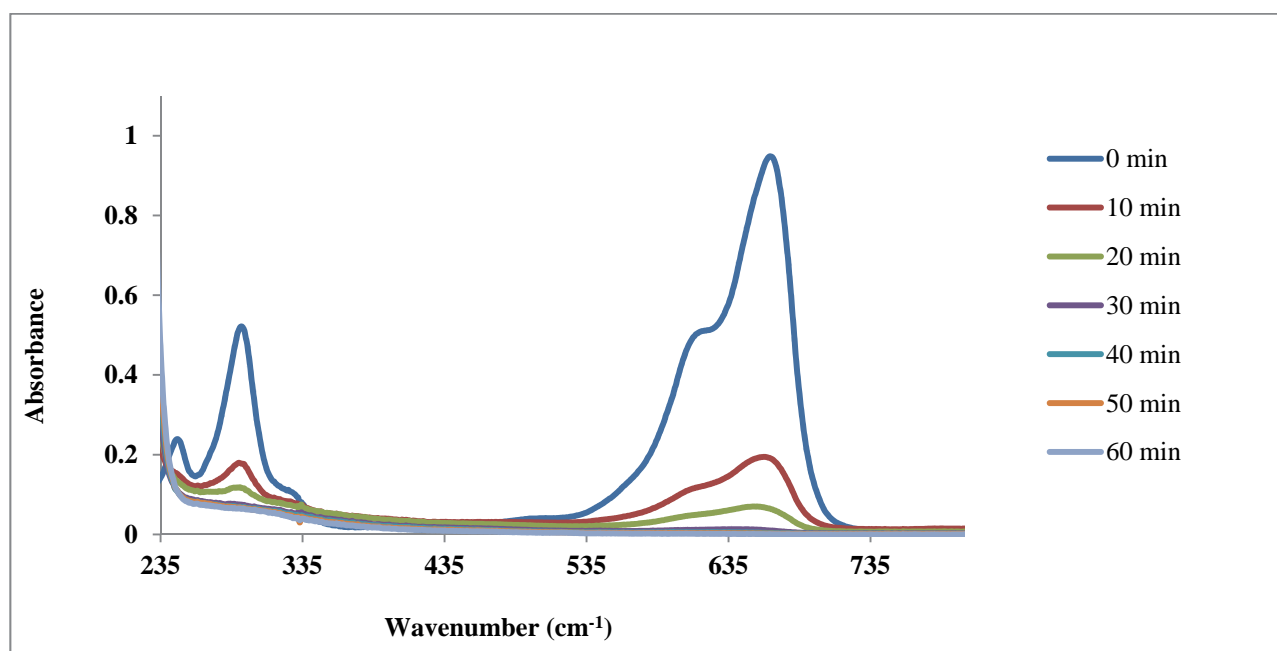


Figure 4.19: Ultra violet – Visible Spectra of untreated and treated MB solutions at different times at the following experimental conditions: applied voltage 25 V, Peak voltage 7.8 kV, pH (various), air gap 2 mm, air flow rate 3 L/min, MB volume 1500 mL, 50 g/L NaCl electrolyte.

Figure 4.19 shows UV spectra of the degradation of MB carried out within 60 minutes and where the solution was sampled every 10 minutes. The UV-vis spectra in Figure 4.19 show that MB absorption bands occurred within two distinct regions. Higher energy absorption bands occurred between 535 cm⁻¹ and 735 cm⁻¹ and lower energy absorption bands appeared in the 235-335 cm⁻¹ range. However, nothing was observed between the two absorption regions. In addition, the spectra show a progressive decrease of the intensity absorption bands over time, and therefore demonstrate a considerable decrease of MB concentration, hence increasing degradation of MB with an increase of the treatment time. In addition, the spectra show that

complete decolourization of MB was achieved within 30 minutes because absorption bands obtained after 40, 50 and 60 minutes overlap one another and lie closely with the x-axis. This implies that after 30 minutes of the experiment, MB was decolourized or totally degraded. This statement is in conformity with the plot of intensity over time results shown in Figure 4.20.

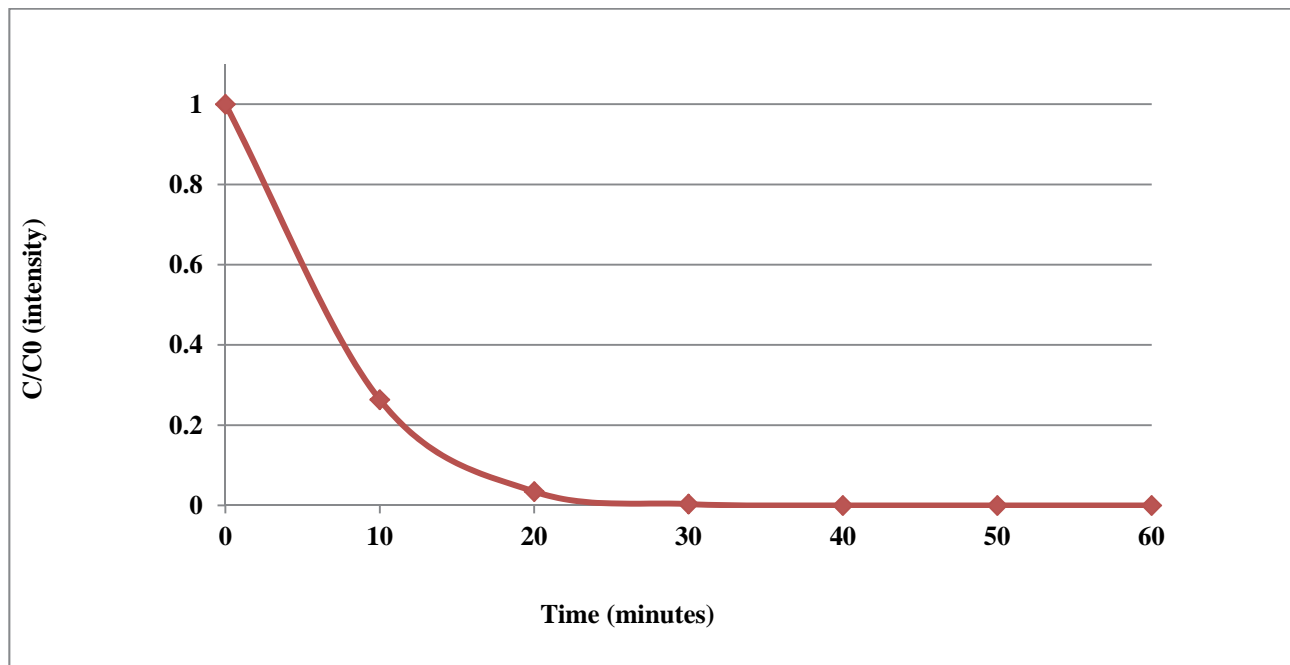


Figure 4.20: Intensity Vs time of MB degradation showing progressive degradation of MB over time (using UV-vis data)

Indeed, some organic molecules and functional groups absorb electromagnetic radiations in the UV/visible region that is, wavelength in the 190-800 nm range. As for electron transition phenomenon in organic molecules, except for alkanes, electrons may undergo several transitions where some are allowed transitions and others are referred to as forbidden transitions. Based on this, the appearance of absorption bands of spectra presented in Figure 4.19 in two different regions could be the result of electron transitions from the highest occupied molecular orbital (HOMO) to the lowest unoccupied molecular orbital (LUMO) of higher energy when MB molecule absorbs energy. Whereas, the region of spectra without absorption bands in Figure 37 might result from the forbidden transitions. Generally, organic molecules such as dyes contain a chromophoric part that is responsible for giving rise to the UV or visible spectrum. An example of this is the $=N^+(CH_3)_2$ group in Methylene blue structure as highlighted by Magureanu et al. (2007). So the rapid decolourization of MB observed within 20 minutes could be due to the destruction of the $=N^+(CH_3)_2$ group by hydroxyl radicals. This is because apart from C-S⁺=C functional group in methylene blue structure, the nitrogen atom in $=N^+(CH_3)_2$ group is also an electrophilic centre that is attacked by powerful OH radicals during plasma exposure. This was also confirmed by Yao et al. (2010). Moreover, substitution of hydrogen by auxochrome groups such as methyl, hydroxyl, alkoxy, halogen and amino groups on a basic chromophoric structure changes the intensity of absorption and possibly the wavelength.

Consequently, the appearance of absorption bands in the higher energy range of spectra (535 cm⁻¹ - 735 cm⁻¹ range) could result from the substitution of hydrogen by methyl group in basic chromophoric structure (=N⁺(CH₃)₂) of MB. Furthermore, the appearance of absorption bands in the range of 250 cm⁻¹ to 310 cm⁻¹ observed from these spectra is probably due to aromatic rings that are detectable in this range because of their conjugated pi electron system.

As a whole, the decline of peak intensity in the UV-vis absorption spectra presented in Figure 37 and results given in Figure 4.20 show a decrease of MB concentration with time. These were just visible observations; however the theoretical observations behind the nature of ionic and molecular species present in treated and untreated MB sample still remain undefined. Therefore analysis of MB samples using FT-IR spectroscopy could give qualitative information of the samples' organic content to determine if intermediate products still remain in solution.

4.6 FT-IR SPECTRUM OF DEIONISED WATER AND MB SAMPLES

The main goal of this section was to compare the existing stretching vibrations of functional groups in the raw and treated MB, hence showing the possible formation of new intermediates during treatment of MB. The FT-IR spectra of deionised water, deionised water + MB and that of treated MB solution are presented in Figure 4.21.

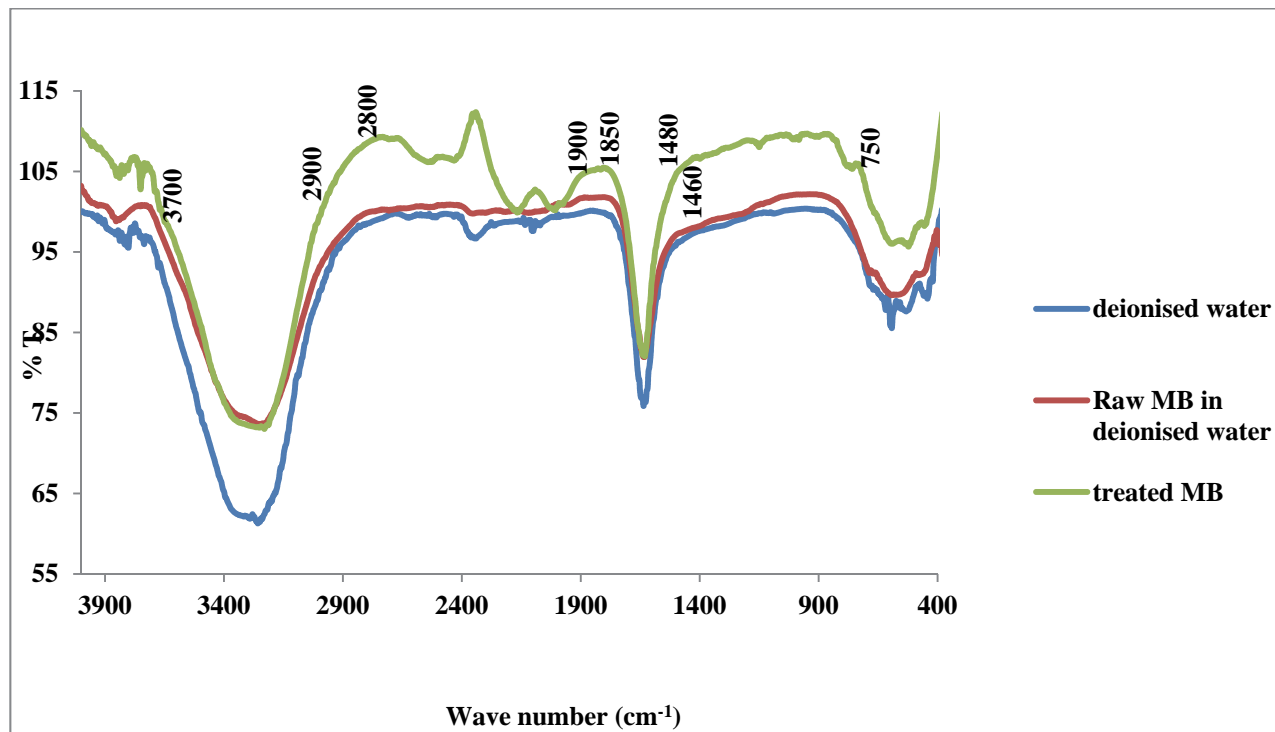


Figure 4.21: FTIR Spectra of deionised water, deionised water + MB and that of treated MB solution

The FT-IR spectra shown in Figure 4.21 can be divided into the following regions: A (3700-2700 cm⁻¹), B (2800-1900 cm⁻¹), C (1850-1480 cm⁻¹), D (1460-750 cm⁻¹). In all these absorption bands it can be noticed that spectral bands of raw and treated MB shifted from that of deionised water even though their shapes around certain regions look similar. This is because when dissolving MB in deionised water, some hydroxyl groups might have been replaced by other functional groups leading to the compression of bands in raw and treated MB spectra, hence their shift. Likewise in certain absorption regions, it can also be seen that the spectrum of treated MB is shifted compared to those of raw MB and that of water. This implies that some chemical reactions, mainly oxidation of MB, might have occurred during the plasma treatment. Moreover, in region A (3700-2700 cm⁻¹), despite the shift of spectral bands of MB samples from that of water, the wide and broad band mostly between 3600 cm⁻¹ and 3040 cm⁻¹ is still persistent. This could be due to the overlap of OH and the symmetric N-H stretching vibrations, whereby OH stretching might be due to water and the N-H could result from amines, or amide functional groups present in treated and untreated MB samples. The anti-symmetric NH₂ stretching vibrations usually observed in 3300-3100 cm⁻¹ and 3140-3350 cm⁻¹ respectively might also appear in this region. As for region B (2800-1900 cm⁻¹), apart from the significant shift of peaks in the spectrum of treated samples compared to those of raw MB and deionised water, about four new absorption bands were formed, whereas such bands were almost invisible in raw MB and deionised water. The resulting vibration bands are probably due to stretching vibrations of new functional groups. The first two bands appearing at 2590 cm⁻¹ and 2392 cm⁻¹ can be attributed to S-H and N-H⁺ stretching vibrations. The last two bands in region B are related to C ≡ C and C ≡ N appearing at 2167 cm⁻¹ and 2000 cm⁻¹ and can probably be due to the presence of unsaturated compounds in the treated MB.

In addition, in region C (1850-1480 cm⁻¹), for treated and untreated samples, MB spectra show a sharp and intense overlapping peak which is shifted compared to that of deionised water. This peak is probably due to the overlapping of C=N, C=C, N-H and probably C=O stretching vibrations. Thus C=N, C=C, N-H bands are more likely to appear in 1740-1650 cm⁻¹ sub-range. The C=O stretching vibrations appears around 1700 cm⁻¹ and characterise the presence of carboxylic acid by-products in treated MB solution. In region D (1460-750 cm⁻¹), although treated MB spectrum is highly shifted compared to that of raw MB and deionised water, a number of small absorption bands appeared. Likewise the band at 1360 and 1430 cm⁻¹ can be assigned to in-phase and out of phase CH₃ groups. Aliphatic NO₂ group in 1390-1300 sub-regions can also be visualized. Finally, C-N and C-O stretching vibration can be localised in the 1220-750 sub-range.

From the analysis of these FTIR results, it can be inferred that oxidation of MB by reactive species (such as OH radicals, H₂O₂, O₃, etc. generated in plasma) during electrical discharge leads to the formation of various intermediate MB by-products. These latter could be further mineralised to CO₂ and H₂O over time. In summary, despite the fact that FT-IR spectra analysed above showed that some functional groups (such as OH and N-H) in the initial MB solution were still present in the treated solution, the appearance of new stretching vibrations, hence the appearance of new organic compounds in the treated sample implies that MB degraded and therefore decomposed to various different intermediates by-products. Apart from these qualitative analysis performed on MB samples, more evidence on the degradation by-products was needed. Therefore quantitative investigation of MB solutions sampled before and after treatment was of great importance.

4.6.1 Quantitative parameters of MB degradation

The degradability of MB during the EHD experiment was evaluated in terms of parameters such as total organic carbon (TOC), chemical oxygen demand (COD), sulphate content, nitrogen (as nitrate + nitrite) content as explained in chapter three. Results obtained from these methods are presented in Table 4.7.

Table 4.7: Ecological parameters of untreated and treated MB solution

Analysis	Unit	Raw MB	Treated MB
Sulphate as SO ₄ Dissolved	mg/L	1.5	1.1
Nitrate + Nitrite as N	mg/L	Not detected	16
Total Organic Carbon (TOC)	mg/L	8.3	3.9
Chemical Oxygen Demand (COD)	mg/L	<5	<5

Table 4.7 shows that, sulphate content in samples decreased from 1.5 mg/L before treatment to 1.1 mg/L after treatment, showing a decrease of sulphur (as sulphate) during the EHD experiment. On the other hand, about 16 mg/L of (nitrate + nitrite) as nitrogen content was found. In addition, the TOC content of untreated MB sample was 8.3 mg/L which decreased to 3.9 after 60 minutes of treatment. MB chemical oxygen demand (COD) content before and after treatment was less than 5 mg/L which is within permissible limit recommended by the World Health Organization (WHO) regulations. The decrease of sulphate content during EHD is probably due to the breaking of C-S⁺=C bonds in the MB molecule. In fact, the sulphur atom in MB frame work is a strong electrophilic centre. So when the dye was exposed to electrical discharge in air, oxidising species such as O₃, H₂O₂ and probably OH generated in plasma are primarily attracted to electron deficient sites. Therefore, the OH[·] radicals attack on bonds in C-S⁺=C functional group probably leads to the formation of SO₄²⁻ ions and other intermediates. This was previously demonstrated by Houas et al. (2001).

Moreover, the 16 mg/L of nitrogen content in the treated solution might have evolved from the decomposition of MB molecule by reactive species or from the introduced air that was used as a feeding gas. Even though air was used as oxygen provider for the EHD system, it should be recalled that air largely consists of nitrogen and a small amount of oxygen. Therefore it can be inferred that the identified nitrogen content is mostly derived from air. A similar opinion was also reported by Magureanu et al. (2013) who demonstrated that nitrogen based compounds detected in plasma treated MB sample mainly evolved from air and not from MB degradation. As for the total organic carbon, its decrease from 8.3 to 3.9 mg/L shows that the long carbon framework of the MB molecule was broken into small carbon chain intermediates. This was also highlighted by Houas et al. (2001). So the TOC efficiency was then calculated according to the formula suggested by Reddy et al. (2014) and given by:

$$\text{TOC removal percentage \%} = [(t_0 - t)/t_0] \times 100 \quad \dots\dots\dots (23)$$

So for the current study, TOC removal percentage was calculated as follows:

$$\begin{aligned} \text{TOC removal percentage \%} &= [(8.3 - 3.9)/8] \times 100 \\ &= 53\% \end{aligned}$$

This means that at 5 mg/L, about 53% of MB degradation was achieved over time under the applied conditions. The degradation pathway of methylene blue is indicated in Figure 4.22. This once again shows that decolourization does not mean degradation. Even if 100% of MB decolourization at 5 mg/L was achieved within 60 minutes, only 53% of its carbon content was removed by the EHD reactor system.

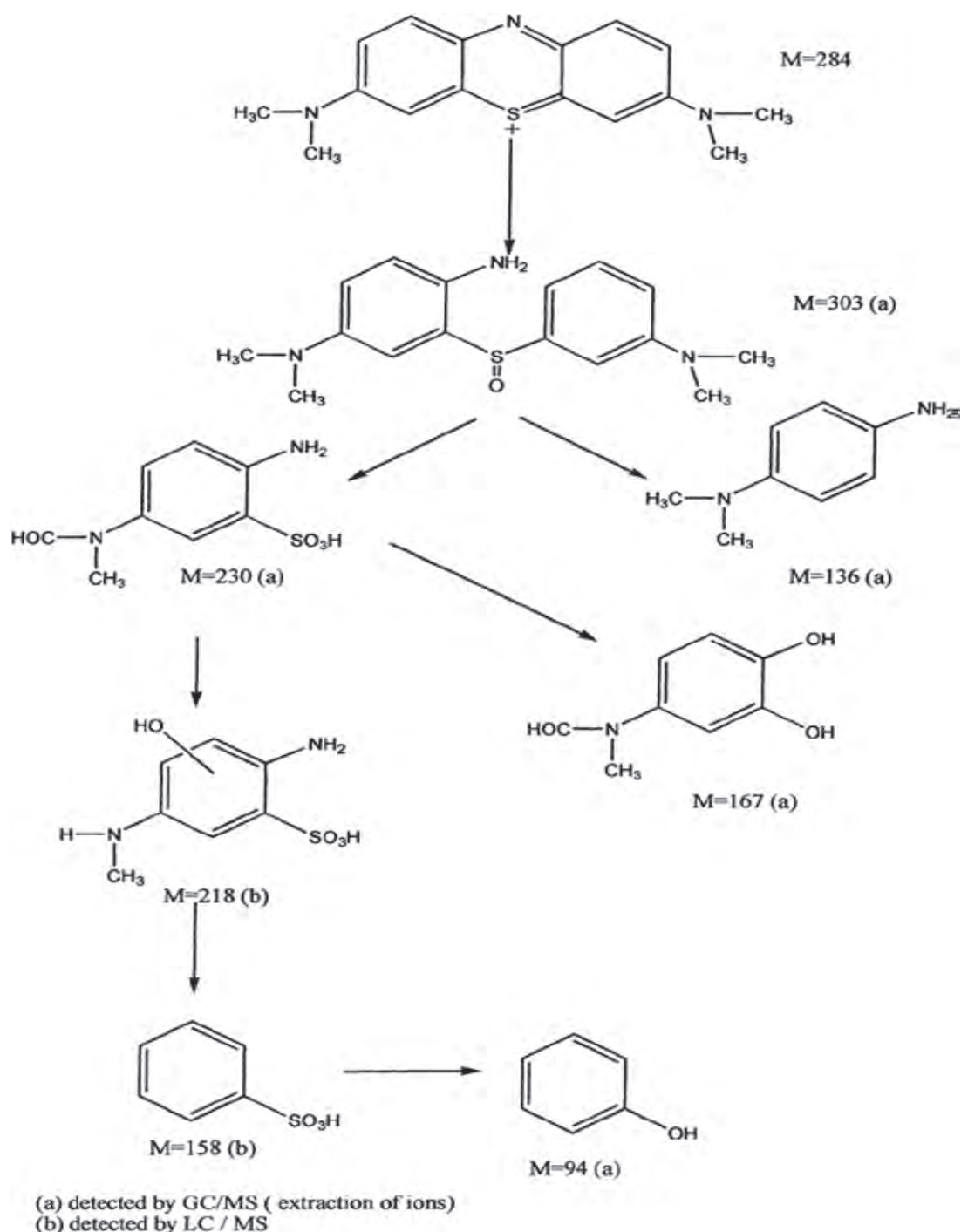


Figure 4.22: Pathway of MB decomposition (Houas et al., 2001).

The above conversion is not in agreement with 98% removal reported by Vujevic et al. (2004) but closely related to 48% removal obtained by Reddy et al. (2012). In addition, the inconsistency of results reported in literature and those of the current work could be due to experimental conditions used. Therefore, implementation of the present EHD system could be significant in achieving higher TOC removal not only for MB but for any other type of pollutants. Furthermore, the large difference between TOC removal percentages reported by Vujevic et al. (2004), Reddy et al. (2012) and 53% of the present study could be explained by the statement about salts and solution pH raised by Salome and colleagues in 2006. In fact, Salome et al. (2006) highlighted that the presence of salt in treated wastewater by plasma discharge may positively affect the TOC removal and negatively impact the colour removal percentage of organic pollutants. For instance, Table 18 of this section shows that during treatment of MB by corona discharge, about 16 mg/L of nitrogen based compounds largely resulting from air used as the feeding gas (Jo and Mok, 2009) were detected in the treated sample. On the other hand, sulphur content (1.5 mg/L) as SO₄ in the untreated MB decreased to 1.1 mg/L. So the reduction and production of these by-products might have led to the formation of acidic species such as HNO₃, HOON, H₂SO₄, etc. (Magureanu et al., 2013) which eventually decreased solution pH and raised its electrical conductivity.

Based on the pH evidence, Salome and co-workers (2006) emphasized that organic compounds may be hydrolysed when the pH of the solution is close to 7 after ozonation. Likewise, the pollutant is not hydrolysed when the solution pH is around 3.9. This meant that the decrease of solution pH favours colour removal at the expense of dye mineralization, hence a lower TOC removal. In other words, in the present research, MB was decomposed to various intermediates/by-products, the resulting aliphatic compounds such as carboxylic acids, aldehydes, amines, amides, etc. were not oxidised into CO₂ and H₂O but remained in the solution. This finding was also reported by Jun et al. (2008) who stated that during treatment of dyes by NTP, both parameters, TOC and colour removal percentage cannot be successfully achieved at the same time. Thus, optimization of the current EHD system is significant in order to overcome the limitation between TOC and decolourization percentage removal.

Based on evidence supported by UV-vis results, FT-IR, TOC, COD, (SO₄ and nitrites + nitrates) content, MB was also proved to degrade to intermediates during electrohydraulic discharge instead of only being decolourized. In that case, the colour removal concept was neglected over MB degradation and it was worthwhile to evaluate the impact of initial concentration on MB degradation efficiency.

4.7 DECOLOURIZATION EFFICIENCY OF MB AT NORMAL AND OPTIMUM CONDITIONS

After recording the absorbance of the solution at each sampling time, the unknown concentration of MB was approximated using the calibration curve of absorbance vs concentration of standard MB solutions. In addition, from the initial and the determined MB concentrations, the decolourization efficiency of MB was calculated and presented in Tables 4.8 and 4.9. Furthermore, the decolourization efficiency of MB at normal and optimum conditions were plotted versus time and presented in Figure 4.23.

Table 4.8: EHD experiment at normal conditions (Applied voltage 25 V, peak voltage 7.8 kV, [MB] = 5 mg/L, V= 1500 mL, air flow rate 3 L/min, 0.5 mm silver electrode, 50 g/L NaCl electrolyte, air gap 2 mm and running time of 60 minutes).

Time (minutes)	Absorbance	Concentration (mg/L)	Decolourization %
0	1.146	5	0
10	0.219	1.897	62.06
20	0.037	0.320	93.6
30	0.000	0.000	99.99
40	0.000	0.000	99.99
50	0.000	0.000	99.99
60	0.000	0.000	99.99

Table 4.9: EHD experiment at optimum conditions (Applied voltage 25 V, peak voltage 7.8 kV, [MB] = 5 mg/L, V= 1500 mL, air flow rate 3 L/min, 1.5 mm silver electrode, 50 g/L NaCl electrolyte, air gap 2 mm and running time of 60 minutes)

Time (minutes)	Absorbance	Concentration (mg/L)	Decolourization %
0	1.144	5	0
10	0.170	1.473	70.54
20	0.001	0.0086	99.82
30	0.000	0.000	99.999
40	0.000	0.000	99.999
50	0.000	0.000	99.999
60	0.000	0.000	99.999

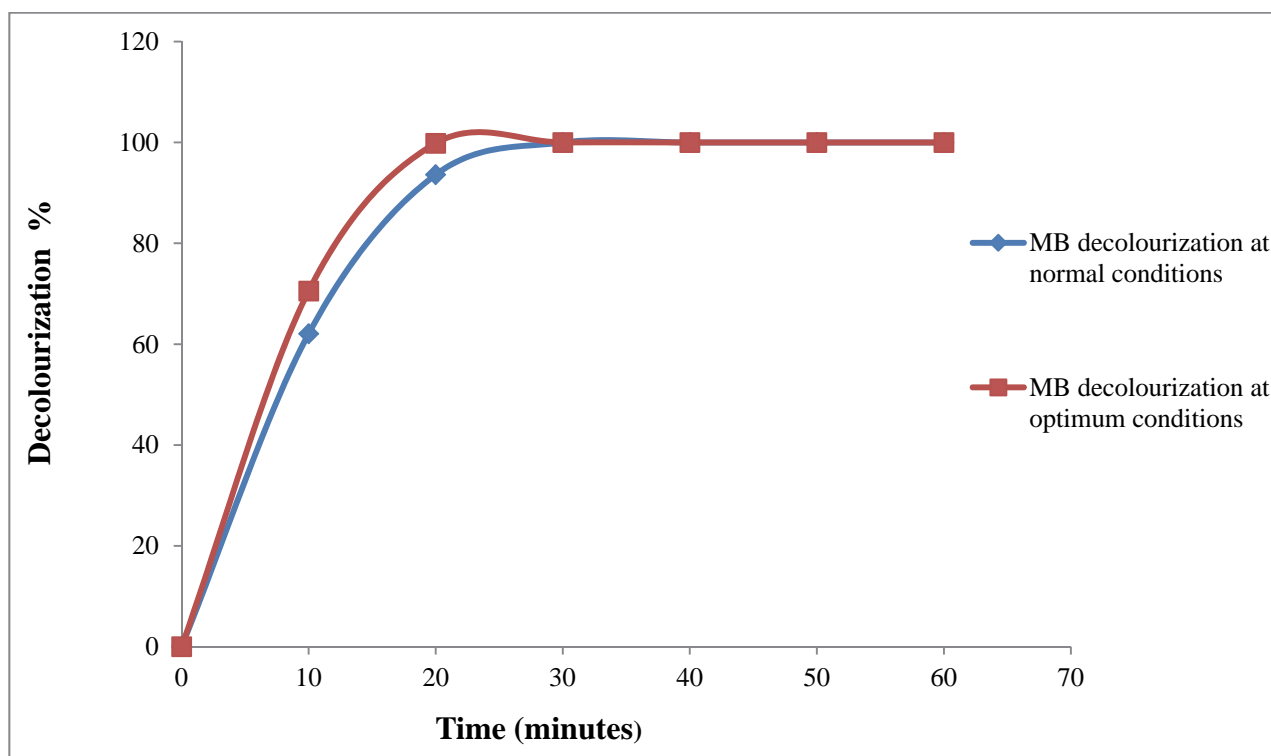


Figure 4.23: Decolourization efficiency of MB at normal and optimum conditions

The results presented in Table 4.8 show that at normal conditions, MB degraded progressively with increase in treatment time and complete decolourization was achieved within 30 minutes. In the case of EHD experiment run at optimum conditions, the same trend was observed whereas the results exhibited in Table 4.9 indicate that total colour removal of MB almost occurred within 20 minutes. To recall, MB dye is a chromophoric molecule as any coloured material contains a chromoric form responsible for its intense blue colour. Therefore the progressive decolourization of MB noticed during these experiments could be explained by the destruction of the chromoric form by free reactive species such as O₃, H₂O₂, etc. generated during plasma treatment. The reduction in treatment time from 30 to 20 minutes at which complete MB decolourization was achieved shows that the optimized EHD system has improved MB colour removal. This can also be observed in the results plotted in Figure 4.23, the graph of MB degradation at optimum lies on top of the one obtained at normal conditions. Hence the shortening of treatment time for total decolourization of MB shows the performance of the optimized EHD system which can further be used for treatment of water/wastewater effluents.

4.8 PRELIMINARY RESULTS FOR TREATMENT OF A REAL TEXTILE EFFLUENT WITH EHD

In order to determine and enhance the efficiency of colour removal, TOC and COD from a real textile wastewater sample by EHD, the optimal conditions were determined for the use of various flocculents separately and in combination with coagulant or EHD.

The results presented in Table 4.10 represent an optimum dosage of each coagulant and flocculent without or in combination with electrohydraulic discharge system. Among the investigated coagulants, alum (Al₂(SO₄)₃) seemed to be most effective as 0.8 g of alum lowered the COD value to 7543 mg/l which is about 36.87% of the influent COD of the textile wastewater. With the addition of 0.8 g of Ca(OH)₂, a further decrease in the COD by 5% was observed. This was due to the destabilization of organic flocs resulting in almost stable COD values. Correspondingly, pH was observed to be 10.35, which is slightly higher than the favourable pH range. Furthermore, the addition of 1.6 kg/m³ of Fe-Mn reduced the odour and enhanced the COD reduction. Therefore, coagulation-flocculation process reduced the COD value by 41.87%. The incorporation of Fe-Mn and electrohydraulic discharge system further enhanced the COD reduction by 96.79%. Integration of coagulation-flocculation and electrohydraulic discharge system is considered to be advantageous for lowering the COD level in the effluent. This preliminary study with model and real dye effluents has demonstrated that a single technology processing is not sufficient for complete removal of COD, TOC and other parameters.

Table 4.10: COD, TOC and pH value before and after flocculation/EHD treatment

	pH	COD (mg/l)	TOC (mg/l)
Before treatment	6.02	20456	5950
After treatment with Al ₂ (SO ₄) ₃	2.44	7, 543	1456
After treatment with FeSO ₄ .7H ₂ O	5.03	11,134	2310
After treatment with FeCl ₃	1.88	8369	1650
After treatment with Ca(OH) ₂	11.32	12, 653	2568
After treatment with Al ₂ (SO ₄) ₃ + Ca(OH) ₂	10.35	6, 521	1340
After treatment with Fe-Mn	5.74	19,987	5893
After treatment with electrohydraulic discharge system alone	5.99	18,057	4953
After treatment with Al ₂ (SO ₄) ₃ + electrohydraulic discharge system	4.56	4, 532	986
After treatment with Fe-Mn + electrohydraulic discharge system	5.75	18,466	4820
After treatment with Al ₂ (SO ₄) ₃ + Ca(OH) ₂ + electrohydraulic discharge system	9.63	958	224
After treatment with Fe-Mn + Al ₂ (SO ₄) ₃ + Ca(OH) ₂ + electrohydraulic discharge system	8.51	656	200

Redesign of EHD reactor for better recirculation of generated reactive species and the development of TiO₂ photocatalysts in supported form for incorporation in the EDH was further considered in this project.

4.9 REDESIGN OF THE EHD REACTOR

This section deals with the designing and construction of a scaled up multiple electrode electrohydraulic discharge (EHD) reactor, in a specific way. The detail of the proposed design is given in Appendix A and the constructed cell as well as the newly built power supply/AC convertor is presented in the images that follow (Figures 4.24-4.27).



Figure 4.24: New constructed EHD reactor

With respect to borosilicate glass there is also the problem that it is opaque to UV radiation, which is supposed to shine into the cell water. In the new design the outer glass tube of each discharge cell is made of fused quartz for reasons of durability and UV permittivity. Once the benefits and constraints of the new cell are properly investigated a further configuration may be developed in collaboration with the Department of Electrical Engineering at the University of Stellenbosch and continuous mode operation of this redesigned system with integrated supported photocatalysts will form part of future work on the EHD reactor.

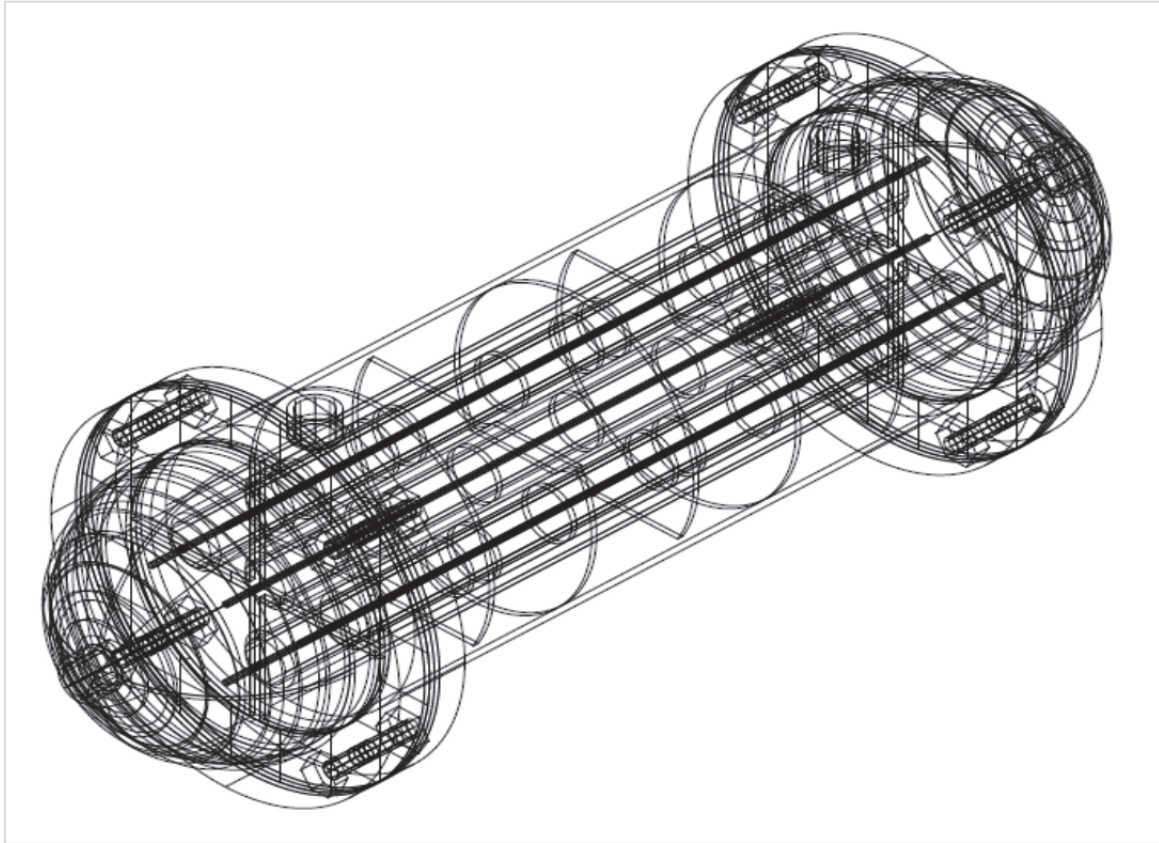


Figure 4.25: Isometric wireframe view of reaction vessel

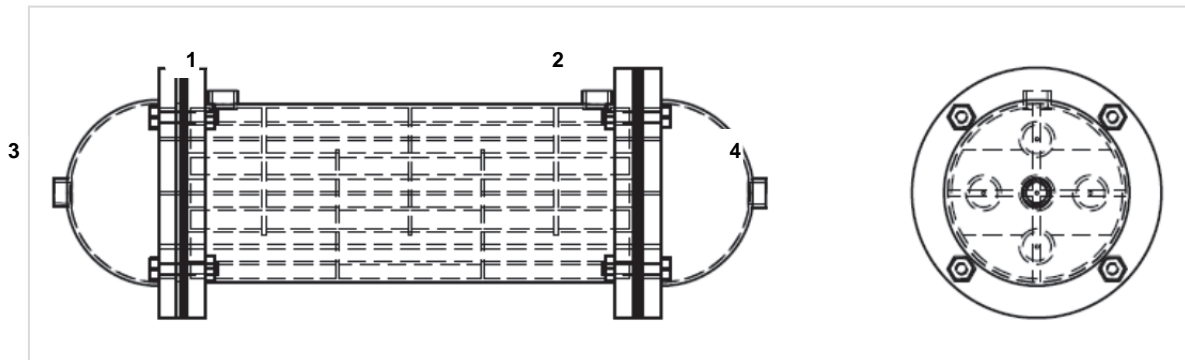


Figure 4.26: Front and left hand wireframe view of reaction vessel

4.9.1 Materials of reactor construction

The main body of the reactor is built from Perspex and Teflon. The Perspex is used to construct the outer shell of the reactor and the end caps as it is translucent, allowing the process to be observed, and is shock resistant. The flanges which enclose the shell and hold the tubes in position are constructed from Teflon as this is a high temperature resistant and non-conductive material. The baffles and electrode placement disks are constructed from Teflon for similar reasons. This will make the reactor robust and reduce the chances of it being damaged easily. The tubes in the shell are constructed from a dielectric material which has a high tolerance for temperature and which does not absorb UV light. For this reason it is constructed from quartz

as previous experiments have shown quartz to be ideal in this type of application. For the electrodes, 2 mm diameter silver rods will be used, as the electrodes must be stiff to ensure the arcing distance will be equal in all directions. The electrode placement disks are bolted in place between the shell and the end caps. Appendix A contains a systematic disassembly and dimensions of the reactor to aid the explanation given above.



Figure 4.27: New power supply and AC convertor to drive the EHD reactor

The power supply has had a KV meter added in the design as this will allow display of the output voltage directly without the use of an oscilloscope and probe. The new power supply has fewer losses than the previously used one. The power source generates a nearly pure sinusoidal voltage wave with no offset, i.e. the Integral of $V = 0$.

4.9.2 Results for optimization of supported TiO₂ photocatalysts

In the previous WRC funded study, K5//1897, proof of concept of the beneficial incorporation of TiO₂ photocatalysts in the EHD system were presented. However, in that system, the photocatalyst preparation protocols were laborious and difficult to replicate. Therefore, it was necessary to develop a protocol which was well controlled and replicable to support the photocatalyst of a suitable stable support. In this study, the protocol was optimized and simplified as set out in the experimental section and the results are presented in

this section. The mass percentage of the deposited TiO₂ nanocrystals on the stainless steel mesh that was achieved through the stainless steel mesh coating method using 8% PAN/DMF/TiO₂ sol gel solution and decomposed by calcination using the new protocol as set out in experimental is presented in Figure 4.28.

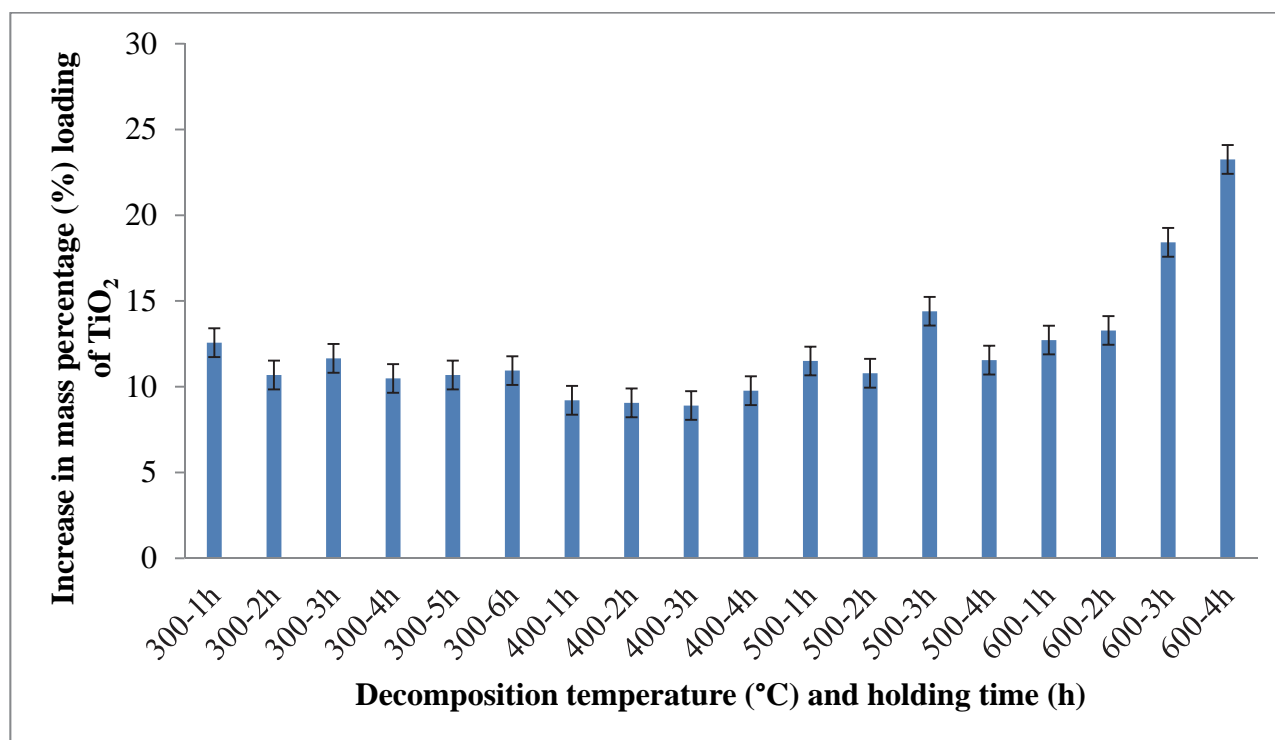


Figure 4.28: Mass percentage of immobilised TiO₂ obtained by various decomposition temperatures and holding times using the 8% PAN/DMF/TiO₂ sol gel solution coating method

Figure 4.28 shows that the mass of TiO₂ decomposed onto the stainless steel support at 300°C for between 1 up to 6 h holding time fluctuated slightly between 10-12 mass percent loading. The mass percent loading of the TiO₂ composite decomposed at 300°C is higher than the mass loading decomposed at 400°C as polymer is not fully decomposed. The mass percentage loading decomposed at 400°C is fairly even and probably the polymer is mainly decomposed. The samples with the mass loading decomposed at 500°C vary between 10-14 mass percent loading. The mass percentage loading decomposed at 600°C is gradually increasing with an increase in the holding time and this increase may be due to the excess formation of oxides, furthermore the anatase may be starting to transform to rutile phase, as the rutile is denser than the anatase (4.25 g/cm³ versus 3.894 g/cm³) (Ahmad et al., 2008). The increase in temperature causes the TiO₂ anatase to expand its crystal structure and forming more oxides, hence increasing the mass of the sample loaded on the support.

Figure 4.29 shows representative patterns of the X-ray diffraction (XRD) obtained for TiO₂ nanocrystals with the anatase crystal phase. All samples prepared by various methods produced the anatase phase with varying degrees of crystallinity. The peaks illustrated in the XRD patterns correspond to the (101), (103), (004), (112), (200), (105), (211), (204), (116), (220) and (215) planes of TiO₂ tetragonal anatase phase.

These patterns can be well indexed to tetragonal anatase. The recorded XRD matches with the JCPDS pattern of TiO₂ anatase, body centered tetragonal, $a = 3.8101 \text{ \AA}$, $b = 3.8101$, $c = 9.3632$, $\alpha = 90^\circ$, $\beta = 90^\circ$, $\gamma = 90^\circ$ (Hackeyley and Ferraris, 2001).

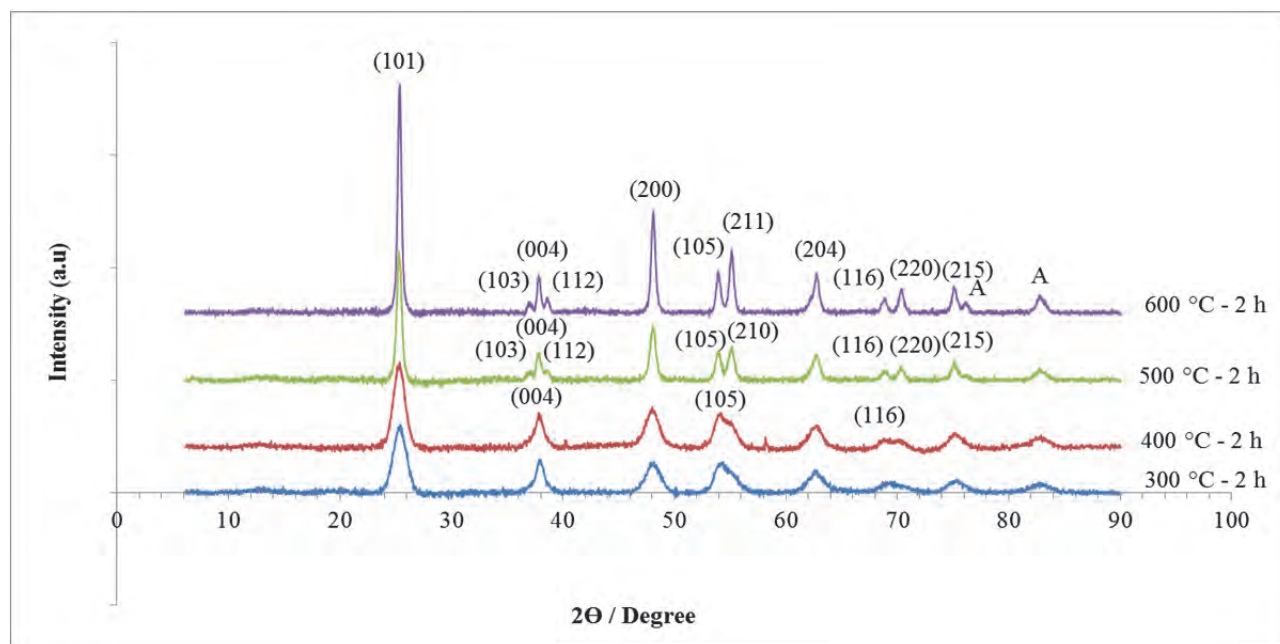


Figure 4.29: XRD pattern of 8% (PAN/DMF/TiO₂) decomposed TiO₂ at 50°C/min and different holding temperatures for 2 h: Samples (TT4.1B), (TT4.2B), (TT4.3B) and (TT4.4B)

The HRSEM micrographs of 8% (PAN/DMF/TiO₂) sol gel solution coated stainless steel mesh calcined at 300 °C with the heating rate of 50 °C/min and different times are presented in Figure 4.30. In Figure 4.30A (TT4.1) there are no TiO₂ crystals to be seen after carbonization in air for 1 h at 300°C while in B (TT4.1) TiO₂ crystals appear after 2 h carbonization at 300°C but are not fully developed and are still embedded inside the polymer (PAN). In C (TT4.1) after 3 h carbonization at 300°C the crystals are visible with clear morphology; they are large with spaces in between them and have a 3 dimensional hexagonal structure. In D (TT4.1) after 4 h at 300°C the TiO₂ crystals are smaller and more densely packed with hexagonal structure morphology compared to the crystals obtained at a shorter time. Image E (TT4.1) shows the TiO₂ crystals obtained after 5 h at 300°C, which had a rod-like agglomerated morphology. In sample F (TT4.1) there are agglomerated TiO₂ nanocrystals to be seen after carbonization for 6 h at 300°C, with cracks appearing in the film on the stainless steel support. HRSEM images of samples obtained between 4 h and 6 h (Figure 4.30) show that the morphology of the supported TiO₂ nanocrystals is agglomerated and as time increased to 6 h at 300°C the TiO₂ nanocrystals are not fully developed on the surface of the stainless steel mesh.

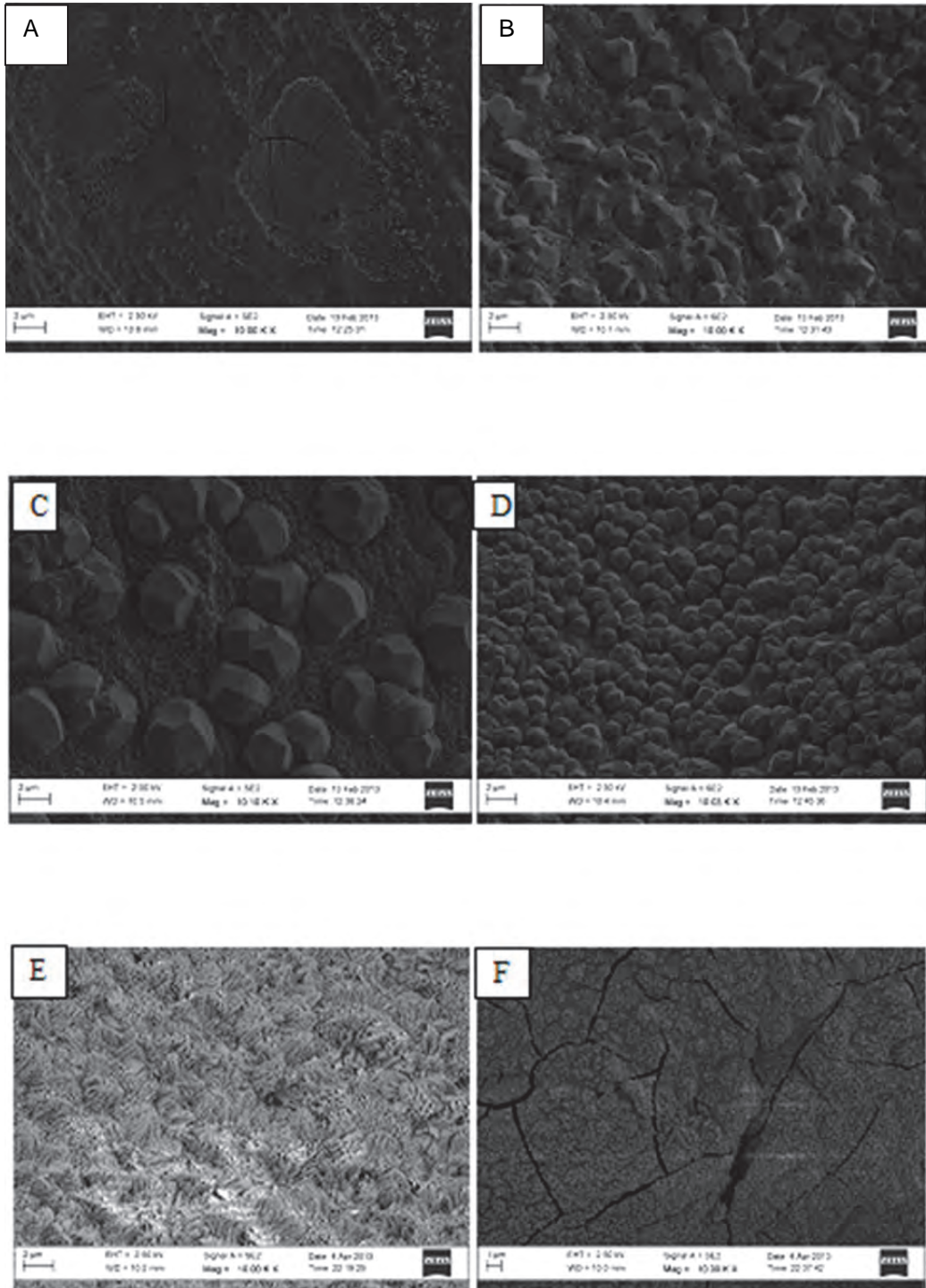


Figure 4.30: HRSEM micrographs of 8% (PAN/DMF/TiO₂) sol gel solution coated stainless steel mesh calcined at 300 °C with the heating rate of 50 °C/min and different times, where [A] = 1 h, [B] = 2 h, [C] = 3 h, [D] = 4 h, [E] = 5 h and [F] = 6 h.

In the images shown in Figure 4.31 all samples prepared at 400°C at the specified holding time have a crystalline TiO₂ structure. The image of sample (TT4.2) A shows that after 1 h the crystal structure was not fully formed, while in B of the (TT4.2) sample prepared at 400°C for 2 h, crystal structures are small. In C of the sample (TT4.2) prepared at 400°C for 3 h the leaf-like TiO₂ crystal structures are large and aligned in a structured manner with clear morphology, have high surface area and are aggregated. In (TT4.2 D) of the sample prepared at 400°C for 4 h the leaf-like crystal structures are again small and have different sizes and are aggregated. Therefore these series of experiments showed that the most well developed TiO₂ structure could be obtained when using 8% PAN/DMF/TiO₂ sol gel solution made of 8% PAN/DMF sol solution and 99% pure TiCl₄ titanium precursor followed by carbonization using a heating rate of 50°C/min in air, up to 400°C and held at 400°C for 3 h. For HRSEM images of the samples obtained from the 8% (PAN/DMF/TiO₂) sol gel solution decomposed at 400°C for up to 3 h, it was observed that the mass is gradually decreasing and when it reaches 4 h then increases.

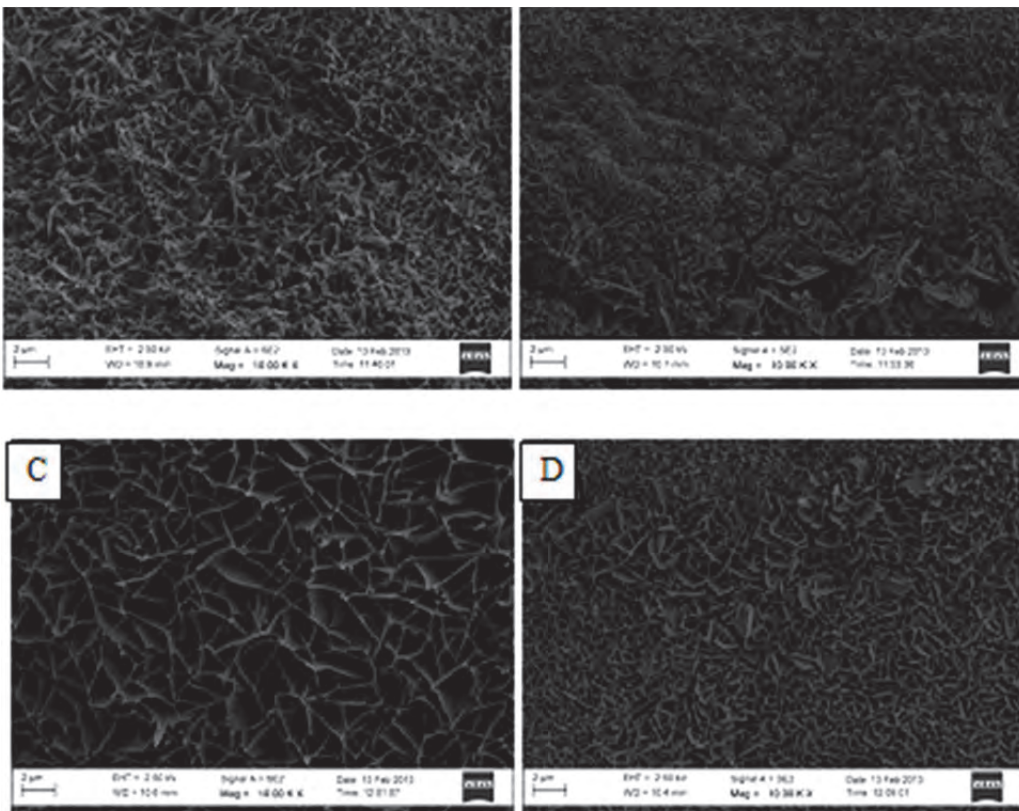


Figure 4.31: (TT4.2) 8% (PAN/DMF/TiO₂) sol gel solution coated stainless steel mesh calcined at 400°C with heating rate of 50 °C/min and holding times of [A] = 1 h, [B] = 2 h, [C] = 3 h and [D] = 4 h.

In Figure 4.32 of sample (TT4.3) all the images show that at 500°C a leaf like crystallite structure of the TiO₂ crystals was obtained between 1-3 h but not for the sample carbonized at 4 h (image D) which had a sharp needle-like structure. The higher temperature of 500°C caused the TiO₂ structures to be less uniform than those obtained at 400°C and cracks were apparent in image TT4.3 B. The decomposed structures for 1 h (TT4.3) A up to 4 h (TT4.3) D holding time does not correlate throughout.

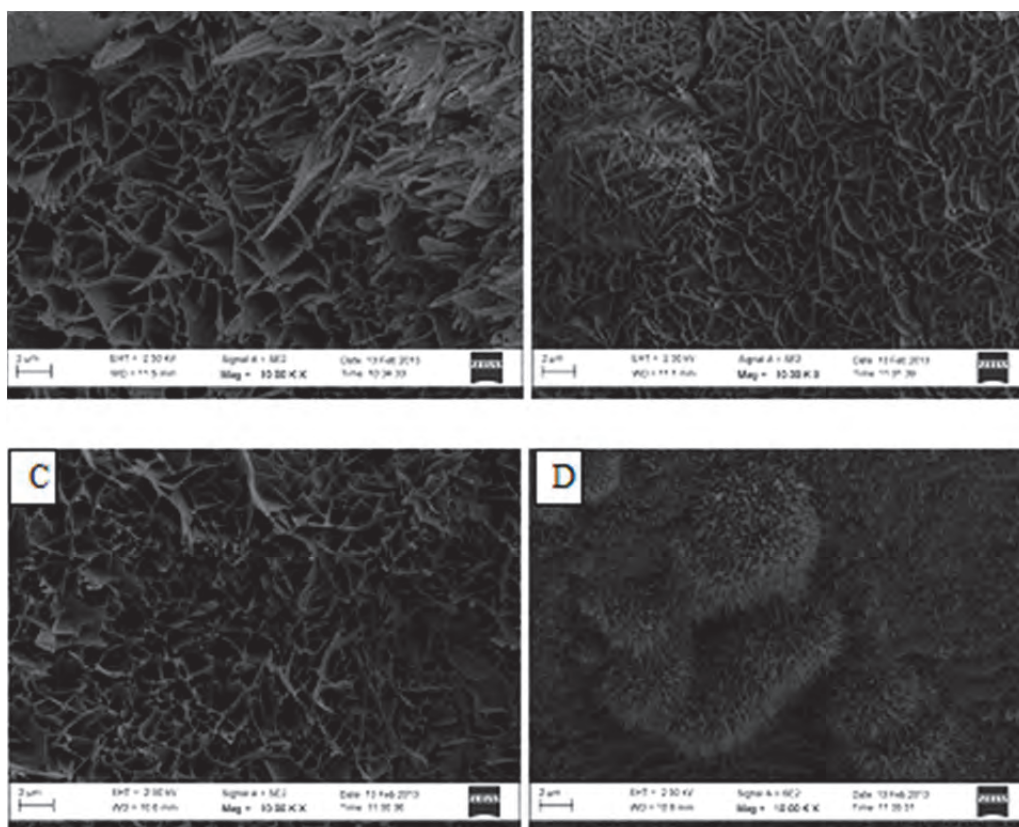


Figure 4.32: 8% (PAN/DMF/TiO₂) sol gel solution coated stainless steel mesh was calcined at 500 °C with heating rate of 50 °C/min and holding times were [A] = 1 h, [B] = 2 h, [C] = 3 h and [D] = 4 h.

In Figure 4.33 (TT4.4) the applied temperature of 600°C resulted in various needle-like structures that were inhomogeneous and not well adhering to the stainless steel substrate. The HRSEM illustrated that the heating time and temperature had a substantial impact on the morphology of the supported TiO₂ nanocrystals and resulted in equ-dimensional structures at 400°C. The supported TiO₂ nanocrystals decomposed at 300°C resulted in different hexagonal morphology with the change in holding time, whereas the higher temperature (500-600°C) resulted in inhomogeneous structures. The trend for 1 h (TT4.4) A up to TT4.4 - 4 h D holding time showed an increasing mass of oxide. In another study on nucleation and growth kinetic of titania nanoparticles prepared by sol gel method it was shown that the rate constant for coagulation of particles increased with temperature because the velocity of monomer through the particles had a high dependency upon temperature (Mehranpour et al., 2011). This present study that was undertaken in this research is novel due to the process to improve the adhesion of TiO₂ nanocrystals on a stainless steel

support; and the method used for the adhesion of such nanocrystals was very simple with fewer chemicals used than usual processing steps, therefore the findings of this research are unique.

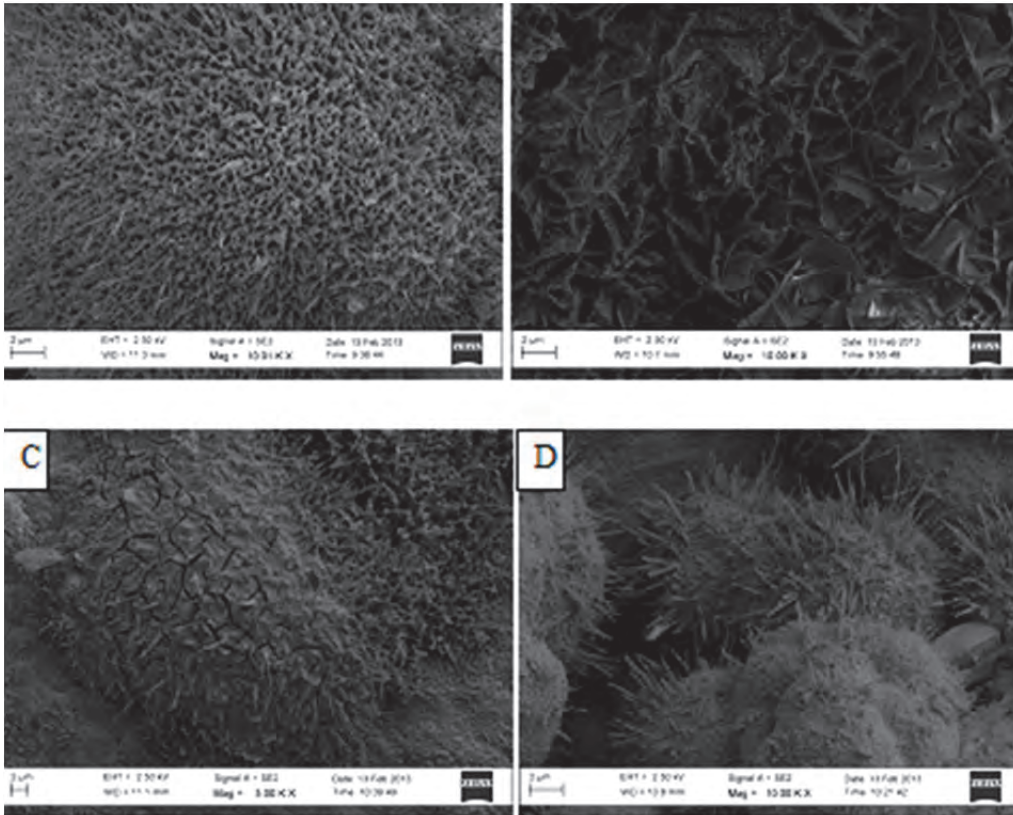


Figure 4.33: HRSEM of samples made with 8% (PAN/DMF/TiO₂) sol gel solution coated on stainless steel mesh calcined at 600 °C with heating rate of 50 °C/min and holding times [A] = 1 h, [B] = 2 h, [C] = 3 h and [D] = 4 h.

The characteristic HRTEM image is shown in Figure 4.34A while the SAED pattern of the samples is presented in Figure 4.34B. The sample (TT4.2) was composed of aggregated TiO₂ nanocrystals when decomposing PAN at a high heating rate of 50°C/min using the calcination process. The images shown in Figure 7 possess equidimensional nanocrystals with polycrystalline particles. The SAED of the nanocrystals confirms their polycrystallinity. The polycrystalline diffraction ring indexed confirmed that the TiO₂ nanocrystals were composed of highly nanocrystalline anatase phase. The SAED pattern and XRD as well as EDS confirmed the presence of the TiO₂.

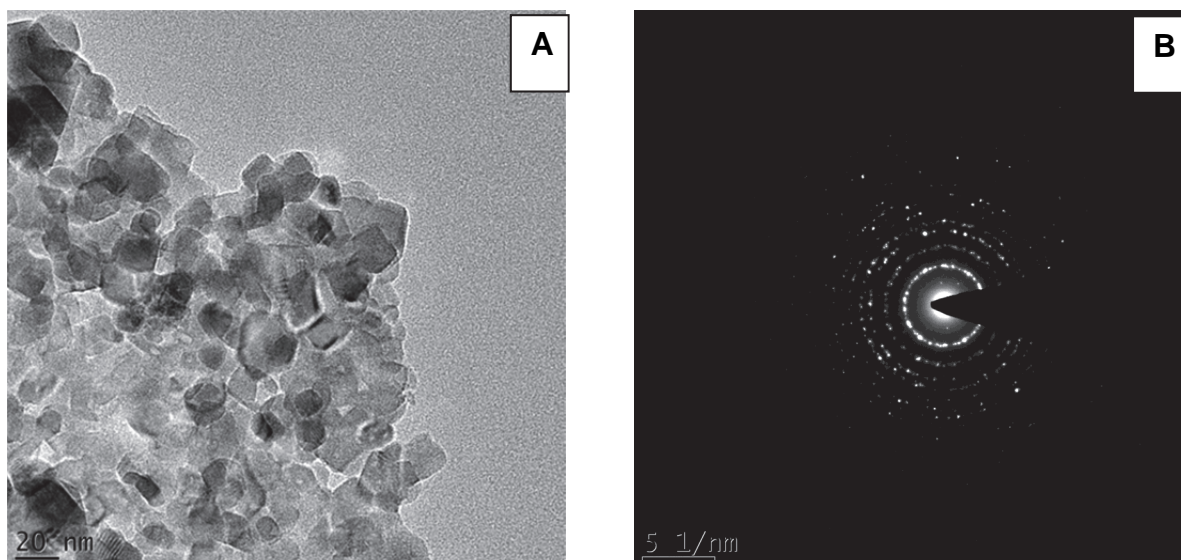


Figure 4.34: HRTEM image for the TiO₂ nanocrystals (TT4.2) formed after decomposing by heating at 50°C/min and holding at: 400°C for 2 h, B = SAED pattern of 400°C for 2 h

Figure 4.35 presents a characteristic FTIR spectral data of sample (TT4.2) with the vibrational bands of the anatase TiO₂ functional groups. Vibrational bands that appeared at 528-544 cm⁻¹ were ascribed to the vibration of the skeletal O-Ti-O bonds of anatase phase (Cristallo et al., 2001). The characteristic C=O, C=C and C-N stretching vibrations were seen at 1737-751, 1440-1457, and 1217-1218 cm⁻¹, and the good adhesion of TiO₂ nanocrystals onto the support was ascribed to these carbon bonds formed by the decomposition of the polymer precursor used.

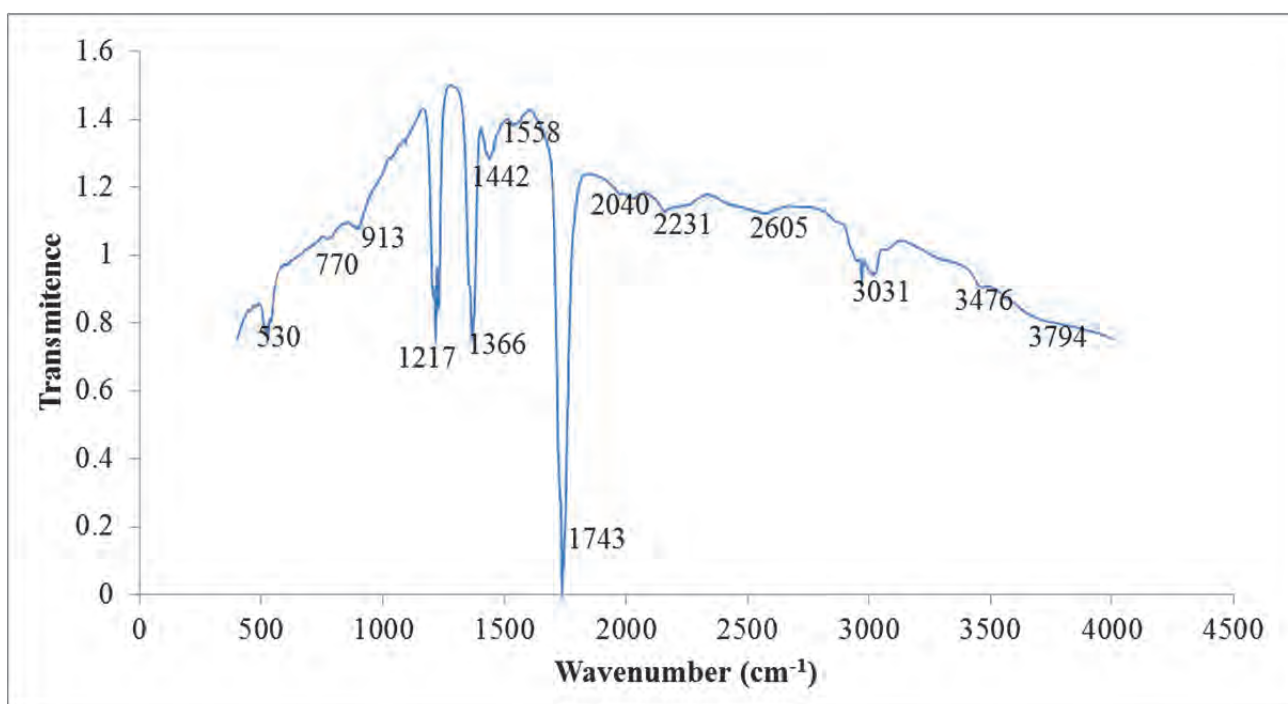


Figure 4.35: FTIR of sample (TT4.2) prepared at 400 °C for 2 h

The band at 3000-3500 cm⁻¹ was attributed to the hydroxyl group of Ti-O-H. Hence the conspicuous bands at 528-544 cm⁻¹ represented the Ti-O and Ti-O-Ti stretching vibration modes and according to Saravanan et al. (2010) the same stretching vibration modes were distinguished at 542 cm⁻¹. The peaks observed between 1440 and 1457 cm⁻¹ can also be attributed to the Ti-O-Ti vibration. The peak around 1737-1751 cm⁻¹ was due to the bending vibration of the O-H bond of chemisorbed water and it was believed that the prominent peaks around at around 1500-1650 cm⁻¹ corresponds to the surface adsorbed water.

Methylene degradation over the supported TiO₂ photocatalysts was undertaken and results are shown in Figure 4.36. For the samples treated at 400°C (TT4.2), the percentage removal for the MB degradation ranged between 96.02 ± 0.0054 – 59.83 ± 0.0083%. The highest percentage MB removal obtained was 96.02 ± 0.0054% after 30 min degradation time in the presence of the 0.3 g supported TiO₂ nanocrystals decomposed at 400°C for 2 h (TT2.2). Other samples prepared at other temperatures were not as active and are not shown. This research showed that the supported TiO₂ nanocrystals prepared at 400°C for various degradation time intervals possessed photocatalytic activity except for the supported TiO₂ nanocrystals decomposed at 400°C for 3 h which did not degrade MB. Even though all the immobilised TiO₂ nanocrystals possessed photocatalytic activity the supported TiO₂ nanocrystals decomposed at 400°C for 2 h gave the highest degradation percentage ± 100% and at the lowest degradation time interval of 30 min. The variability of the UV vis results was due to the stirring of the supported PAN/DMF/TiO₂ nanocomposite that may have resulted in damaging the nanocomposite. This photocatalytic degradation experimental setup was not optimized, thus the random movement of the catalyst means that the sample was not exposed to constant UV flux.

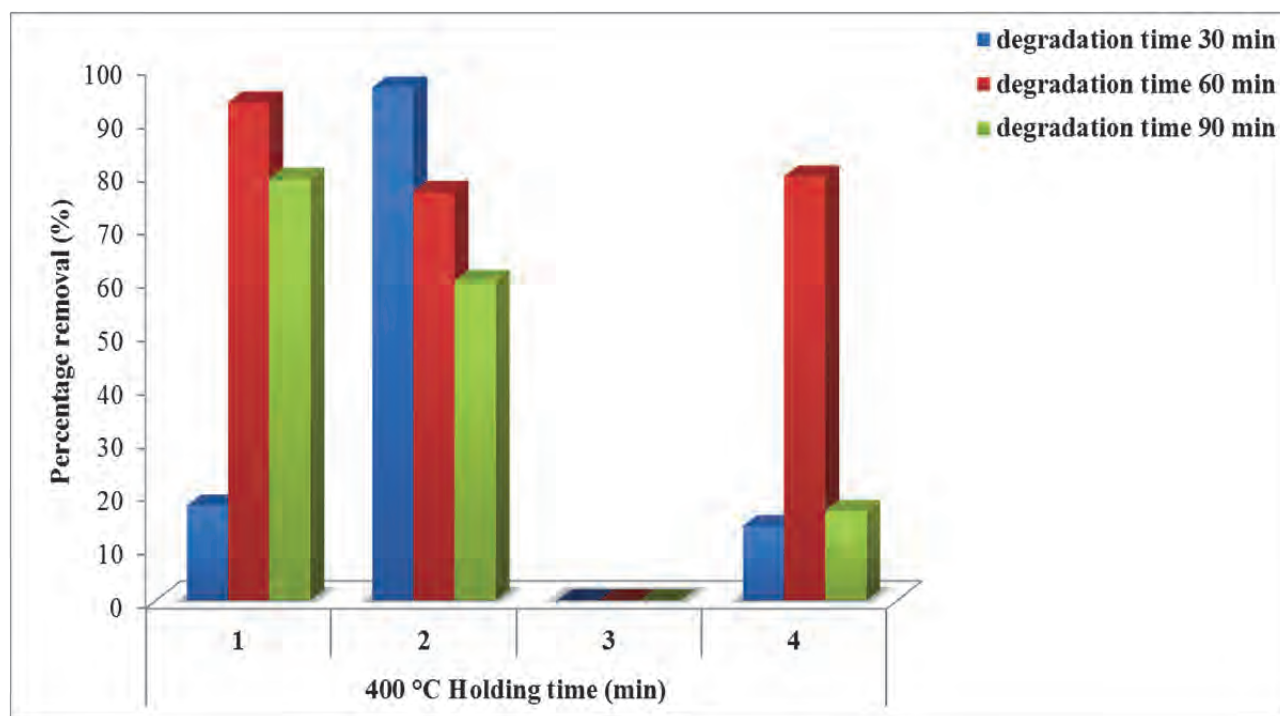


Figure 4.36: Degradation of MB for 30, 60 and 90 min using the carbonized supported TiO₂ nanocrystals prepared by heating at 50°C/min to 400°C for 1 h, 2 h, 3 h or 4 h (TT4.2)

The preparation of the nanocomposites, TiO₂ nanocrystal supported on the stainless steel mesh, by a coating technique was achieved. The XRD patterns has demonstrated that TiO₂ crystallized above 300°C in the anatase form, which phase remarkably remained stable up to 600°C. The stabilization of this TiO₂ phase in composite form is due to the nanometric size of the crystals immobilized onto the stainless steel mesh. The crystalline phase and morphology of the nanocomposites are supported by XRD and HRSEM analyses, which has shown homogeneous and monodisperse distribution of nodular anatase nanocrystals (crystal size 17.26 nm) onto stainless steel mesh for the sample calcined in air at 400°C for 2 h. The anatase nanocrystals are thermally stable, smaller than 20 nm, well dispersed and immobilized on the surface of stainless steel mesh. The various supported anatase nanocomposites were successfully made and it was possible to replicate and tailor the crystal size depending on the processing conditions such as the heating temperature and holding time. The XRD and SEM characterization elucidated the crystallinity and morphology of the prepared nanocomposites. The TiO₂ anatase phase changed the crystal structural morphology and the surface area with the change in temperature and holding time. The HRSEM showed that the heating time and temperature had a substantial impact on the morphology of the supported TiO₂ nanocrystals and the result of equi-dimensional structures at 400°C, hexagonal morphology at 300°C and inhomogeneous (500-600°C). The degree of anatase coating on the stainless steel mesh was inhomogeneous but sufficient for the stainless steel mesh piece.

4.10 DISINFECTION OF *E. coli* BY DIELECTRIC BARRIER DISCHARGE

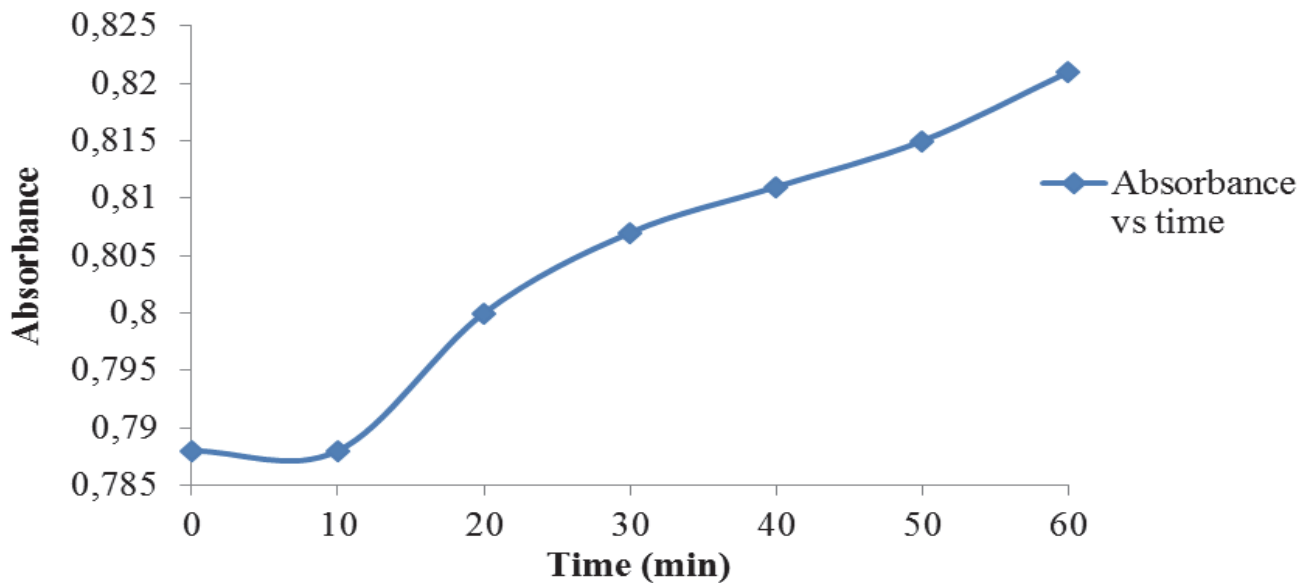
This section presents the results of *E. coli* inactivation and blank by dielectric barrier discharge system.

4.10.1 Simulation of *E. coli* solution by stirring with a magnetic stirrer within 60 minutes at room temperature

During the stirring process of *E. coli* solution, the solution was sampled every 10 minutes. The optical density (absorbance) of samples was measured and recorded in Table 4.11. It can be seen that the absorbance of *E. coli* samples recorded within 60 minutes of stirring process. In addition, the absorbance/optical density of the micro-organisms continuously increased with increase in treatment time. The behaviour of *E. coli* during the stirring process was assessed by plotting the optical density of samples versus time and presented in Figure 4.37. The results shown in Table 4.11 and Figure 4.37 proved that within 60 minutes of stirring process, *E. coli* bacteria were still growing and were in the log phase of their lifetime. These results correlate with the expectation of a continuous growth when the colony was taken at a specific point in the log phase. The *E. coli* growth exhibited in Figure 4.37 showed that the bacteria were still active and therefore guaranteed that the DBD experiment could be performed in that period of time. Hence the efficiency of the present double cylindrical DBD reactor could be tested on *E. coli* inactivation within the time scale.

Table 4.11: Optical density/absorbance of *E. coli* recorded within 60 minutes at room temperature and a stirring speed of 50 rpm

Time (min)	Absorbance
0	0.788
10	0.788
20	0.800
30	0.807
40	0.811
50	0.815
60	0.821

**Figure 4.37: Evolution of *E. coli* optical density recorded within 60 minutes at room temperature and stirring speed of 50 rpm**

4.10.2 Inactivation of *E. coli* by dielectric barrier discharge system

During disinfection of *E. coli* by the DBD reactor, the absorbance also called optical density of the solution sampled within 60 minutes was measured and the results are presented in Table 4.12. Based on these results, the efficiency of the DBD reactor was assessed by plotting the absorbance of samples against time (Figure 4.38).

Table 4.12: Absorbance/optical density of *E. coli* solution sampled within 60 minutes of DBD experiment at room temperature. Experimental conditions (Applied voltage 25 V, peak voltage 7.8 kV, *E. coli* volume 1500 mL, NaCl electrolyte concentration 50 g/L, 1.5 mm silver

Time (min)	Absorbance	% Inactivation
0	0.500	Growing period
10	0.754	Growing period
20	0.669	11.3
30	0.567	24.8
40	0.459	39.1
50	0.355	52.9
60	0.306	59.4

$\% \text{ Inactivation} = [\text{Initial absorbance} - \text{final absorbance} / \text{initial absorbance value}] \times 100$

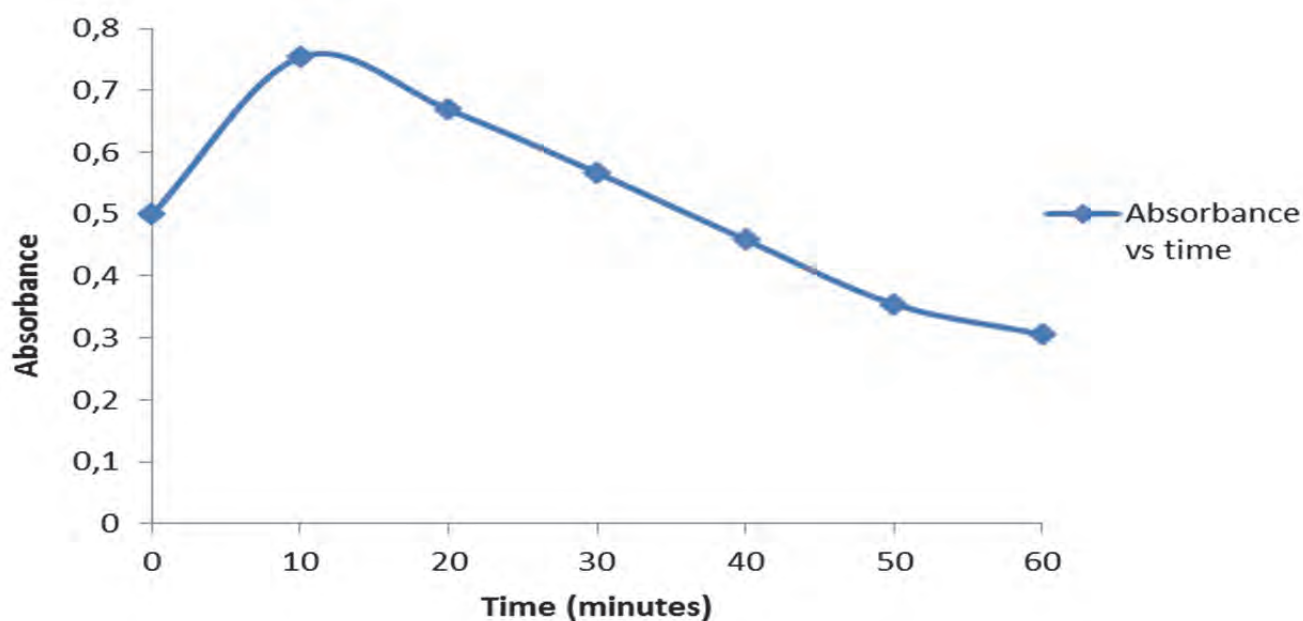


Figure 4.38: Effect of DBD reactor on *E. coli* sterilization. Experimental conditions (Applied voltage 25 V, peak voltage 7.8 kV, *E. coli* volume 1500 mL, NaCl electrolyte concentration 50 g/L, 1.5 mm silver electrode, treatment time 60 minutes)

Table 4.12 presents the optical densities of *E. coli* solution during DBD experiment while Figure 4.38 shows the plot of optical densities recorded in Table 4.12. The results obtained showed that the density of the bacteria increased in the first 10 minutes and then decreased with an increase of treatment time. This indicates that *E. coli* bacteria were still active in the first 10 minutes probably due to the fact that the amount of active species such as ozone was very low at that period of time. Thus, there was neither decrease nor increase in the inactivation percentage. Likewise, the continuous decline in the optical density after 10

minutes of DBD experiment showed that *E. coli* bacteria were being inactivated by the DBD system. The UV radiation and the presence of various highly reactive species such as ozone, atomic oxygen, hydrogen peroxide and hydroxyl radicals largely contributed to the sterilization of the bacteria. Also, the abrupt decrease in the bacteria optical density as shown in Figure 4.38 could be attributed to the fact that, after 10 minutes, the active chemical species being formed could react with the aqueous environment. The OH radicals were suspected to have interacted with the cytoplasmic membrane of *E. coli* and hence inhibiting the activity of the micro-organism (Chen et al., 2009; Hernández-Arias et al., 2012 and Sato, 2008).

Furthermore, Pompl et al. (2009) argued that reactive oxygen species (ROS) and hydroxyl radicals were believed to be responsible for the physical destruction of the cytoplasmic membrane of the bacteria when exposed to plasma discharge. Nevertheless, Rajbarath, (2005) proposed a comprehensive approach of bacteria inactivation during plasma exposure. According to Rajbarath (2005), the destruction of the microorganism DNA by UV photon is the first step in bacteria inactivation. In that case, the UV radiation generated during the DBD process might have strongly stressed the *E. coli* membranes causing the cell injuries or their lyse depending on the energy associated with the photons produced during the DBD experiment. Also, during the first step, the accumulation of cell debris forming a layer on top of the active spores or living cells might have occurred, shielding them from the UV. Thereafter, the photo-desorption and etching facilitated by the radicals and other active species generated during DBD process could probably led to volatile debris. Once volatilization occurred, the UV radiations have access to the rest of the bacterial cells for inactivation.

Despite the various explanations on the deactivation of microorganisms by plasma exposure, the oxidative chemical mechanistic pathways of bacteria such as *E. coli* in DBD configurations are still unclear. It was generally observed that after the first 10 minutes of exposure of *E. coli* to plasma discharge, the inactivation percentage increased from 11.3 to 59.4% as shown in Table 4.12. Even though, the analytical techniques such as Scanning Electron microscopy (SEM) was not used to show the progressive death of *E. coli* bacteria, the actual DBD system has demonstrated its efficiency on the inactivation of microorganisms as shown by the continuous decrease of the optical density of the bacteria. However, many aspects such as conversion of the optical density into normal concentrations, sample analysis using other sophisticated techniques still need to be covered, which fell outside of the scope of this project. Therefore the results of this study expressed in terms of optical density could not be compared with those found in literature and expressed in terms of disinfection rates per mL.

CHAPTER 5: CONCLUSIONS AND RECOMMENDATIONS

5.1 CONCLUSIONS

This study showed the optimization of the electrohydraulic discharge unit and quantification of free radicals in electrohydraulic discharge system as well as the preparation of stable, active, supported TiO₂ photocatalysts. Conclusions are as follows:

The effect of physicochemical, electrical and reactor configuration on MB decolourization and degradation was evaluated at the following fixed conditions: applied voltage 25 V, peak voltage 7.8 kV, MB volume 1500 mL, air flow rate 3 L/min, air gap 2 mm, 0.5 mm silver electrode (25 cm long) and contact time of 60 minutes. The reactive species H₂O₂ and O₃ were also detected and quantified at the same conditions.

The effect of concentration was firstly determined on MB decolourization and degradation and the dye MB concentration was varied from 0.5 to 10 mg/L with 0.5 mg/L increments. MB decolourization efficiency decreased with an increase in concentration. For concentrations ranging from 0.5 to 5 mg/L, the final solution sampled within 60 minutes was clear indicating complete decolourization. At concentrations above 5 mg/L, the colour of the final solution sampled after 60 minutes changed progressively from yellow to deep green. This study shows that complete MB decolourization was achieved within 60 minutes with MB concentration ranging from 0.5 to 5 mg/L. Thus, 5 mg/L was further used as the optimum MB concentration for the EHD system being investigated.

The UV-vis analysis of the treated MB solution showed that complete decolourization of MB was achieved in the first 30 minutes contact time due to the breakdown of the chromophoric [=N+(CH₃)₂] group in Methylene blue structure. The presence of the following functional groups: C=C, C=O, C=N, NH, NH₃, NO₂, etc. which are characteristics of carboxylic acids, amines, amides, nitrogen based compounds (salts), aliphatic and unsaturated by-products in the bulk solution was proved by the FT-IR analysis. Apart from this, 16 mg/L of nitrates and nitrites and 1.1 mg/L of sulphates mainly originating from air and MB were present in the treated solution. Therefore, during EHD experiment, the organic pollutant MB was destroyed into various saturated and unsaturated by-products as well as salts such as sulphates and nitrogen based species which mainly resulted from the air feed and from the decomposition of MB in the EHD system.

The study carried out to determine the effect of chemical parameters on MB degradation efficiency showed that when varying the pH from 2.5 to 10.5 with increment of 2, MB decolourisation efficiency decreased with an increase in solution pH. Therefore, solution pH had a significant effect on MB degradation efficiency. This indicated that acidic dyes such as MB easily decolourize in acidic conditions. When the solution pH increases, hydroxyl radicals become unselective and react easily with scavengers such as carbonate ions that form during oxidation of organic materials and thus, reducing the efficiency of the oxidation process

significantly. It was observed that after 10 minutes of the EHD experiment, 83.02% of MB removal was achieved at a pH of 2.5 compared to 71.4%, 67.08%, 60.32% and 56.16% MB removal achieved at pH 4.5, 6.5, 8.5 and 10.5, respectively. Therefore, pH significantly affected MB degradation efficiency. In this case, the optimum pH value was 2.5.

Additionally, the conductivity of the MB solution was adjusted with diluted solutions of NaOH and HNO₃. So, increasing the conductivity values from 5 to 20 mS/cm with increment of 5 at the same conditions did not show a significant impact on MB degradation efficiency as a continuous increase trend between MB removal efficiency and solution conductivity was not defined. However, 84.76% MB removal was achieved at conductivity of 10 mS/cm followed by 82.32%, 71.06% and 69.16% at conductivities of 15, 20 and 5 mS/cm, correspondingly. Hence, the optimum solution conductivity in this study was considered to be 10 mS/cm.

Even though MB removal efficiency slightly increased when the volume of the solution increased from 500 to 2000 mL with 500 increments at the same experimental conditions, it does not mean that the solution volume affected MB degradation efficiency. This is because at low volume, some of the UV-vis radiations generated by corona discharge were wasted due to the fact that the reactor tube was not completely immersed in the polluted water, thereby decreasing MB percentage removal at low volumes. After 30 minutes of experiment, 92%, 97.58%, 99.3 and 99.48% of MB removal was achieved with volume of 500, 1000, 1500 and 2000 ml, respectively. 1500 mL was chosen as the best volume for the EHD reactor because any volume above 1500 mL would induce overloading of the present system which needed to be redesigned to a flow through configuration.

NaCl electrolyte was used in the central electrode compartment of the EHD system to avoid sparking between the 0.50 mm silver electrode and the inner quartz tube of the reactor. The concentration of NaCl was varied from 10 to 50 g/L with 20 units using the same experimental conditions. Thus, 58.58% MB degradation efficiency was achieved with 50 g/L of NaCl while 47.32% and 41.4% were reached with 10 and 20 g/L of NaCl, accordingly. Since the decreasing trend was not strongly observed between electrolyte concentration and MB degradation efficiency, therefore NaCl electrolyte concentration in the central compartment was not deemed to impact MB degradation significantly. Therefore, 50 g/L of NaCl was chosen as the optimum electrolyte concentration used for further EHD experiments.

The physical parameter air flow rate was varied from 2 to 4 L/min at the following experimental conditions: voltage (25 V), peak voltage (7.8 kV), MB volume (1500 mL), air gap (2 mm), 0.5 mm silver electrode (25 cm long) and contact time of 60 minutes. After 10 minutes contact time, the results showed that MB degradation efficiency increased with an increase in the air flow rate. That is, 49.2%, 60.14% and 73.32% MB removal were consecutively obtained at air flow rates of 2, 3 and 4 L/min, respectively. This could be explained by the fact that the introduction of O₂-containing gas in the EHD system induced the generation of O₃ and other O-based active species that boosted OH• production and together with H₂O₂ and other reactive species significantly augmented MB degradation. Therefore, 3 L/min was chosen to be the optimum air flow rate for this system because any value above 3 L/min produced an excessive amount of bubbles resulting in short-circuits. Thus, air flow rate significantly affected MB removal efficiency.

In the case of the electrical parameters that were varied, MB degradation efficiency was affected by the increase of voltage and current under the following conditions: MB volume 1500 mL, air flow rate 3 L/min, air gap 2 mm, 0.5 mm silver electrode (25 cm long) and contact time of 60 minutes. When voltage was varied from 20, 22 to 25 V, about 48.02% 72.46% and 73.66% MB degradation were respectively achieved after 10 minutes of contact time. The optimum voltage suitable for the EHD system was 25 V corresponding to a peak voltage of 7.8 kV and a current of 4 A. On the other hand, the current was varied from 2 A to, 3 A to 4 A and 67.4%, 75.92% and 85.78% MB removals were achieved, respectively. The optimum current was 4 A. The increase of MB degradation efficiency was due to the fact that increasing voltage resulted in an increase of both the number and the length of streamers generated in corona electrohydraulic discharge. The strong electric field around the anode electrode therefore accelerated the production of reactive species and hence achieving an increase in MB degradation/decolourization efficiency.

In the study carried out to optimise the electrode, the optimum 1.5 mm silver electrode was the best compared to copper and stainless steel. After 10 minutes of experiment, 55.8% of MB removal was achieved with silver compared to 38.3% and 48.7% removal that were reached with copper and stainless steel, respectively. Besides the fact that the three types of electrodes (copper, silver and stainless steel) were immersed in NaCl electrolyte in the inner tube of the reactor, the highest percentage removal of MB was achieved with silver wire and its dominance over copper and stainless steel electrodes was also due to the following reasons:

The thermal conductivity of silver (429 W/m-K) is superior to that of copper (329 W/m-K) and that of stainless steel (304 W/m-K).

The thermal conductivity of copper might be affected by the mechanical work and NaCl electrolyte used in the inner tube of the reactor.

In spite of having a low thermal conductivity, the exposure of stainless steel to moisture, NaCl salt, and heat accelerated corrosion.

The 1.5 mm silver electrode was considered as optimal compared to 0.5 mm silver electrode. The reason being that the pre-oxidation zone which is the distance between the anode (in electrolyte in the inner tube) and water surface was short with 1.5 mm silver wire and longer with a small 0.5 mm silver electrode. In fact, with 1.5 mm silver electrode, the anode-water surface distance is shortened as the electric field becomes much stronger in the presence of high-energy electrons, yielding a significant amount of reactive free radicals and hence, a considerable 71.24% MB removal compared to 55.8% of MB degradation obtained with the 0.5 mm silver electrode whereby the anode-water surface is longer and the produced short lived active species vanish before reaching the dirty water. Therefore the type and the size of electrode influenced MB degradation significantly mainly because of the change in physical distances.

At the following conditions: applied voltage (25 V), peak voltage (7.8 kV), MB volume (1500 mL), air flow rate (3 L/min), 0.5 mm silver electrode (25 cm long) and contact time of 60 minutes, the reactor configuration also

impacted MB degradation efficiency in such a way that MB removal decreased with an increase of the air gap from 2 to 6 mm. Therefore, after 30 minutes of contact time the optimum removal of 83.36% was attained with 2 mm air gap while 79.9% and 19% were achieved with 4 and 6 mm air gaps, respectively. This could be explained by the fact that the small 2 mm air gap induced a strong electric field leading to high electron energy around the inner tube and thus, producing a greater amount of reactive species that accelerated MB degradation process.

The detection and quantification of reactive species performed every 10 minutes during experiment (at a voltage 25 V, peak voltage 7.8 kV, MB volume 1500 mL, air flow rate 3 L/min, air gap 2 mm, 0.5 mm silver electrode (25 cm long) and contact time of 60 minutes) showed that the concentration of H₂O₂ reached 3.73 x 10⁻⁵ mol/L in the first 10 minutes of experiment and thereafter decreased to 2.93 x 10⁻⁵ mol/L after 20 minutes. After 30 minutes of the experiment, H₂O₂ increased from 2.93 x 10⁻⁵ mol/L to 3.33 x 10⁻⁵ mol/L while 0.5 x 10⁻⁵ mol/L of ozone was produced. Beyond 30 minutes, concentration of hydrogen peroxide decreased with time whereas that of ozone fluctuated.

The reactive species mainly H₂O₂ and O₃ were detected and quantified, and these reactive species influenced MB degradation. Their interacted with UV radiations generated in the system led to the formation of powerful unselective free radicals such as OH, O., etc. which accelerated the decomposition process. The intermediate by-products of MB degradation could not be measured or detected at 5 mg/L MB because the concentration of MB end-products was very low with respect to the sensitivity of the liquid chromatography/mass spectrometry (LC-MS) and gas chromatography/mass spectrometry (GC/MS) machines used for analysis.

The EHD reaction performed at optimum conditions produced satisfactory results compared to the EHD experiment run at initial conditions. This was shown by the reduction in treatment time which was 30 min at initially applied conditions and decreased to 20 minutes at optimum conditions. Also, when the EHD was performed at optimum conditions, the MB decolourization efficiency increased within 60 minutes and stayed greater than that obtained at the initially applied conditions.

Even though the concept of corona electrohydraulic discharge has been widely used as water/wastewater treatment technique, the technology behind this concept has always been challenging. Trends relating some parameters such as chemical and electrical configuration to dye degradation efficiency have been previously reported on different reactor configurations. These same parameters were optimised in the new EHD system (reactor configuration). Hence, this EHD unit can further be explored as a powerful technique for water/wastewater treatment.

In terms of real textile effluent containing a plethora of dye stuffs, it was demonstrated that a combination of coagulation-flocculation and electrohydraulic discharge treatment was able to remove the colour and lower the COD value of a real textile effluent to well below the discharge limit, depending upon the treatment process combination. The preliminary investigation conducted on the textile effluent indicated that removal of COD below the detection limit remains unrealistic via a single treatment system such as EHD alone. Thus,

process integration was considered to be more economically advantageous and beneficial for the maintenance of environmental sustainability and protection. However, the application of the single cell configuration of the electrical discharge system for industrial wastewater treatment is costly to scale up thus may limit its full scale application for effluent treatment. A preliminary design for a reconfigured recirculating EHD system is being developed which will be utilized in future.

The high surface area supported TiO₂ nanocomposites with high activity for organics degradation were achieved. The photocatalytic degradation of methylene blue over the supported TiO₂ nanocrystals was carried out and UV-vis was used to characterize the degree of degradation of the MB. The findings of this research were that the supported TiO₂ nanocrystals possessed obvious photocatalytic activity at various degradation time intervals. Of all the immobilised TiO₂ nanocrystals prepared that possessed photocatalytic activity, the supported TiO₂ nanocrystals (decomposed at 400°C for 2 h), showed the highest degradation activity for methylene blue of 96.02 ± 0.0054% after 30 min degradation time in the presence of the 0.3 g supported TiO₂ nanocrystals that were decomposed at 50°C/min up to 400°C with a holding temperature of 2 h at 400°C in air. This work contributes to the preservation of water by efficient treatment of organic pollutants in waste waters with a new composite photocatalyst that can in future be integrated into the EHD system to utilize the generated UV. The supported photocatalyst had a high surface area, and would not release particulates into the water to be treated thus not obscuring the penetration of UV light into the system, thus overcoming the problems experienced with current photocatalysts.

On the disinfection of bacteria using dielectric barrier discharge system, the study has demonstrated that dielectric barrier discharge system has a significant impact on the sterilization of *E. coli* colonies. However, further investigation on the inactivation of bacteria by the system need to be carried out using the killing factor as well as other analytical techniques.

The aim and objectives of this study were achieved. Physico-chemical, electrical and reactor configuration were optimized for the DBD. It was shown that the following parameters: MB concentration, solution pH, voltage and current, air flow rate and air gap significantly affected MB decolourization/degradation efficiency in the DBD reactor. The current optimized EHD system is feasible, efficient, and environmentally friendly and has proved to decolourize and degrade organic pollutants at ambient conditions and the incorporation of a stable, reproducible, supported photocatalyst is now possible to fully utilize the generated UV radiation. Design flaws were identified and improvements as recommended below can be incorporated in future studies.

5.2 RECOMMENDATIONS

- It would be important to consider quantification of hydroxyl radicals produced in the EHD system for better understanding of MB mineralization.
- Future research should identify the intermediates by-products of the degradation of MB and elucidate the degradation mechanisms of the model pollutant which can be achieved using LC-MS, GC-MS or HPLC-MS.
- To avoid undesirable by-products such as nitrites and nitrates during the treatment of pollutant by EHD system, pure oxygen should be used instead of air.
- The future work should also attempt to trap and quantify the CO₂ produced as one of the final end-products even if its presence might be in the order of pico mg/L.
- Full integration of the TiO₂ photocatalyst into the EHD should be optimized.
- A flow through design should be based upon the findings of this optimization study
- Quantification of the free reactive species during inactivation of *E. coli* by DBD and their correlation with the progressive death of bacteria would be necessary.
- The use of various possible analytical and characterization techniques for a better analysis of bacteria samples is recommended.

REFERENCES

- Akpan, U.G. and Hameed, B.H. (2009). Parameters affecting the photocatalytic degradation of dyes using TiO₂-based photocatalysts: A review: *J. Hazardous Materials*: 170: 520-529
- Ahmed, S., Rasul, M.G., Martens, W.N., Brown, R.J., and Hashib, M.A. (2010) Heterogeneous photocatalytic degradation of phenols in wastewater: a review on current status and developments. *Desalination*, 261(1-2): 3-18.
- Arjunan K. Priya, Gary Friedman, Alexander Fridman and Alisa Morss Clyne, (2012). Non-thermal dielectric barrier discharge plasma induces angiogenesis through reactive oxygen species. *Journal of the Royal Society*. Interface 9,
- Ayan, H., Staack, D., Fridman, G., Gutsol, A., Mukhin, Y., Starikovskii, A., Fridman, A. & Friedman, G. (2009). Application of nanosecond-pulsed dielectric barrier discharge for biomedical treatment of topographically nonuniform surfaces. *J. Phys. D: Appl. Phys.* 42, 125202 (5pp).
- Bader H. and Hoigne, J. (1981). "Determination of ozone in water by the indigo method," *Water Research*. 15:449-456
- Behnajady M.A., Modirshahla N., Shokri M. and Rad B. (2008). Enhancement of photocatalytic activity of TiO₂ nanoparticles by silver doping: photodeposition versus liquid impregnation methods, *Global NEST Journal*, 10: pp1-7.
- Blake D. M., Maness P. C., Huang Z., Wolfrum E. J. and Huang J. (1999), "Application of the photocatalytic chemistry of titanium dioxide to disinfection and the killing of cancer cells", *Separation and Purification Methods*; 28, 1-50.
- Brisset J-L, Benstaali B, Moussa D, Fanmoe J, Njoyim-Tamungang E (2011). Acidity control of plasma chemical oxidation: applications to dye removal, urban waste abatement and microbial inactivation. *Plasma Sources Sci Technol*, 20: 034021
- Byrne, J. A., Fernandez-Ibañez, P. A., Dunlop, P. S. M., Alrousan, D. M. A and Hamilton, J. W. J. (2011). "Photocatalytic enhancement for solar disinfection of water: a review," *International Journal of Photoenergy*, vol. 2011, Article ID 798051, 12
- Bruggeman, P.J., and Locke, B.R. (2013). Assessment of Potential Applications of Plasma with Liquid Water, in *Low Temperature Plasma Technology: Methods and Applications*, P. Chu, and X. Lu (Eds.), Taylor and Francis Group, Pp. 368-369.

Chen, X. and Mao, S.S. (2007). Titanium dioxide nanomaterials synthesis, properties, modifications and applications, *Chemical Reviews*, 107: 2891.

Chen, C. W., Lee, H. M. & Chang, M. B., (2009). Influence of pH on inactivation of aquatic microorganism with a gas-liquid pulsed electrical discharge. *J. Electrostat.* 67, 703-708

Choi, H., Al-Abed, S. R., Dionysiou, D. D., Stathatos, E. and P. Lianos, (2010). "TiO₂-based advanced oxidation nanotechnologies for water purification and reuse," *Sustainability Science and Engineering*, 2: 229-254

Choi Jai Hyuk, Inho Han, Hong Koo Baik, Mi Hee Lee, Dong-Wook Han, Jong-Chul Park, In-Seob Lee, Kie Moon Song, Yong Sik Lim, (2006). Analysis of sterilization effect by pulsed dielectric barrier discharge. *Journal of Electrostatics*, 64 17-22

Chong, M. N., Jin, B., Chow, C. W. K., and Saint, C. (2010). Recent developments in photocatalytic water treatment technology: a review. *Water Resources*, 44, 2997-3027.

Conrads H., and Schmidt, M. (2000). Plasma generation and plasma sources, *Plasma Sources Sci. Technol.* 9: 441-454.

Chuangchote S., Jitputti J., Sagawa T. and Yoshikawa S. (2009), "Photocatalytic activity for hydrogen evolution of electrospun TiO₂ nanofiber", *Applied Materials & Interfaces*; 1, 1140-1143

Dang TH, Denat A, Lesaint O, Teissedre G (2008). Degradation of organic molecules by streamer discharges in water: coupled electrical and chemical measurements. *Plasma Sources Sci Technol*, 17: 024013

Deng Sanxi, Cheng Cheng, Guohua NI, Yuedong Meng, and Hua Chen, (2008). Bacterial inactivation by atmospheric pressure dielectric barrier discharge plasma jet. *Japanese Journal of Applied Physics*, 47(8): 7009-7012

Dindarloo Inaloo K., K. Naddafi , A. R. Mesdaghinia , S. Nasser , R. Nabizadeh Nodehi, A. Rahimi, (2011). Optimization of operational parameters for decolorization and degradation of c. i. reactive blue 29 by ozone. *Iran. J. Environ. Health. Sci. Eng.* 8(3): 227-234

Dojcinovic BP, Roglic GM, Obradovic BM, Kuraica MM, Kostic MM, Nesic J, Manojlovic DD (2011). Decolorization of reactive textile dyes using water falling film dielectric barrier discharge. *J Hazard Mater*, 192:763-771

Fisher, M. B., Keenan, C. R., Nelson, K. L. & Voelker, B. M., (2008). Speeding up solar disinfection (SODIS): effects of hydrogen peroxide, temperature, pH, and copper plus ascorbate on the photoinactivation of *E. coli*. *J. Water Health* 6, 35-51.

Foo, K. Y. and Hameed, B. H. (2010). "Decontamination of textile wastewater via TiO₂/activated carbon composite materials," *Advances in Colloid and Interface Science*, 159:(2): 130-143

Gaya, U. I., and Abdullah, A. H. (2008). Heterogeneous photocatalytic degradation of organic contaminants over titanium dioxide: a review of fundamentals, progress and problems. *Journal of Photochemistry and Photobiology C*, 9(1): 1-12.

Gilmour Charles (2012). Water treatment using advanced oxidation processes: application perspectives. Thesis of Masters in Engineering Science. Graduate program in engineering science department of chemical and biochemical engineering. University of Western Ontario London, Ontario, Canada.

Girginov Ch., Stefchev, P., Vitanov, P. and Dikov, Hr. (2012). Silver Doped TiO₂ Photocatalyst for Methyl Orange Degradation. *Journal of Engineering Science and Technology Review*, 5 (4): 14-17

Gogate P.R. and Pandit A.B. (2004a) A review of imperative technologies for wastewater. *Chemosphere*, 73:848-853.

Gupta S. B., (2007). Investigation of a physical disinfection process based on pulsed underwater corona discharges, MSc thesis. *Institut für Hochleistungsimpuls- und Mikrowellen-technik*.

Gultekin, I., & Ince, N. H. (2007). Synthetic endocrine disruptors in the environment and water remediation by advanced oxidation process. *Journal of Environmental Management*, 85: 816-832.

Hernández-Arias, AN., Rodríguez-Méndez, BG, López-Callejas, R, Alcántara-Díaz, D., Valencia-Alvarado, R., Mercado-Cabrera, A., PeñaEguiluz, R, Muñoz-Castro, AE, Barocio, SR and de la Piedad-Beneitez, A. (2012). Inactivation of *Escherichia coli* in water by pulsed dielectric barrier discharge in coaxial reactor. *Journal of Water and Health*, 10(3): 371-379

Houas A., Lachheb H., Ksibi M., Elaloui E., Guillard C., Herrmann J.-M. (2001) Photocatalytic degradation pathway of methylene blue in water. *Applied Catalysis B: Environmental* 31(2): 145-157.

Hu G., Meng X., Feng X., Ding Y., Zhang S. and Yang M. (2007), "Anatase TiO₂ nanoparticles/carbon nanotubes nanofibres: preparation, characterization and photocatalytic properties", *Journal of Materials Science*; 42, 7162-7170.

Huang, C.P.; Dong, C. and Tang, Z. (1993). Advanced chemical oxidation: Its present role and potential future in hazardous waste treatment, *Waste Management*, 13: 361-377.

Jin-Oh JO, Mok, Y.S. (2009). In-situ production of ozone and ultraviolet light using a barrier discharge reactor for wastewater treatment. *Journal of Zhejiang University Science A*. 10(9):1359-1366

Jiang, B., Qiu, J. Z. S., Mingbo, W., Yan, Q. Z. Z., & Xue, Q. (2014). Review on electrical discharge plasma technology for wastewater remediation. *Chemical Engineering Journal*, 236: 348-368

Joshi G. Suresh., Moogega Cooper, Adam Yost, Michelle Paff, Utku K. Ercan, Gregory Fridman, Gary Friedman, Alexander Fridman, and Ari D. Brooks, (2011). Nonthermal dielectric-barrier discharge plasma-induced inactivation involves oxidative DNA damage and membrane lipid peroxidation in *Escherichia coli*. *Antimicrobial Agents and Chemotherapy*, 55(3p):1053-1062.

Joshi, S. G. (2010). Control of methicillin-resistant *Staphylococcus aureus* in planktonic form and biofilms: a biocidal efficacy study of nonthermal dielectric-barrier discharge plasma. *Am. J. Infect. Control* 38: 293-301. 12.

Kaunas, (2012). Report on the different plasma modules for pollution removal MO 03. *Plasma for environment protection*

Kogelschatz Ulrich, (2003). Dielectric-barrier Discharges: Their History, Discharge Physics, and Industrial Applications. *Plasma Chemistry and Plasma Processing*, 23, No. 1.

Koivunen, J. and Heinonen-Tanski, H., (2005). Peracetic acid (PAA) disinfection of primary, secondary and tertiary treated municipal wastewaters. *Water Res.* 39: 4445-4453.

Konelschatz U., B. Eliasson and W. Egli, (1997). Dielectric-barrier discharges. Principle and applications. *Journal de physique IV. France* 7

Kostov K.G., V. Rocha, C.Y. Koga-Ito, B.M. Matos, M.A. Algatti, R.Y. Honda, M.E Kayama, R.P. Mota, (2010). Bacterial sterilization by a dielectric barrier discharge (DBD) in air. *Surface & Coatings Technology* 204 (2010) 2954-2959

Krause, H., Schweiger, B., Schuhmacher, J., Scholl, S., and Steinfeld, U. (2009). Degradation of the endocrine disrupting chemicals (EDCs) carbamazepine, clofibric acid, and iopromide by corona discharge over water. *Chemosphere*, 75:163-168.

Li Youji, Mingyuan Ma, Wei Chen, Leiyong Li, Mengxiong Zen. (2011). Preparation of Ag-doped TiO₂ nanoparticles by a miniemulsion method and their photoactivity in visible light illuminations. *Materials Chemistry and Physics*, 129:501-505

Locke, B. R., Sato, M., Sunka, P., Hoffmann, M. R., and Chang, J. S. (2006). Electrohydraulic discharge and non-thermal plasma for water treatment. *Industrial and Engineering Chemistry Research*, 45(3): 882-905.

Lomoră, M., Drăghici, C., and Eneșca, Al. (2011). Intermediary compounds in advanced oxidation processes for wastewater treatment. *Bulletin of the Transilvania University of Brașov Series I: Engineering Sciences* 4 (53) : 1-2011

Lopez Jose L., (2008). Dielectric barrier discharge, ozone Generation, and their applications. *Complex Plasmas Summer Institute*

Lu J., Zhang T., Ma J. and Chen Z. (2009). Evaluation of disinfection by-products formation during chlorination and chloramination of dissolved natural organic matter fractions isolated from a filtered river water. *J. Hazard. Mater.* 162: 140-145

Malik, M. A. (2010). Water purification by plasmas: which reactors are most energy efficient? *Plasma Chemistry and Plasma Processing*, 30: 21-31

Manoj Kumar Reddy P., B. Rama Raju, J. Karupiah, E. Linga Reddy, Ch. Subrahmanyam, (2013). Degradation and mineralization of methylene blue by dielectric barrier discharge non-thermal plasma reactor. *Chemical Engineering Journal*, 217: 41-47

Mark P. Cal and Martin Schluep, (2001). Destruction of benzene with non-thermal plasma in dielectric barrier discharge reactors. *Environmental Progress*, 20, No.3

Martínez-Huitle, C. A. and Brillas, E. (2009). "Decontamination of wastewaters containing synthetic organic dyes by electrochemical methods: a general review," *Applied Catalysis B*, 87(3-4): pp. 105-145

Matthew Pavlovich J, Hung-Wen Chang, Yukinori Sakiyama, Douglas S Clark and David B Graves, (2013). Ozone correlates with antibacterial effects from indirect air dielectric barrier discharge treatment of water. *Journal of physics d: applied physics* 46 145202 (10pp).

Magureanu M., Mandache NB, Parvulescu VI, (2007). Degradation of organic dyes in water by electrical discharges. *Plasma Chemistry and Plasma Processes* 27:589-598

Martínez, C., Canle L.M., Fernández, M.I., Santaballa, J.A., , Faria,J. (2011). Kinetics and mechanism of aqueous degradation of carbamazepine by heterogeneous photocatalysis using nanocrystalline TiO₂, ZnO and multi-walled carbon nanotubes-anatase composites. *Applied Catalysis B: Environmental*, 102(3-4) :563-571

Mastanaiah Navya, Judith A. Johnson, Subrata Roy, (2013). Effect of dielectric and liquid on plasma sterilization using dielectric barrier discharge plasma. *LoS ONE* 8(8): e70840. doi:10.1371/journal.pone.0070840

Monica Magureanu, Corina Bradu, Daniela Piroi, Nicolae Bogdan, Mandache Vasile Parvulescu, (2013). Pulsed Corona Discharge for Degradation of Methylene Blue in Water. *Plasma Chemistry and Plasma Process* DOI 10.1007/s11090-012-9422-8

Muranyi P., J. Wunderlich and M. Heise, (2007). Sterilization efficiency of a cascaded dielectric barrier discharge. *Journal of Applied Microbiology* 103 1535-1544

Naik Bhanudas, Chinthan Hemapa Manoratne, Akash Chandrashekhar, Abhishek Iyer, Vadakkethonippurathu Sivankutty Prasad and Narendra Nath Ghosh. (2012). Preparation of TiO₂, Ag-doped TiO₂ nanoparticle and TiO₂-SBA-15 nanocomposites using simple aqueous solution-based chemical method and study of their photocatalytic activity. *Journal of Experimental Nanoscience*, 1-18

Nainani Roshan, Pragati Thakur and Manohar Chaskar. (2012). Synthesis of silver doped TiO₂ nanoparticles for the improved photocatalytic degradation of methyl orange. *Journal of Materials Science and Engineering*, B 2 (1): 52-58

Nehra Vijay, Ashok Kumar and H K Dwivedi, (2008). Atmospheric non-thermal plasma sources. *International Journal of Engineering*, 2(1): 53-68

Paunekar Waman, Swapnil Sanmukh, Krishna Khairnar, Rajshree Chandekar, Chetan Khapekar, Naresh Bokade, Udit Pal, Ram Prakash, Ghanshyam L Bodhe, (2014). Future Prospects of Plasma Treatment Technology for Disinfection. *Emerging Technologies of the 21st Century*

Pavlovich Matthew J, Hung-Wen Chang, Yukinori Sakiyama, Douglas S Clark and David B Graves, (2013). Ozone correlates with antibacterial effects from indirect air dielectric barrier discharge treatment of water. *Journal of Physics d: Applied Physics*, 46: 145202 (10pp).

Prendiville, P. W., (1986). Ozone. *Science and Engineering*, 8, 77-93.

Porter D, Poplin MD, Holzer F, Finney WC, Locke BR (2009) Formation of hydrogen peroxide, hydrogen, and oxygen in gliding arc electrical discharge reactors with water spray. *IEEE Trans Ind Appl* 45:623-629

Reddy P. Manoj Kumar and Ch. Subrahmanyam, (2012). Green Approach for Wastewater Treatment – Degradation and Mineralization of Aqueous Organic Pollutants by Discharge Plasma. *Industrial & Engineering Chemistry Research*, 51: 11097-11103

Reddy P. Manoj Kumar, B. Rama Raju, J. Karupiah, E. Linga Reddy, Ch. Subrahmanyam, (2013). Degradation and mineralization of methylene blue by dielectric barrier discharge non-thermal plasma reactor, *Chemical Engineering Journal*, 217:41-47

Reddy P. Manoj Kumar, Sk. Mahammadunnisa, Ch. Subrahmanyam, (2014). Catalytic non-thermal plasma reactor for mineralization of endosulfan in aqueous medium: A green approach for the treatment of pesticide contaminated water. *Chemical Engineering Journal*, 238:157-163

Rong Shaopeng, Yabing Sun, Zehua Zhao and Huiying Wang, (2014). Dielectric barrier discharge induced degradation of diclofenac in aqueous solution. *Water Science & Technology*, 69.1

Sato, M., (2008). Environmental and biotechnological applications of high-voltage pulsed discharges in water. *Plasma Sources Sci. Technol.* 17, 024021 (7pp).

Sato, M. (2009). Environmental and biotechnological applications of high-voltage pulsed discharges in water. *Plasma Sources Sci. Technol.* 17, 024021 (7pp).

Shannon, M.A., Bohn, P.W., Elimelech, M., Georgiadis, J.G., Marin^ˆas, B.J and Mayes, AM. (2008). Science and technology for water purification in the coming decades. *Nature*, 452(20):301-310.

Shen Yong Jun, LEI LeCheng and Zhang XingWang, (2008). Evaluation of energy transfer and utilization efficiency of azo dye removal by different pulsed electrical discharge modes. *Chinese Science Bulletin* vol. 53 | no. 12 | 1824-1834

Suresh G. Joshi, Moogega Cooper, Adam Yost, Michelle Paff, Utku K. Ercan, Gregory Fridman, Gary Friedman, Alexander Fridman, and Ari D. Brooks. (2011). Nonthermal Dielectric-Barrier Discharge Plasma-Induced Inactivation Involves Oxidative DNA Damage and Membrane Lipid Peroxidation in *Escherichia coli*. *Antimicrobial agents and chemotherapy*, 55(3): 1053-1062

Tarr M. (2003), *Chemical Degradation Methods for Wastes and Pollutants*, Marcel Dekker Inc., New York, NY.

Tsai, Wen-Tien., Mei-Kuei Leeb, Ting-Yi Suc, & Yuan, M. Chang. (2009). Photodegradation of bisphenol-A in a batch TiO₂ suspension reactor. *Journal of Hazardous Materials*, 168:269-275

Ubonchonlakate, K. Sikong, L. and Saito, F. (2012). Photocatalytic disinfection of *P. aeruginosa* bacterial Ag-doped TiO₂ film. *Procedia Engineering*, 32: 656-662

Uher G., E. Gilbert, U. Siegfried, H. Eberle, (1991). "Determination of hydrogen peroxide in presence of organic peroxides" *Vom Wasser*, 76, pp. 225-234

Vujevic D., N. Koprivanac, A. Loncaric Bozic and B.R. Locke, (2004). The Removal of Direct Orange 39 by Pulsed Corona Discharge from Model Wastewater, *Environmental Technology*, 25(7):791-800

Yao Z., Baiye Sun, Shihuai Deng, Yingjun Wang, Hong Peng, Yuanwei Li, Xiaohong Zhang, (2010). Methyl orange degradation by pulsed discharge in the presence of activated carbon fibers. *Chemical Engineering Journal* 159 47-52 (Journal homepage: www.elsevier.com/locate/cej)

Yang H. and Cheng H. (2007). Controlling nitrite level in drinking water by chlorination and chloramination. *Sep. Purif. Technol.* 56: 392-396.

Yue Ma, Guan-Jun Zhang, Member, IEEE, Xing-Min Shi, Gui-Min Xu, and Yun Yang, (2008). Chemical Mechanisms of Bacterial Inactivation Using Dielectric Barrier Discharge Plasma in Atmospheric Air. *IEEE Transactions on Plasma Science*, 36: 4

Zhang, R., Wang, L., Wu, Y., Guan, Z. & Jia, Z., (2006). Bacterial decontamination of water by bipolar pulsed discharge in a gas-liquid-solid three-phase discharge reactor. *IEEE Trans. Plasma Sci.* 34, 1370-1374.

Zhang Y, Zhou M, Hao X, and Lei L (2007) Degradation mechanisms of 4-chlorophenol in a novel gas-liquid hybrid discharge reactor by pulsed high voltage system with oxygen or nitrogen bubbling. *Chemosphere* 67:702-711

Zhang Y., Zheng J., Qu X., Chen H., (2008). Design of a novel non-equilibrium plasma-based water treatment reactor, *Chemosphere*, 70:1518-1524

Zhang Jiao, Deqi Liu, Wenjuan Bian, and Xihua Chen, (2012). Degradation of 2,4-dichlorophenol by pulsed high voltage discharge in water. *Desalination*, 304 :49-56

Zhang, Y., Zhang, R., Ma, W., Zhang, X., Wang, L., and Guan, Z. (2013). Purification of water by bipolar pulsed discharge plasma combined with TiO₂ catalysis. *Journal of Physics: Conference Series* 418: 012125

Zhou, B., Parasher, S., Wu, Z.W., Zhou, Z.H.: US20087326399 (2008) Titanium dioxide nanoparticles and nanoparticle suspensions and methods of making the same. US Pat. 20087326399, 2005. Headwaters Technology Innovation, LLC (United States).

APPENDIX A: Multiple unit EHD reactor

A1. Systematic reactor disassembly:

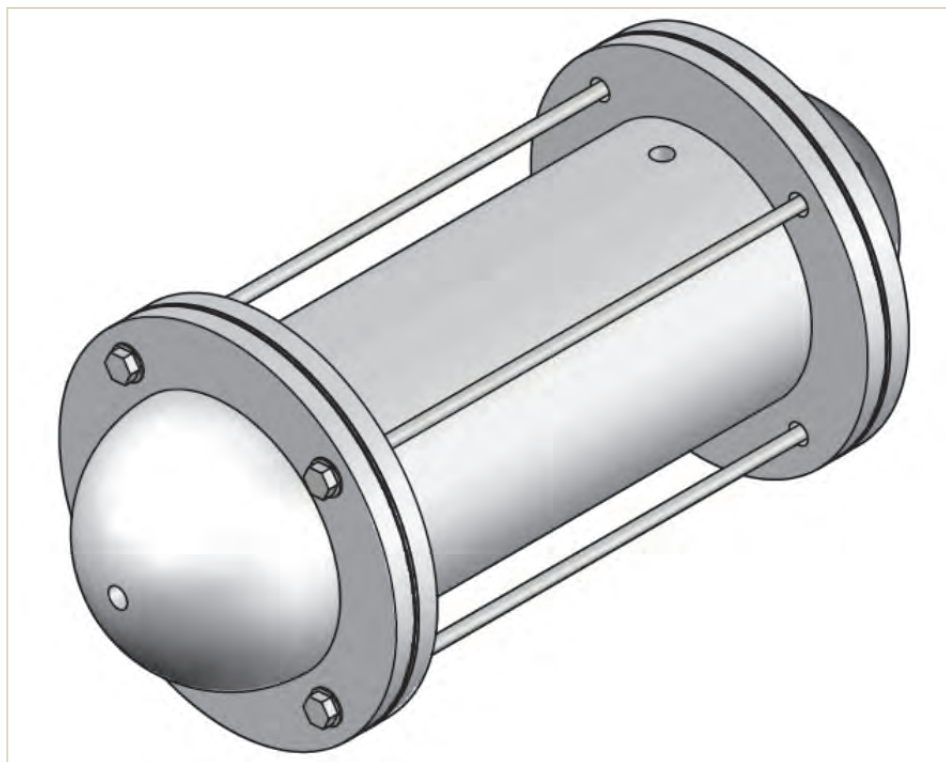


Figure A1.1: Fully assembled reactor vessel

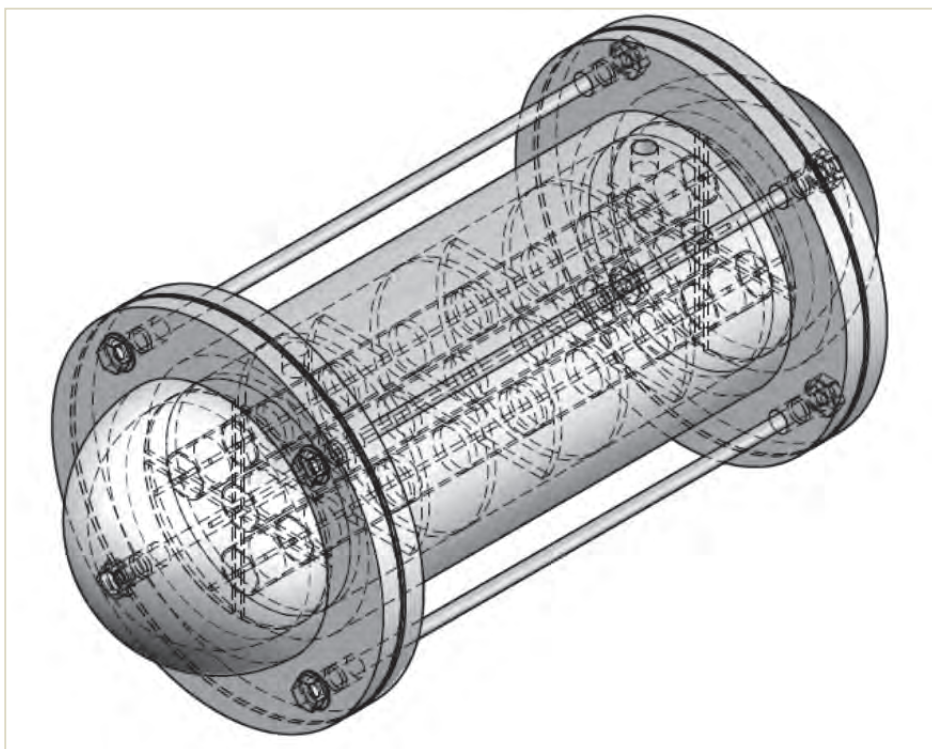


Figure A1.2: Fully assembled reactor vessel (wire frame view)

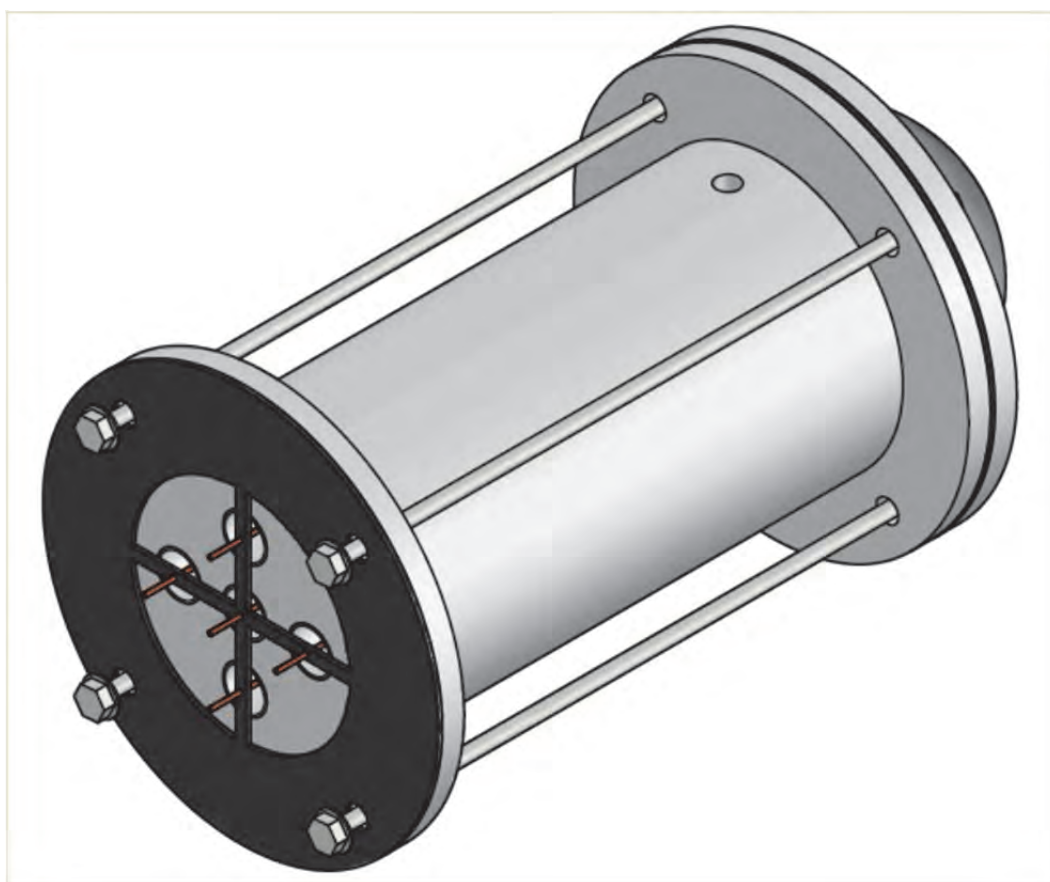


Figure A1.3: Reactor vessel with end cap removed

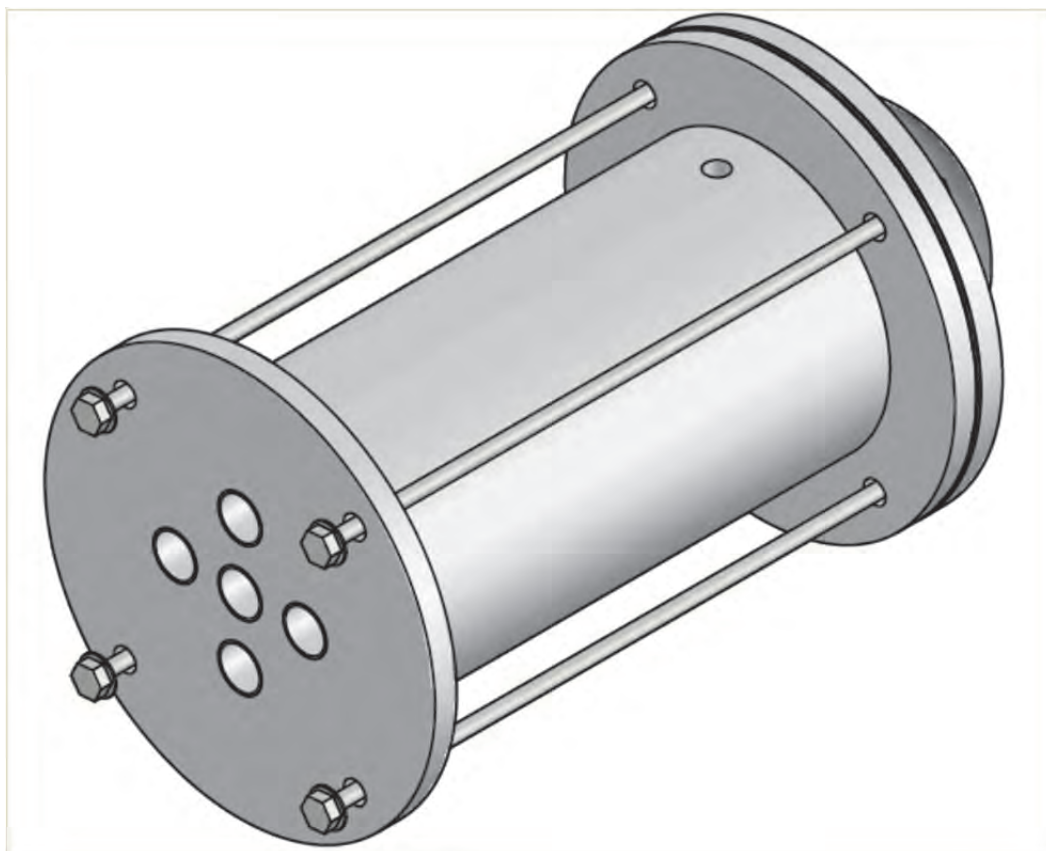


Figure A1.4: Reactor vessel with electrode placement disk and electrodes removed

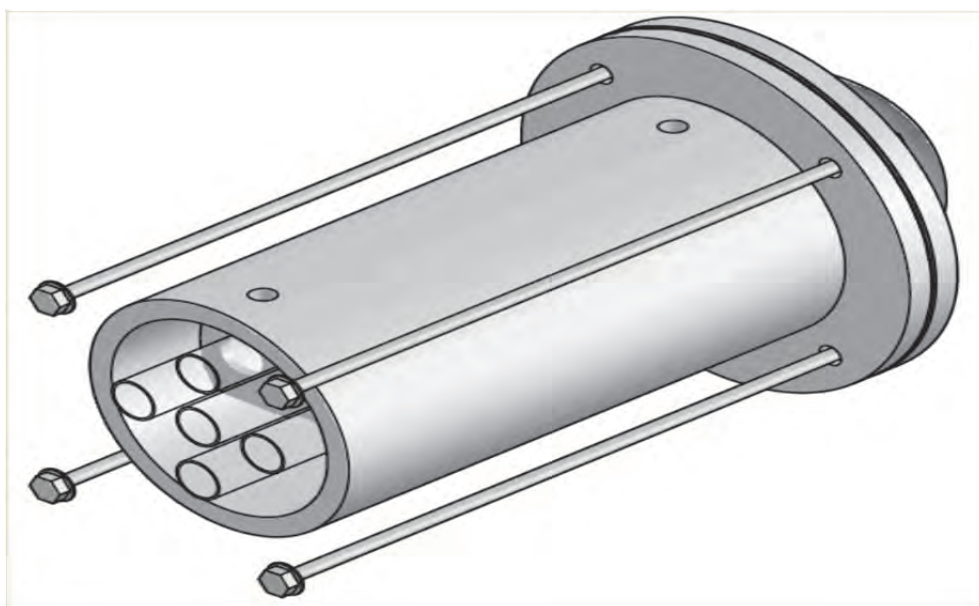


Figure A1.5: Reactor with shell flange removed

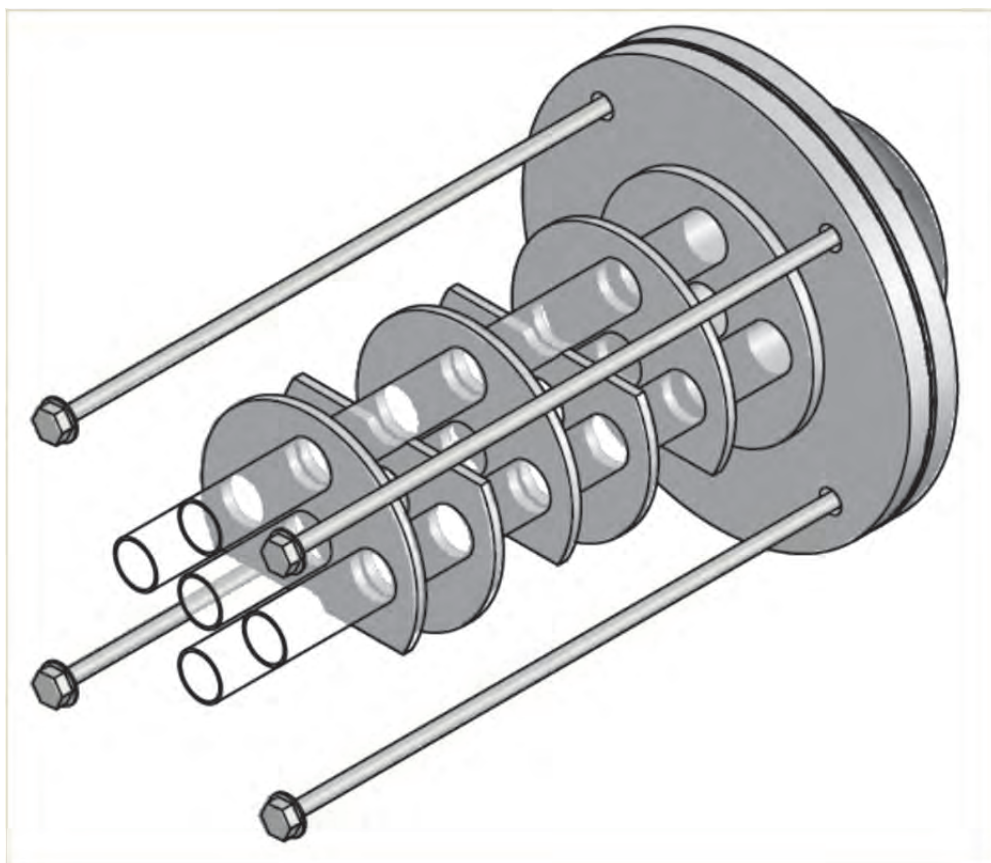


Figure A1.6: Reactor vessel with shell removed

A2. Dimensioned parts

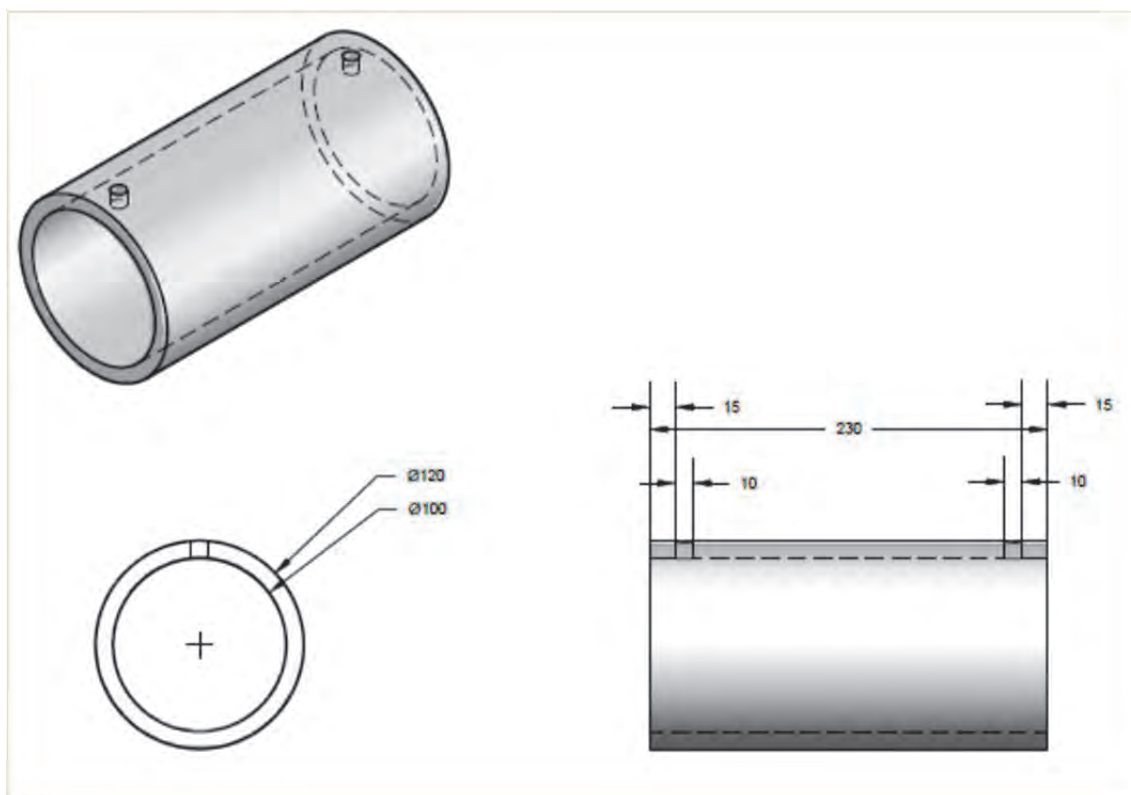


Figure A2.1: Perspex shell dimensions

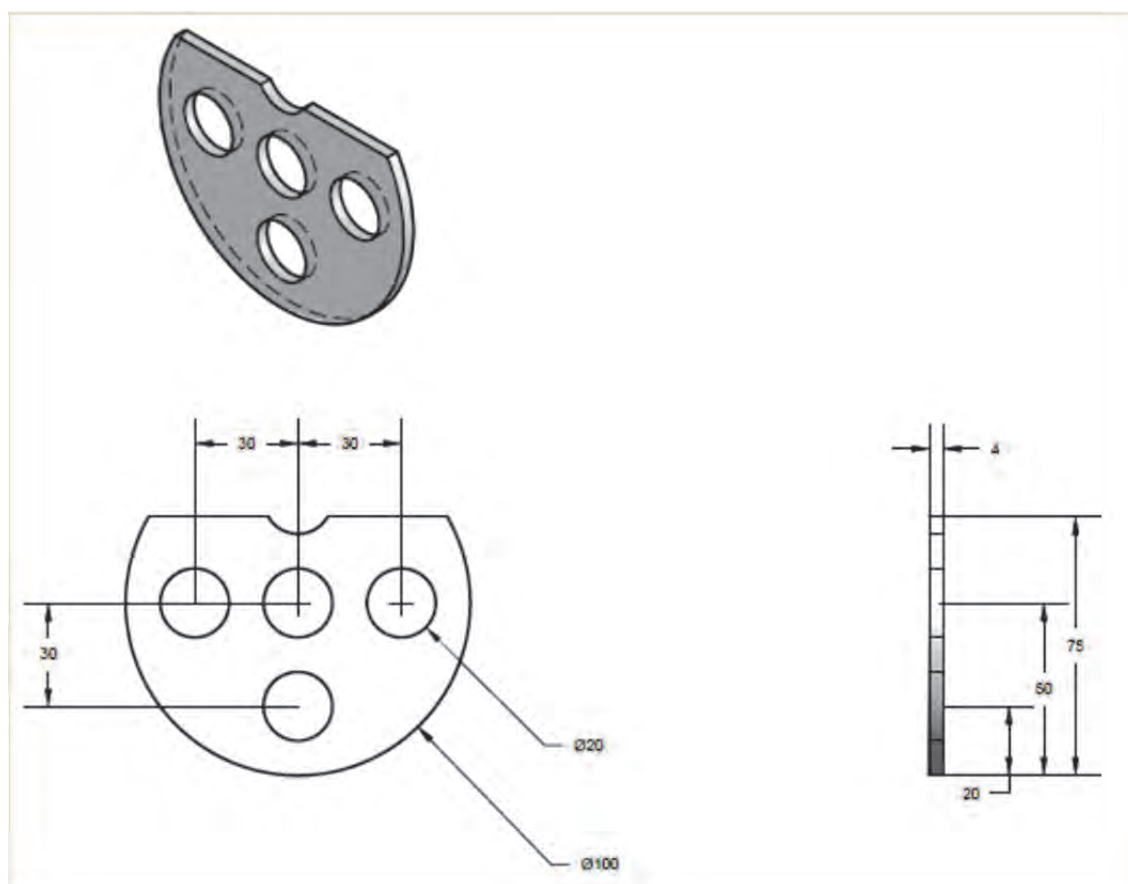


Figure A2.2: Teflon baffle dimensions

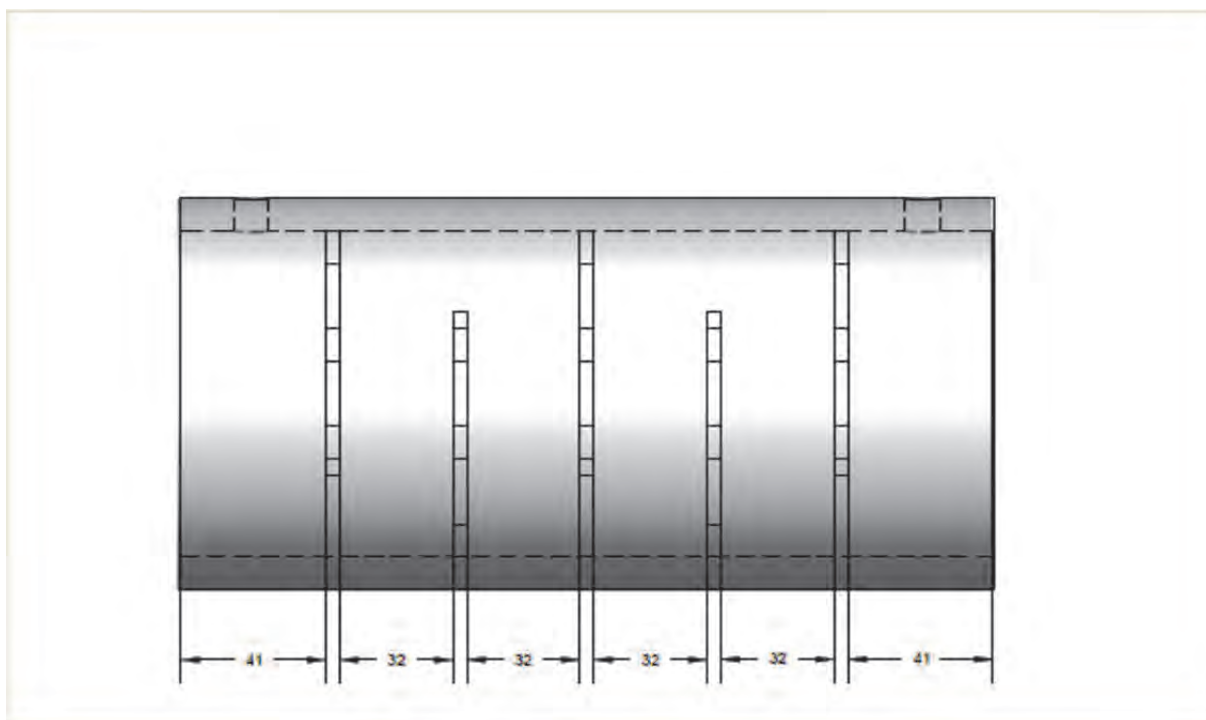


Figure A2.3: Baffle placement in shell

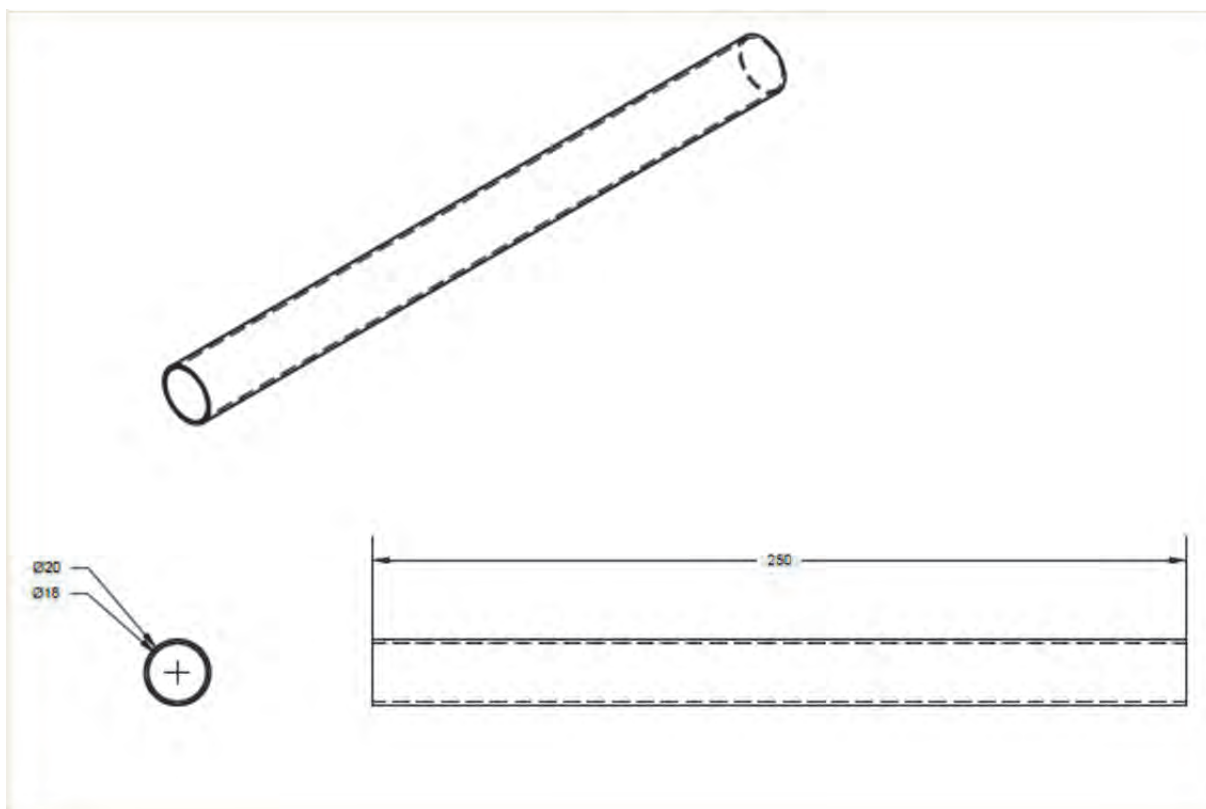


Figure A1.10: Quartz tubes dimensions

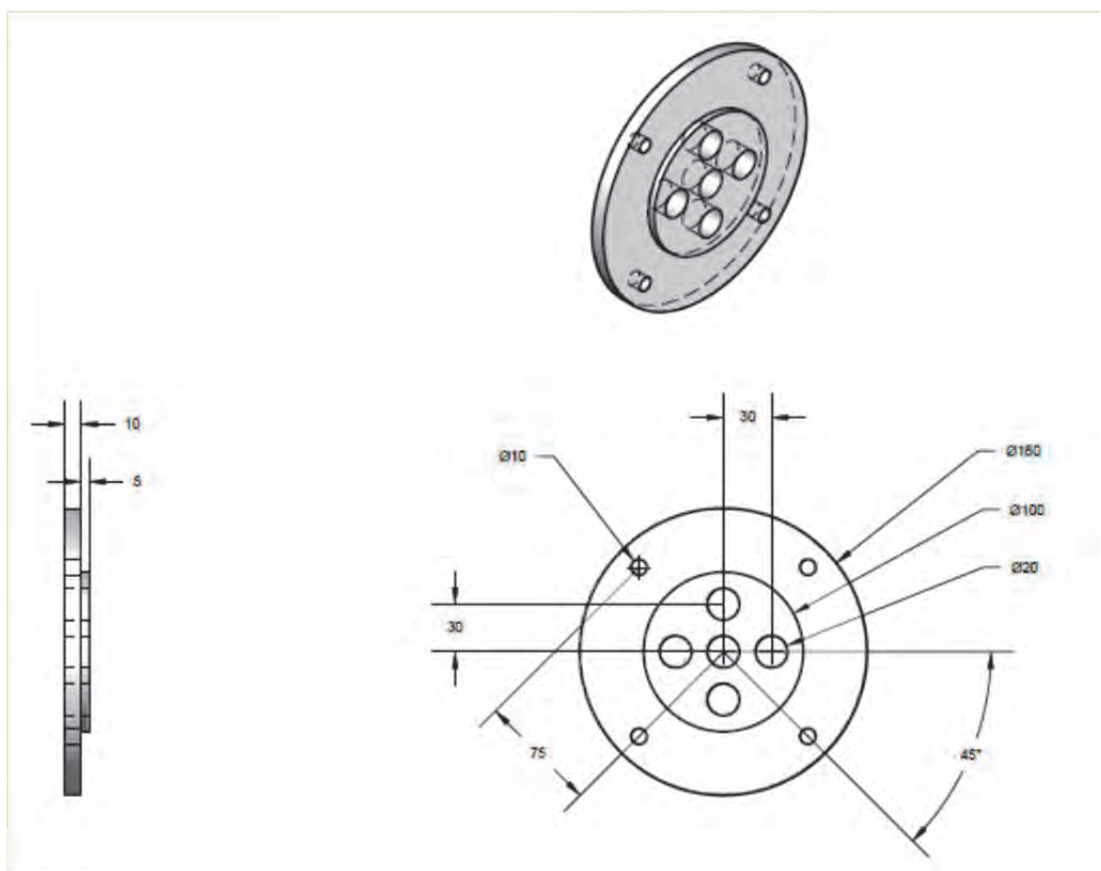


Figure A1.11: Teflon shell flange dimensions

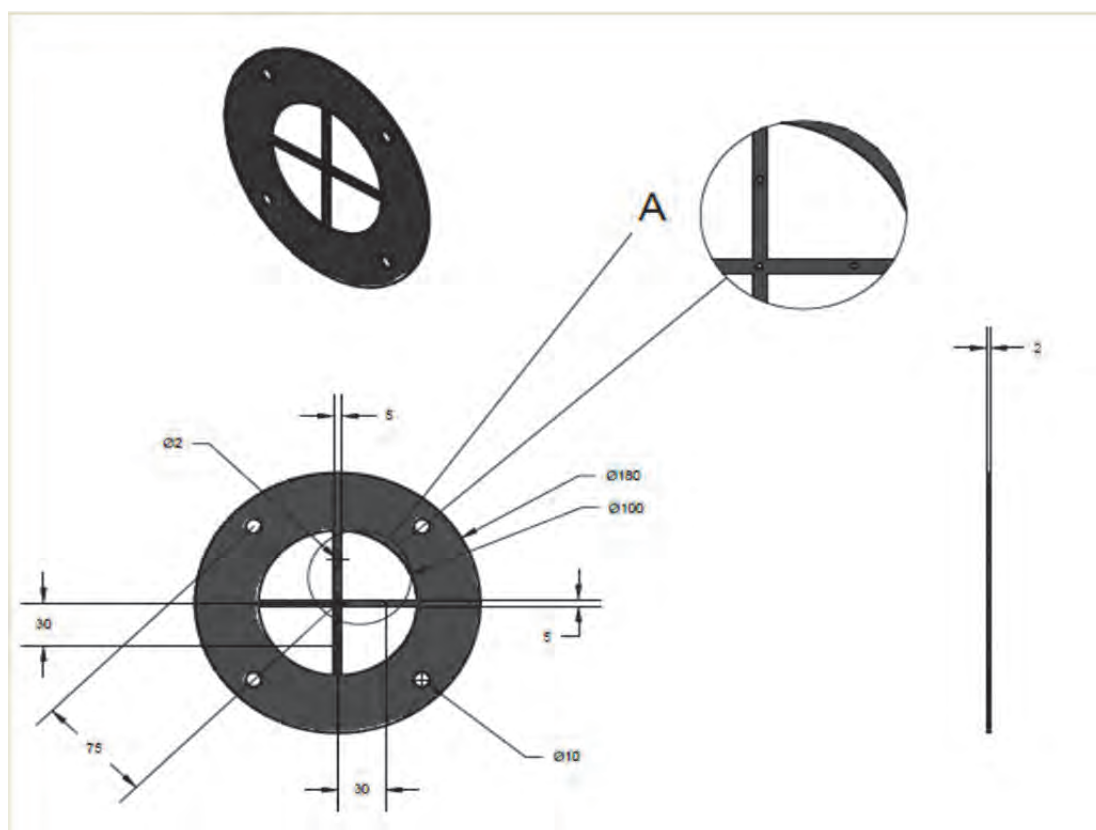


Figure A1.12: Teflon electrode placement disk dimensions

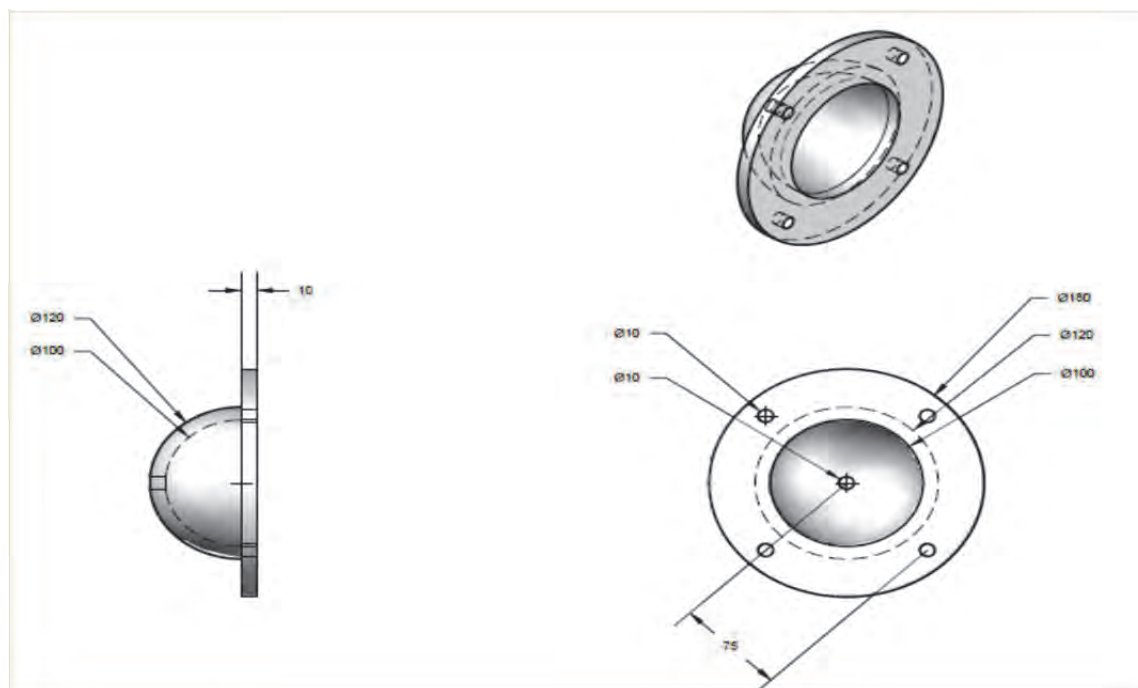


Figure A1.13: Perspex end cap dimensions

Reactor description

The reactor consists of a shell and tube design (water flows through the shell and electrodes are placed in the tubes) which contains 5 evenly spaced baffles. The baffles were incorporated in the design after fluid flow simulations were done. Computer simulation showed that large dead zones were present. After the baffles were introduced the simulation was repeated and it was found that the dead zones had been reduced to almost nothing. It was important to reduce the dead zones as organic material growth could occur in these areas and residence times vary widely as a result of these dead zones. The electrodes, connected to the AC power supply are situated in the tubes running coaxially through the shell. These electrodes, diameter of 2 mm, connected in series, are held central to the tubes, having a diameter of 20 mm, by electrode placement disks situated at the ends of the central body (shell) creating an arcing distance of 9 mm, 8 mm of which is air and 1 mm of which is quartz, between the outside surface of the electrode and the grounded water feed. And there is a 6 mm diameter hole in the left hand side end cap through which the electrodes are connected to the power source.

Reactor operation

Water enters the shell at the inlet marked as (1) on the above figures where the in situ oxidation compounds (H₂O₂ and OH radicals) are formed. These compounds then mineralize the organic compounds present in the water while still in the reactor. The water then leaves the shell through the outlet marked as (2). The high voltage causes electricity to move from the electrode toward the shell containing the grounded water by way of a corona discharge. This process causes plasma to form which ionizes the water to form the oxidation compounds. While this is taking place air is fed in at the inlet marked (3). This air flows through the tubes containing the electrodes and plasma is formed in which oxygen is converted to ozone. This mixture of ozone and air leaves the reactor through the outlet marked (4) and is mixed in line with the water entering at inlet 1 so as to allow the ozone to take part in the mineralization of the organic compounds inside the reactor.